Final Report on WIPANO Research Project

A New Test Method for Evaluating Prestressing Steels' Susceptibility to Stress Corrosion Cracking

Acronym:	Safety of Prestressing Steels
Reporting period:	October 2019 to September 2022
Funding source:	Federal Ministry of Economic Affairs and Climate Action (BMWK) 11019 Berlin
Support program:	WIPANO - Knowledge and technology transfer through patents and standards, Project Management Jülich (PTJ)

Authors:

Lando Seifert[1], Markus Philipp[2], Gino Ebell[1], Jörg Moersch[3], Thoralf Müller[1]

[1]Bundesanstalt für Materialforschung und -prüfung (BAM), Unter den Eichen 87, 12205 Berlin, Germany (FKZ: 03TNH019A)

[2]Stahlwerk Annahütte Max Aicher GmbH & Co. KG (SAH), Max-Aicher Allee 1+2, 83404 Hammerau, Germany (FKZ: 03TNH019D)

[3]Max Aicher GmbH & Co. KG, Teisenbergstraße 7, 83395 Freilassing, Germany (FKZ: 03TNH019B)

English Version, Berlin, **2023**

DOI: 10.26272/opus4-58126

Gefördert durch:

aufgrund eines Beschlusses
des Deutschen Bundestages

Cite: Lando Seifert; Markus Philipp; Gino Ebell; Jörg Moersch; Thoralf Müller, A New Test Method for Evaluating Prestressing Steels' Susceptibility to Stress Corrosion Cracking, Final Report on WIPANO Research Project (FKZ: 03TNH019A/B/D), Berlin **2023**. https://doi.org/10.26272/opus4-58126

Abstract

For the safety of prestressed concrete structures, a test of prestressing steel products for hydrogen-induced stress corrosion cracking is mandatory. The current standardized test methods according to DIN EN ISO 15630-3 have proven deficiencies concerning the reproducibility of the results and thus make it difficult to assess the susceptibility clearly. The WIPANO research project funded by BMWK aimed to improve the test method regarding reproducibility and reliability of results. The project created constant and reproducible test conditions by modifying material, electrolyte, and process parameters. The new test method aims not to simulate the entire corrosion process in the structure up to failure, as is done with the previous test according to DIN EN ISO 15630-3, but only tests the material-specific sensitivity of the microstructure under high tensile load. The new method is also independent of the triggering corrosion conditions that were previously necessary for the formation of hydrogen and were time-determining for the test. This leads to a reduction of the test time with more controllable test conditions, so that the method is also suitable for factory production control.

As part of the project, a round robin test was initiated to confirm the applicability and reproducibility of the new test method. The round robin test also confirms a clear differentiation between susceptible and robust products.

The new test method was evaluated for its applicability to the prestressing steel product wire. A draft standard with a proposed conformity criterion for these products was submitted to the responsible ISO committee for approval. According to the current feedback from the committee, the draft standard will be included in the informative annex of the testing standard, which could pave the way for mirroring at European and national standardization levels.

Table of Contents

1 Presentation of Project

1.1 Current Technology

The durability of prestressing steel performance should guarantee that the formation and propagation of hydrogen-induced cracks can be excluded both during the construction phase and during the long-term operation of a structure when applying the technical code for prestressed concrete construction. For prestressed concrete, this means that only those prestressing steels or prestressing methods should be technically approved, which have a sufficiently low susceptibility to hydrogen-induced stress corrosion cracking. Therefore, examination and test methods are necessary, which set requirements for the prestressing steels' safety level (conformity criteria) and thus can separate good from bad conditions. A prestressing steel is considered suitable for construction if the conformity criteria are met.

Normative testing of prestressing steels is carried out by determining the so-called stress corrosion test. In this process, prestressing steels are provided with test cells filled with test solutions containing thiocyanate (test solution A or test solution B) and prestressed to a defined load level. The load level and temperature are kept constant during the test period. The time to fracture of prestressing steel under the given test conditions is defined by the failure of the sample due to brittle fracture. These brittle fractures are caused by hydrogen-induced stress corrosion cracking. In Germany, stress corrosion tests to assess the susceptibility of prestressing steels to stress corrosion cracking are required for the initial type testing of prestressing steel products as well as for internal factory production control and external continuous surveillance of the production.

For prestressing steels in the product forms strand, wire, and bar, the susceptibility to stress corrosion cracking must be tested in accordance with DIN EN ISO 15630-3 [1] and the DIBt guideline for approval and monitoring tests for prestressing steels [2]. The standards prEN 10138, parts 1-4 [3] provide information on the conformity criteria regarding the type and number of tests as well as the requirements for the minimum time to fracture. For ease of reference, the conformity criteria are listed in Table 1.

Table 1: Requirements for minimum time to fracture according to prEN 10138 part 1-4:2000 [3]. The number of tests is n=6.

	Product form	Nominal diameter d [mm]	Minimum time to fracture [h]	Median time to fracture [h]
Test solution A	strand	-	2	5
	wire	-	2	5
	bar	up to 15	20	50
		$15 < d < 25$	60	250
		$25 < d < 50$	100	400
Test solution B	strand, wire, bar	-	2000	-

The results of the tests must be representative and reliable. This is also important to avoid safety risks.

In prestressed concrete structures, hydrogen-induced stress corrosion cracking (HiSCC) can occur if a corrosion induced hydrogen evolution on the steel surface meets a prestressing steel, which is for the applied load susceptible for brittle failure. The resulting hydrogen-induced cracks will reduce the load-bearing cross section of the prestressing steel and may lead to brittle fracture of the steel. In the recent past, this type of damage to people and structures in Germany has been prevented or detected promptly using monitoring systems and periodic inspections. Not least, the manual for the inspection and assessment of older bridge structures built with quenched and tempered prestressing steel that is susceptible to stress corrosion cracking introduced so-called hazard classes for prestressed concrete structures. [4,5] A current example is the timely closure and dismantling of the prestressed concrete bridge at the Altstädter Bahnhof in Brandenburg an der Havel made of prestressed steel from Hennigsdorf, which was examined in detail by means of structural diagnostics. [6]

However, history has shown for a long time that brittle fracture of prestressing steels can lead to damage of prestressed concrete structures without any prior warning. In the technical report of the International Federation for Structural Concrete (fib), Task Group 9.5, damage cases related to HiSCC are divided into those caused by unsuitable materials and those caused by design and construction errors. [7] On the one hand, problems in the composition and application of concrete and grout were cited as construction material causes. On the other hand,

susceptible prestressing steel was the cause of damage. Several damage cases with cracks and wire breaks have been documented in bridge structures with prestressing wires of the so-called "old type" with the trade names Neptun, Sigma alt, and Hennigsdorfer. [8] Therefore, the stress corrosion test should be able to assess "old type" wires as highly susceptible.

1.2 Issue

As part of a project sponsored by the Deutsches Institut für Bautechnik (DiBt) and organized by the Bundesanstalt für Materialforschung und -prüfung (BAM) in 2012 and 2013,
it was found that the results of individual test institutes diverged significantly, which calls into question the reliability of the stress corrosion test [9]. A new graphical representation of the raw time to fracture data of the round robin test on prestressing steel bars St 950/1050 with a nominal diameter of 18 mm in test solution A, published in the report, is shown in Figure 1.

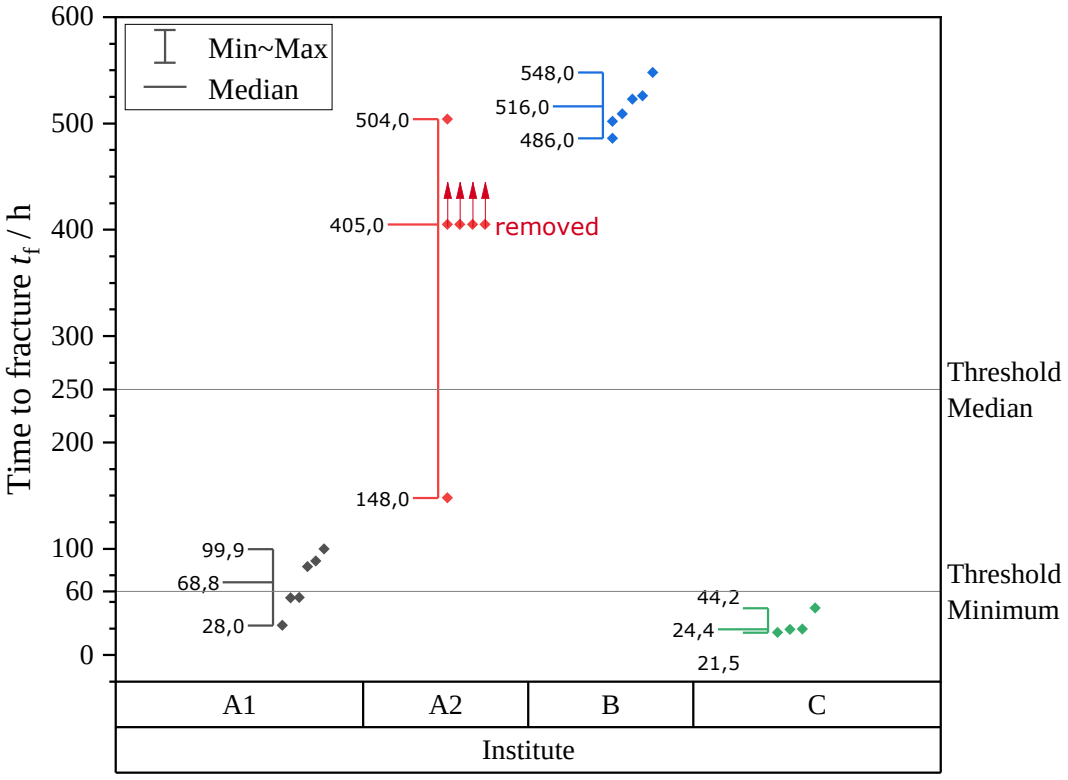

Figure 1: The results of the round robin test with prestressing steel bars St 950/1050, nominal diameter 18 mm, in test solution A, the raw data from [9] have been used.

The results of a round robin test initiated a few years ago by the Arbeitsgemeinschaft Deutscher Zertifizierungsstellen für Bewehrungen (ADZB) also showed considerable variation. These scattered results concerned both tests with test solution A and tests with test solution B. The results of this Round Robin test have not been published to date. A further complicating factor

is that when test solution B is used, an extended test duration of a maximum of 2000 hours must be achieved to demonstrate the insusceptibility of a prestressing steel product. For this reason, test solution A is used by default in external monitoring, while test solution B is mainly used in approval tests.

The problem for prestressing steel producers is that the time to fracture results from monitoring tests can only be reproduced to a limited extent and are, therefore, of limited significance. However, for the safety and reliability of prestressed concrete structures such as bridges, hall roofs, tanks, and wind turbines, but also for geotechnical applications, a low susceptibility of the steel used is an essential requirement.

Prestressing steel producers plan to develop and market new innovative products that differ significantly from previously approved products in alloy and mechanical properties. It is more than desirable for prestressing steel producers and users to have a reliable test method that ensures reproducible results under similar test conditions for the susceptibility of prestressing steels to stress corrosion cracking and that can sharply distinguish between susceptible and robust conditions. In the same way, the stringent development of materials and products requires a reproducible test method that can be evaluated quantitatively. At present, this test is not suitable for assessing the possible use of new prestressing steels to be developed, such as higher-strength steels, since no reference values for the time to fracture of such higher-strength steels are defined or known.

1.3 Test Method Requirements

As a result of the previous findings, requirements for a test method to evaluate stress corrosion cracking susceptibility were defined for the project:

- Reproducibility of results independent of the testing laboratory
  (verified by a round robin test)
- Reasonable test duration
- Differentiation/separation between susceptible and robust condition
- Clear limit value for passing the test (conformity criterion)
- Representation of realistic conditions in terms of load level

The objective of this research project is to develop a modified test method that meets the above requirements. The prestressing steel industry and its stakeholders should benefit from the project results. Among these are

- Prestressing steel producers
- Testing institutes
- Approval authorities
- Those involved in the design and production of prestressed concrete structures
- Contractors
- Building owners

Representatives of these bodies were included in the extended project monitoring committee to transfer the results to the stakeholders. In addition, a round robin test with a new test method was carried out in WP 5 involving both third-party testing institutes and prestressing steel producers with internal production control.

1.4 Scientific and Technical Approach

In standardized stress corrosion tests using Test Solution B, the prestressing steel is considered to be the corrosion system in the test electrolyte. The purpose of test solution B is to simulate unfavorable corrosive environmental conditions in the construction phase, such as the ingress of concrete settling water into the jacket pipes or the condensation of moisture on the prestressing steel. This is not to be considered a purposeful practice and can be justified in the following way:

- Although simulated corrosive conditions can be defined, the resulting corrosion systems are not reproducible in terms of charge conversion due to varying anode/cathode ratios and thus inevitably exhibit significant differences in time to fracture.
- Stress corrosion testing under free corrosion conditions is subject to many interferences limiting the reproducibility of test results.
- The simulation of realistic corrosive conditions during testing gives the false impression that a durability assessment for prestressed concrete structures can be derived from the test results. Prestressing steel shows the tendency that the susceptibility against HISCC increases with strength. Limits of strength for a durable application varies depending on manufacturing technology. The stress corrosion test should only be able to separate low-susceptible prestressing steels from high-susceptible prestressing steels. (Classification into susceptible and robust condition).

To optimize the method, reasonable solutions must be sought during the project. Stress corrosion cracking must be understood as a material property and tested accordingly.

The test standard DIN EN ISO 15630-3 [1] provides two test solutions. Test solution A consists of distilled or demineralized water and ammonium thiocyanate (NH_4SCN) at a concentration of 20% by weight. Test solution B consists of distilled or demineralized water, potassium sulfate (K_2SO_4), potassium thiocyanate (KSCN), and potassium chloride (KCl) in concentrations of 5.0 g l^{-1} SO_4^{2-}, 1.0 g l^{-1} SCN^- and 0.5 g l^{-1} Cl^-.

The test solutions induce local corrosion on the surface of the prestressing steel, potentially leading to hydrogen-induced stress corrosion cracking. The adsorbable amount of atomic

hydrogen at the surface of corroding steels increases with (i) decreasing pH, (ii) decreasing corrosion potential, (iii) in the presence of promoters (recombination poisons) such as thiocyanates, and (iv) decreasing oxygen content. [10] Changes in the corrosion-related quantities, such as the free corrosion potential during the experiment, could explain the large scatter of the experiments performed in the past [11].

In principle, it is known that during the tests with free corrosion in test solution A and test solution B, corrosion-related quantities such as the free corrosion potential and the polarization resistance change during the test in ways that were not investigated in detail.

Surface examinations have shown that the production-related drawing layer, scale layer, or rolled skin residues cover the delivery surface unevenly and incompletely, resulting in inhomogeneities and microgaps. The test method has not yet taken this into account. Adhesions of the drawing layer or other surface components are not specified and, therefore, not part of the product. Without affecting the geometry, these can be removed.

To answer the question of whether the surface influences the test result, the knowledge of the influence of the surface during the test must be extended.

1.5 The Project Consortium

The partners in the project "Safety of prestressing steels" were as follows.

- Bundesanstalt für Materialforschung und -prüfung (BAM)

The Bundesanstalt für Materialforschung und -prüfung (BAM) is a senior scientific and technical federal institute responsible to the Federal Ministry for Economic Affairs and Climate Action (BMWK). The scientific investigations and tests required for the project are carried out by Department 7.6, "Corrosion and Corrosion Protection," which has many years of experience in corrosion in the construction industry, particularly in the field of prestressing steels. [4, 11-18] The focus of the work at BAM is on electrochemical investigations on the different prestressing steels under different boundary conditions (test solution, temperature, surface, and potential). These investigations form the basis for developing a new, more reliable test method. In addition, BAM will accompany the construction or modification of the test equipment at the partners and the various testing institutes. BAM will also supervise and evaluate a round robin test.

- Stahlwerk Annahütte Max Aicher GmbH & Co KG

Stahlwerk Annahütte is preparing a comprehensive evaluation of past test results from internal and external monitoring. Detailed characterizations of the prestressing steel bars for the tests are performed. A new test bench for large dimensions has been commissioned. Internally, tests are performed using both old and new test methods. Stahlwerk Annahütte (SAH) is part of the Max Aicher GmbH & Co KG group of companies.

- Max Aicher GmbH & Co KG

Max Aicher GmbH & Co. KG provides Dr. Moersch, the current chairman of the European standardization committees for reinforcing and prestressing steel. As project manager of the subproject, he will organize the integration of the research results into the corresponding building material and testing standards.

The associated partner in the project was

- NEDRI Spanstaal BV/WDI Westfälische Drahtindustrie

The company NEDRI Spanstaal BV/WDI Westfälische Drahtindustrie is participating in the project as an associated partner. It will contribute its experience with the old test method gained during internal and external monitoring. As part of the verification process, it is also planned to test the new test method in the Venlo plant. NEDRI Spanstaal BV in Venlo, the Netherlands, is a subsidiary of Westfälische Drahtindustrie GmbH (WDI-Spannstahl) and is one of the most important prestressing wire producers in Europe with a recognized high level of competence in the field of prestressing steel production. NEDRI Spanstaal BV produces prestressing steel in both Hamm (Germany) and Venlo (The Netherlands) and employs a total of 150 people.

1.6 Literature

[1] DIN EN ISO 15630-3, Ausgabe Februar **2011**: Stähle für die Bewehrung und das Vorspannen von Beton – Prüfverfahren – Teil 3: Spannstähle.

[2] DIBt-Berlin, Richtlinie für Zulassungs- und Überwachungsprüfungen für Spannstähle, Fassung **2004**.

[3] prEN 10138-1, -2, -3, -4, Ausgabe **2000**: Spannstähle, Teil 1: Allgemeine Anforderungen, Teil 2: Draht, Teil 3: Litze, Teil 4: Stäbe.

[4] J. Lingemann, K. Zilch, R. Ehmann, G. Marzahn, D. Krüger, Die neue Handlungsanweisung zur Überprüfung und Beurteilung des Ankündigungsverhaltens von älteren Brückenbauwerken mit spannungsrisskorrosionsempfindlichem Stahl, *Bauingenieur* **2010**, 85, 297.

[5] G. Marzahn, V. Angelmaier, W. Beul, R. Ehmann, R. Frenzl, G. Garthof, T. Hampel, D. Krüger, J. Lingemann, R. Maurer, W.-M. Nitzsche, M. Raupach, U. Schölch, J. Steiner, T. Zichner, K. Zilch, Handlungsanweisung zur Überprüfung und Beurteilung von älteren Brückenbauwerken, die mit vergütetem, spannungsrisskorrosionsgefährdetem Spannstahl erstellt wurden (Handlungsanweisung Spannungsrisskorrosion), BMDV, Abteilung Straßenbau, **2011**, Ausgabe 6.

[6] O. Steinbock, T. Bösche, G. Ebell, F. Kaplan, G. Marzahn, Erfahrungen aus dem Rückbau der Brücke am Altstädter Bahnhof in der Stadt Brandenburg – Teil 1 Untersuchung und Erkenntnisse zum Ankündigungsverhalten bei großformatigen Spanngliedern mit spannungsrisskorrosionsgefährdetem Spannstahl. *Beton- und Stahlbetonbau* **2022**.

[7] Fédération Internationale du Béton (FIB), Task Group 9.5, U. Nürnberger, Technical Report on Influence of Material and Processing on Stress Corrosion Cracking of Prestressing Steel – Case Studies, **2003**.

[8] J. Lingemann, *Ph.D. Thesis*, TU München, Germany, **2010**.

[9] J. Mietz, J. Fischer, *Ringversuch zur Prüfung der Spannungsrisskorrosion an Spannstählen*, Bauforschungsbericht T 3306, Fraunhofer IRB Verlag, Stuttgart **2014.**

[10] U. Nürnberger, *Mater. Corros.* **1997**, *48*, 602.

[11] J. Mietz, K. Pasewald, B. Isecke, Untersuchungen zum wasserstoffinduzierten Sprödbruch vergüteter Spannstähle, Schlussbericht zum DIBt-Forschungsvorhaben IV 1-5-651/92, Berlin **1998**.

[12] J. Mietz, B. Isecke, *Mater. Corros.* **2002**, *53*, 373.

[13] B. Isecke, *Test Methods for Assessing the Susceptibility of Prestressing Steels to Hydrogen Induced SCC*, EFC Publications Number 37, Maney, London **2004.**

[14] U. Nürnberger, K. Menzel, J. Mietz, B. Isecke, Spannungsrisskorrosion vorgeschädigter Spannstähle im verpressten Zustand, Abschlussbericht des DIBt-Forschungsvorhabens IV 1-5-654/91, Stuttgart und Berlin **1993**.

[15] J. Mietz, U. Nürnberger, W. Beul, Untersuchungen an Verkehrsbauten aus Spannbeton zur Abschätzung des Gefährdungspotentials infolge Spannungsrisskorrosion der Spannstähle, Abschlussbericht zum BMV-Forschungsvorhaben FE 15.209 R91D, Berlin und Stuttgart **1994**.

[16] J. Mietz, B. Isecke, K. Pasewald, Zulässige Krümmungsradien von Spannstählen (Stäbe) bei erhöhter Vorspannung, Abschlußbericht zum DAfStb-Forschungsvorhaben V 341, Berlin, Februar **1995**.

[17] B. Isecke, K. Menzel, J. Mietz, U. Nürnberger, Gefährdung älterer Spannbetonbauwerke durch Spannungsrisskorrosion, *Beton- und Stahlbetonbau* **1995**, 90, 120.

[18] J. Mietz, J. Fischer, Verifizierung zerstörungsfreier Prüfverfahren zur Detektion von Spannstahlschäden an Spannbetonbetonbauteilen mit nachträglichem Verbund, *Beton- und Stahlbetonbau* **2005**, 100, 656.

[19] ASTM International, *Standard Practice for Evaluation of Hydrogen Uptake, Permeation, and Transport in Metals by an Electrochemical Technique*, Designation G148-97, Beuth Verlag, Berlin **2011**.

[20] M. A. V. Devanathan, J. Stachursky, *Proc. Roy. Soc. London A* **1962**, 270, 90.

[21] J. Moersch, *Mater. Corros.* **2003**, *54*, 419.

[22] J. Moersch, *Zur wasserstoffinduzierten Spannungsrisskorrosion von hochfesten Spannstählen*, DAfStb, Beuth, Berlin, **2005.**

1.7 Project Planning and Schedule

Planning:

A total of seven work packages have been defined for the activities within the overall project:

- Work package 0: Formation of a project monitoring committee, reporting
- Work package 1: Expanding the knowledge of damage processes
- Work package 2: Data evaluation and sample preparation
- Work package 3: Development of a new test method
- Work package 4: Commissioning of test benches and implementation of the new test method
- Work package 5: Round robin test
- Work package 6: Evaluation and drafting of a new test standard

The objectives of each work package are described in Chapter 2, Section 2.1, "Use of the grant and results achieved in detail." Work packages 0,1,3,4,5 and 6 were carried out by the Bundesanstalt für Materialforschung und -prüfung (BAM).

Schedule:

To achieve the milestone "New test method developed," the project consortium applied for a cost-neutral extension of 12 months after the 4th quarter of the first year. The request for a cost-neutral extension of 12 months was approved by the project sponsor. Table 2 shows the work and time schedule of the project. The milestone and overall objective of the project were achieved.

Table 2: Work and time schedule of the project (with milestone) from 01.10.2019 to 30.09.2022.

Work packages	**Partner**	**Quarters 1st year**				**Quarters 2nd year**				**Quarters Year 3**			
		1.	2.	3.	4.	1.	2.	3.	4.	1.	2.	3.	4.
AP 0	BAM												
	Annahütte												
	Max Aicher												
AP 1	BAM												
	Annahütte												
AP 2	Annahütte												
AP 3	BAM												
AP 4	BAM												
	Annahütte												
AP 5	BAM												
	Max Aicher												
AP 6	BAM												
	Annahütte												
	Max Aicher												

Milestone: New test method developed;
Cost-neutral extension by 12 months to achieve milestone through work in WP 3

2 In-depth Presentation

2.1 Work Package 0: Project Monitoring Committee

No.	Goal
2.1.1.	Formation of a project monitoring committee, reporting

The aim of Work Package 0 was the formation of a Project Monitoring Committee. In the first online meeting of the project monitoring committee on 12.11.2020, the Bundesanstalt für Materialforschung und -prüfung (BAM) moderated the meeting and presented the objectives and contents of the research project to the committee together with the joint partners. The following institutes, bodies, and prestressing steel producers were represented in the extended project monitoring committee:

- Stahlwerk Annahütte Max Aicher GmbH & Co. KG (SAH)
- Max Aicher GmbH & Co. KG (MAF)
- Bundesanstalt für Materialforschung und -prüfung (BAM)
- Deutsches Institut für Bautechnik (DiBt)
- NEDRI Spanstaal BV/WDI Westfälische Drahtindustrie
- Stahlinstitut Verein deutscher Eisenhüttenleute (VdEh)
- Technische Universität München (TUM)
- CEQMAS/OCAB/SG14 (European certification body)
- Kontrollradet

2.2 Work Package 1: Expansion of Knowledge about Damage Processes

No.	Goal
2.1.2.1	Creation of an Ishikawa diagram
2.1.2.2	Studies of various surface conditions: • Delivery Surface • Grinded • Turned • Polished • Small damage to the delivery surface • Blasted These studies aim to answer whether it is useful to test samples with a delivery surface at all.
2.1.2.3	Study of the electrochemical processes during stress corrosion tests on existing standard cells using current density-potential curves
2.1.2.4	Variation of electrolyte-related parameters • Type of test solution • Temperature (O_2 content)
2.1.2.5	Material characterization for chemical composition and metallography

2.2.1 Creation of an Ishikawa Diagram

To solve the technical problem of non-reproducible results in life testing, six influencing variables were identified in a cause-effect diagram (Ishikawa diagram), see Figure 2.

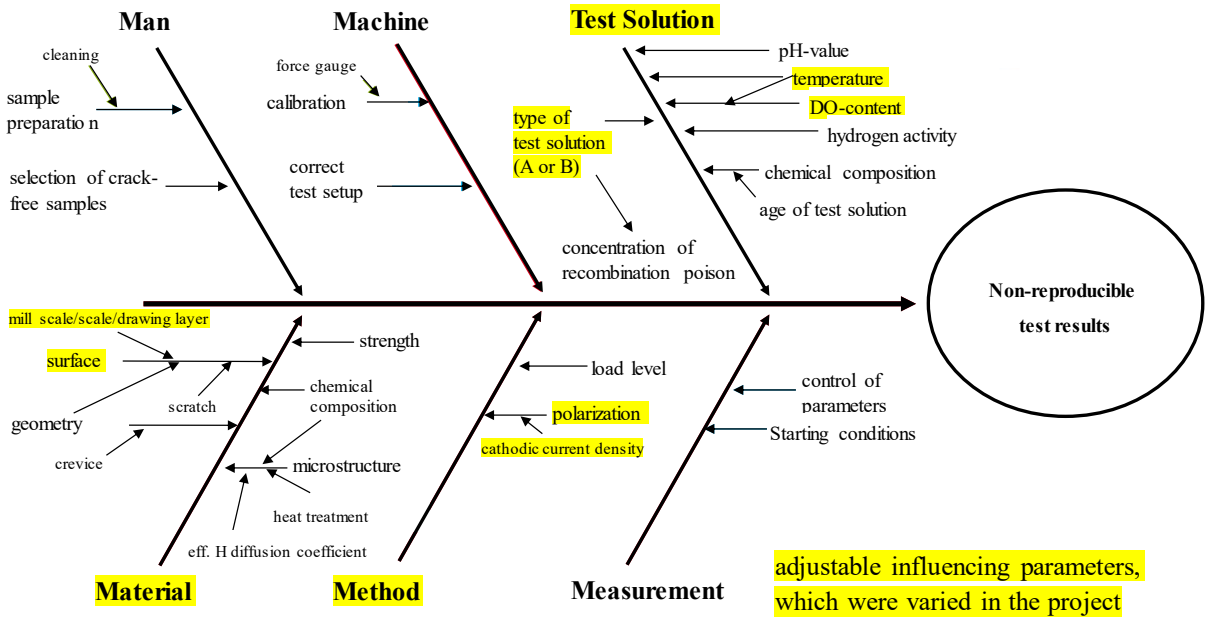

Figure 2: Ishikawa diagram to visualize the influencing parameters of non-reproducible test results.

The main parameters are Man, Machine, Test Solution, Material, Method, and Measurement. The main parameters test solution, material, and method are scientifically quantifiable and verifiable with their respective influencing parameters. They also include controllable influence parameters. The item machine includes both the correct test setup in terms of test cell dimensions and the use of calibrated force gauges. The importance of the material and test solution parameters for the test result has already been pointed out in an earlier publication. [12] In the case of the material, the controllable influence variables that are varied in the project are the surface condition, which is the only material influence that is not a defined product characteristic in the prestressing steel approval. The main influence on the test solution is the type of test solution; in the following sections, we limit ourselves to test solutions A and B. The temperature of the test solution depends on the temperature of the test solution. The temperature of the test solution is directly related to the oxygen content of the test solution. It is well known that oxygen solubility in open systems decreases with increasing temperature. To limit the number of tests for the intended personnel deployment (1 PM), 50°C was chosen for the

temperature, which is the current normative test temperature. On the other hand, a test temperature of 22°C was chosen as an alternative to minimize the subsequent testing effort. This would eliminate the need for solution temperature control equipment in most test laboratories during the stress corrosion test. Depending on the results, the test temperature could then be required in the standard design with a range of, for example, ±3 K accuracy so it would remain feasible for most testing laboratories. The current stress corrosion test uses free corrosion as the "electrochemical" method, which, as explained in Chapter 1, Section 1.4, maybe the reason for the lack of reproducibility. In the project, the prestressing steel is to be cathodically polarized. For this purpose, the cathodic current density will be varied in a two-electrode arrangement. The cathodic polarization protects the prestressing steel against corrosion and, at the same time, increases the formation of atomically adsorbed hydrogen on the surface, which can be absorbed into the microstructure of the prestressing steel (hydrogen charging). Cathodic polarization can bring the prestressing steel to a fracture-critical state earlier by increasing the hydrogen charging in the microstructure.

The load level is also specified under the Method parameter. A load level of 80% of the actual tensile strength is required in most countries worldwide. In principle, the time to fracture can be influenced by changing the load level since the tendency to initiate stress corrosion cracking is also changed. The possibility of changing the existing load level of 80% of the actual tensile strength was discussed in the project consortium. It was agreed not to depart from the existing load levels (usually 80% of tensile strength) and not to explicitly demand this in a draft standard. Instead, the test method with polarization should be the subject of optimization.

2.2.2 Investigations on Different Surface Conditions

Experimental:

Sections of smooth cold-drawn prestressing wire St 1470/1670 with a diameter of 7 mm (CDS-1670) were subjected to grinding, turning, polishing, small-area damage, and blasting to produce various surface conditions which differed from the condition of the delivery surface. During grinding, the samples were machined with SiC abrasive paper (P80 grit) on the grinding machine, reducing the diameter by a maximum of 10 µm. Turning reduces the radius by 250 µm. The surface was polished with polishing paste to a metallic finish on a soft cloth polishing wheel. A scratch was intentionally introduced into the scale layer to simulate damage for further comparison. A marking tool was used to create a scribe approximately 100 µm deep and 2000 µm wide along the circumference of the wire. Blasting was performed at 3.5 bar compressed air with 99.9% Al_2O_3 in an *MHG* blasting machine. After each type of processing, the steel surface was cleaned with acetone and a soft cloth.

A tactile roughness measurement was performed on the delivery surface and the modified surface conditions with a sufficiently periodic surface profile (grinded, turned, polished). Using a *Jenoptic Hommel Etamic WD10* roughness tester, an overview profile was created using the profile method, from which the average roughness value R_a and the average roughness depth R_z in the longitudinal direction were determined. The conical diamond tip had a radius of 2 µm with an angle of 90°. The measuring distance was 4.8 mm.

Results & Discussion:

Metallographically, the as-delivered surface is covered with a dark or grayish drawing layer. See Figure 3. However, there are drawing layer artifacts (scratches) on the delivery surface, which may result from both the cold drawing process and transportation. One such layer artifact, where the drawing layer is missing in a local area, is shown in the longitudinal section of the as-delivered condition (top image in Figure 3). In this localized area, the bare steel can directly contact the test solution.

In producing these cold-drawn prestressing wires, hot-rolled steel wire as the raw material is first pickled to remove the scale layer. The scale layer is formed by the interaction of the lubricant and the high friction of the cold drawing process, during which the wires come into contact with, for example, $Zn_3(PO_4)_2$, borax, and soap. This project did not study the chemical composition of these drawing layers in detail. However, in

WP 1 will investigate the difference in electrochemical corrosion characteristics when these drawing layers are partially or wholly removed. For comparison, metallographic images of different surface conditions were taken in addition to the delivery surface, see Figure 3. As shown in the images, the drawing layer could be removed to a large extent, and different roughnesses could be generated. Roughness parameters were determined on surfaces with sufficiently periodic profiles, see Table 3.

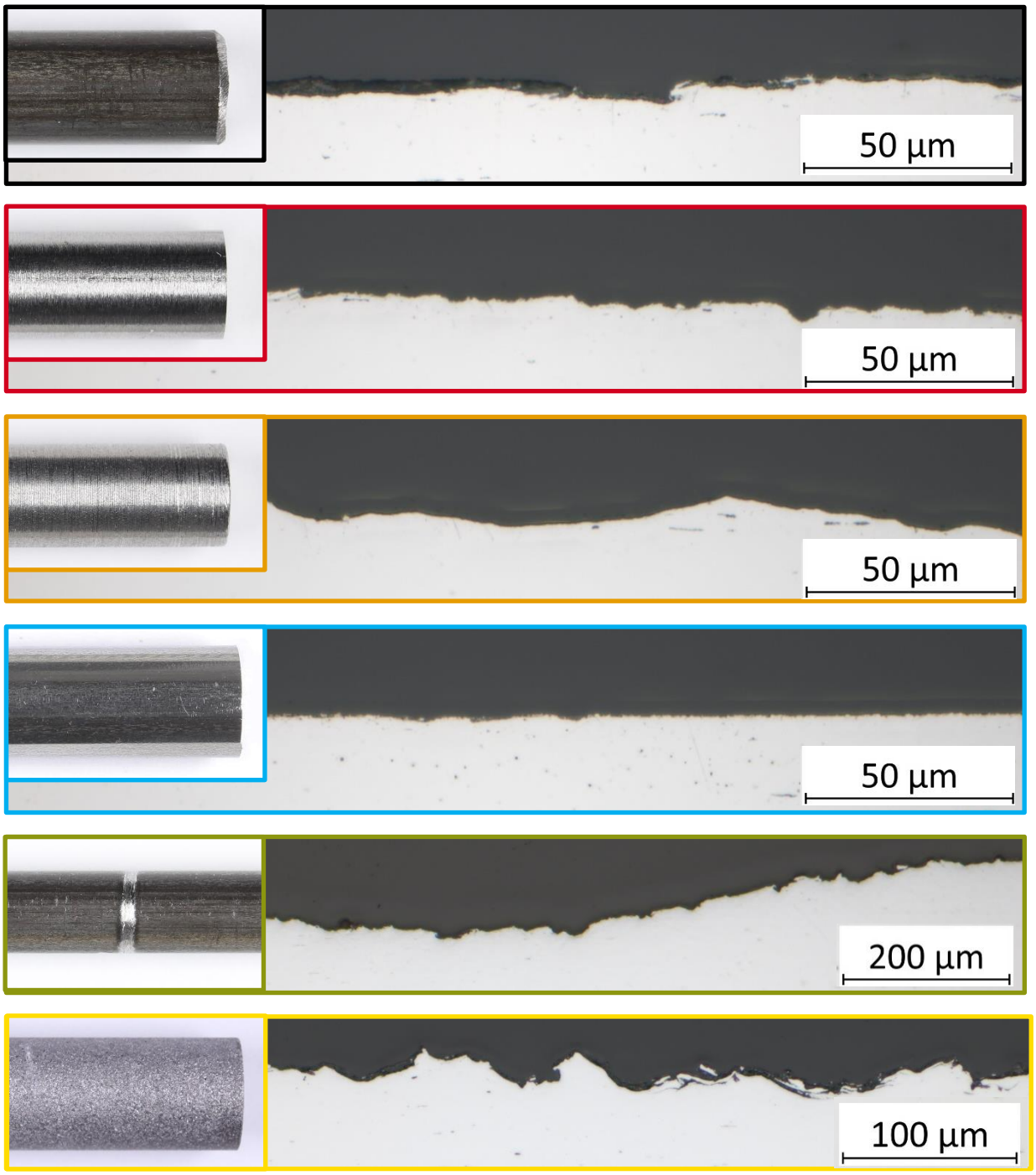

Figure 3: Macroscopic images of the surface (small inset, left) and metallographic images in the longitudinal direction of different surface conditions of the cold-drawn smooth prestressing steel wire, d = 7 mm: with (from top to bottom) delivery surface (black), SiC (P80) grinded (red), turned (dark yellow), polished (blue), scratched (green) and Al_2O_3 blasted (yellow).

Table 3: Roughness characteristics of various surface conditions of the CDS-1670. The center roughness value R_a and the roughness depth R_z are listed for those surface conditions that exhibited a periodic surface profile.

Surface condition	R_a [µm]	R_z [µm]
delivery surface	(0.33±0.05)	(3.14±0.34)
SiC (P80) grinded	(0.61±0.06)	(4.96±0.31)
turned	(2.80±0.16)	(13.70±0.72)
polished	(0.13±0.03)	(1.71±0.48)
scratched	not applied (aperiodic)	
Al_2O_3 blasted	not applied (aperiodic)	

The surface roughness of the SiC (P80) grinded condition shows significantly higher roughness values for both center roughness R_a and roughness depth R_z in the longitudinal direction compared to the as-delivered condition (factor 1.8 for R_a and factor 1.6 for R_z). Compared to the delivery condition, the turned surface condition shows the highest roughness in this study, factor 8.5 in R_a and factor 4.4 in Rz. The polished surface condition shows a significant reduction in roughness, about 60% in R_a and 46% in R_z compared to the delivery condition. The polishing removes most of the drawing layer, creating more homogeneous surfaces without significant artifacts. The edge microstructure of the prestressing steel is unchanged after polishing. More homogeneous surfaces without artifacts such as scratches and low roughness values can help homogenize the distribution of anodically and cathodically active surface areas, reducing scatter in stress corrosion tests. The surface condition with targeted damage to the delivery surface and the blasted condition could not be evaluated due to the lack of longitudinal periodicity of the surface profile. However, from the metallographic images, it can be concluded that the blasted surface has the highest roughness. In general, it should be noted that grinded, turned, and blasted surfaces reduce the cross-section of the wire. This reduces the edge microstructure of the prestressing steel. Changing the edge microstructure is highly detrimental to product testing for hydrogen stress corrosion cracking susceptibility since the edge microstructure is a material or product property. For this reason, comparing the delivery and polished surfaces in an electrochemical study or stress corrosion tests could be particularly interesting since the edge microstructure is unchanged.

2.2.3 Study of Electrochemical Processes

Experimental:

A defined steel surface's free corrosion potential E_{corr} as measured with a *Gamry Interface 1000E* potentiostat against a saturated silver/silver chloride electrode (Ag|AgCl|$KCl_{sat.}$). The samples are stored in a double-walled measuring cell with 500 ml of stagnant test solution, which is tempered at 50°C±1 K via the glass wall using a *Julabo F25-HE* thermostat and a PT100 temperature sensor. The polarization resistance R_P was determined by linear polarization resistance (LPR) measurements after measuring the free corrosion potential in test solutions A and B. For this purpose, a three-electrode arrangement consisting of the steel surface as the working electrode, Ag|AgCl|$KCl_{sat.}$ as the reference electrode, and a grid of titanium mixed oxide as counter electrode was used. A *Gamry Interface 1000E* potentiostat was also used for this purpose. The differential quotient from the change of the electrode potential from -5 mV to +5 mV vs. E_{corr} and the corresponding linear change in current was determined; the potential advance rate was 1 mV s^{-1}. On all samples, the voltage drop across the resistor was also determined R_Ω (voltage drop across R_Ω is referred to as IR drop) of the test solution between the steel surface and the reference electrode was determined. All electrochemical measurements under polarization were IR compensated. Starting from E_{corr}, the R_Ω was determined using a galvanostatic pulse method (GPM). The maximum potential difference during a 0.3 s pulse of 10 mA cm^{-2} is divided by the current value for the calculation of R_Ω. The sampling rate of the potential during GPM was 5 kHz.

Results & Discussion:

The free corrosion potentials E_{corr} of different surface conditions were determined in test solution B at 50°C±1 K, the values after 30 min of free corrosion in test solution B are shown in Figure 4.

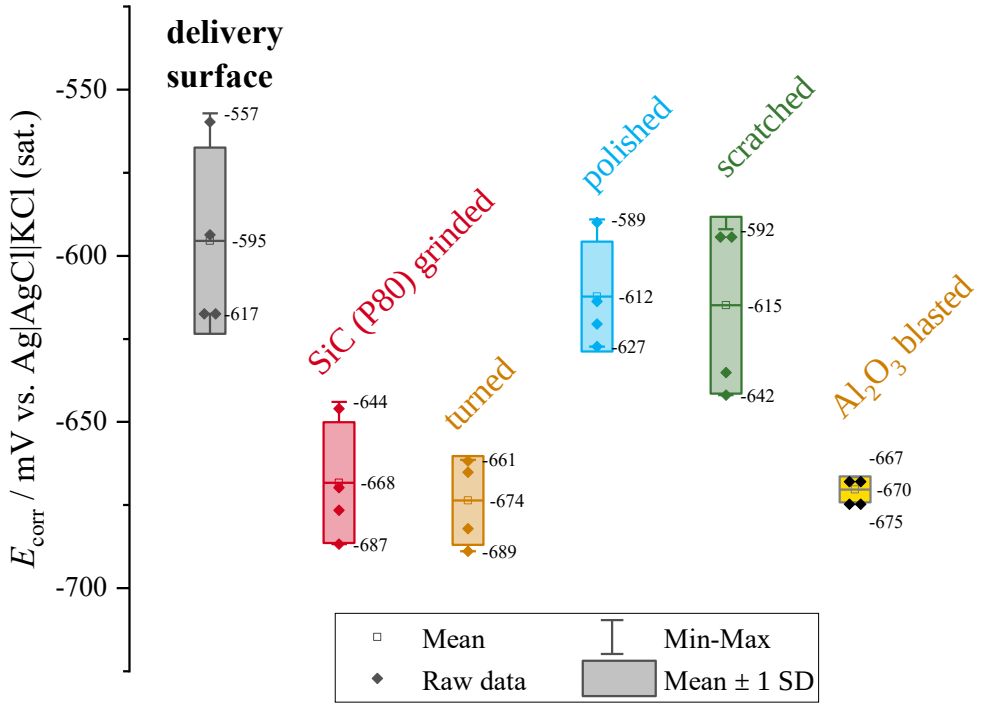

Figure 4: Free corrosion potential E_{corr} of CDS-1670 at different surface conditions after 30 min of free corrosion in test solution B at 50°C±1 K.

Surfaces in the delivery condition in test solution B at 50°C±1 K have a mean value of E_{corr} = -595 $mV_{Ag/AgCl}$. Samples with grinded, turned, and blasted surfaces have a more negative E_{corr} than samples with delivery surfaces. This probably indicates an increase in the anodic surface fractions. The E_{corr} of samples with scratches is not lower compared to samples in delivery condition. Samples with polished surfaces do not show a significant decrease in the E_{corr} compared to samples in the delivery condition. E_{corr} is not sufficient to evaluate corrosion activity as a function of surface condition. For this reason, a second electrochemical process parameter, the polarization resistance R_P of the different surface conditions, was determined and is shown in Figure 5.

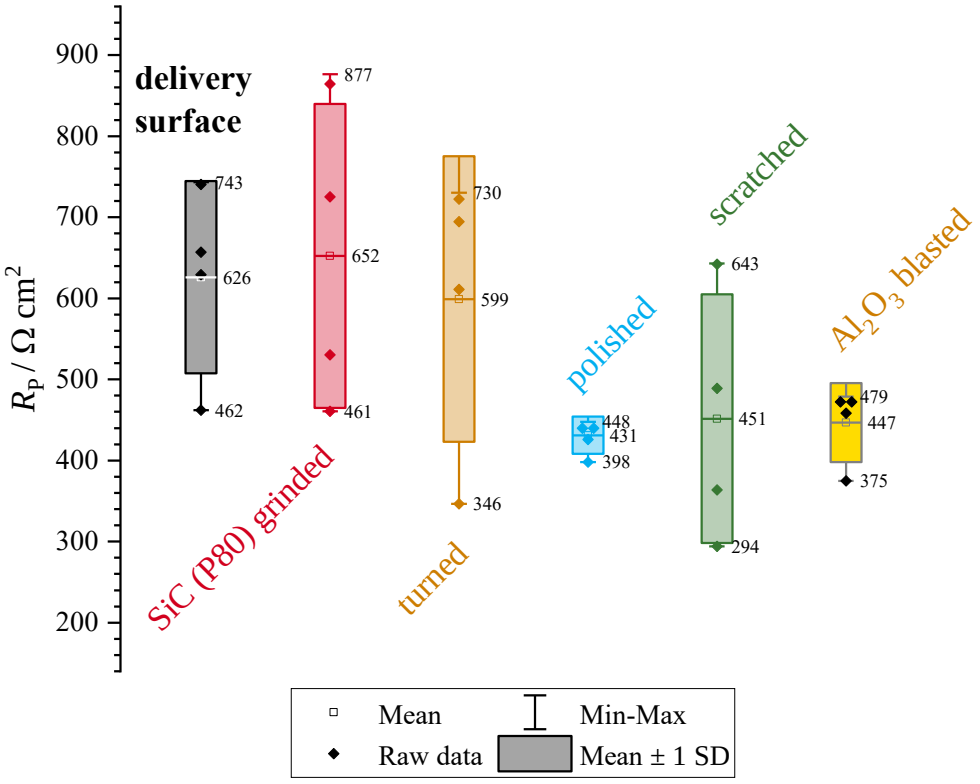

Figure 5: Polarization resistance R_P of the CDS-1670 at different surface conditions after 30 min of free corrosion in test solution B at 50°C±1 K. IR drop corrected.

The value and scatter of R_P after 30 min of free corrosion in test solution B is used to compare the surface conditions. The results are IR drop corrected. The determined polarization resistances for all surface states indicate an active corroding system. However, there are significant differences between the surface states regarding scattering. The R_P values of the grinded and turned surfaces show no significant difference compared to the delivery condition but a higher scatter. The reason for this could be an increase in the effective surface area due to the higher roughness or the presence of a modified edge microstructure.

The R_P values of the scratched samples tend to be lower than those in delivery conditions, but the difference is not significant. The damaged surface area at the scratch acts as an anode, while the remaining area with the delivery surface can act as a cathode. The formation of such a macro element is problematic because it can lead to localized and increased hydrogen charging in the area of the scratch. Depending on the distribution of the artifacts on the surface, the formation

of corrosion elements can lead to highly scattered results in time to fracture, an indication of this is the greater scatter of the R_P values.

The polished surface has a significantly lower R_P value with less scatter in comparison to the delivery surfaces. Low scattered R_P values are considered advantageous to reduce scattering in stress corrosion tests. Blasted surfaces also tend to have low R_P values and low scatter compared to the delivery surface, but the clearly visible increase in roughness and change in edge microstructure argue against the use of blasted surfaces.

As a result of the variation in the surface conditions, the following sections will continue with the delivery surface and the polished surface.

2.2.4 Variation Electrolyte-related Parameters

Experimental:

To evaluate the corrosion behavior of steels with delivery surfaces and polished surfaces in test solutions A and B over a practical test period, the free corrosion potential E_{corr} and the polarization resistance R_P (IR drop corrected) were determined in the interval at the time points of 0.5 h, 1 h, 4 h, 7 h, 10 h, 40 h, and 70 h of free corrosion. The dissolved oxygen (DO) concentration in the test solutions was measured using a *Hanna Instruments HI 5421* laboratory meter with a *HI76483* DO probe with a built-in temperature sensor.

The permeation was measured with steel membranes made of unalloyed steel type 1.0978 and a thickness of d of 0.05 mm. The chemical composition is shown in Table 8.

The steel membrane separates the charging cell from the oxidation cell, both cells have the same surface area A_{geo} in contact with the test solution, which is 1.13 cm^2 each. The ratio of electrolyte volume to A_{geo} on both sides of the membrane is 194.5 ml cm^{-2}.

In the oxidation cell, a three-electrode arrangement was used, with the steel membrane as the working electrode, a silver/silver chloride reference electrode (Ag|AgCl|KCl(sat.)), and a grid of titanium mixed oxide as the counter electrode. The surface area of the counter electrode is at least ten times that of the working electrode. According to the recommendations of ASTM standard G148 [19], an electrode potential of +541 mV against the standard hydrogen electrode (SHE) was potentiostatically adjusted in a 0.1 mol l^{-1} sodium hydroxide (NaOH) solution.

During the experiment, the temperature was kept constant by a temperature-controlled and electrically screened housing surrounding the permeation cell. The test solution and 0.1 mol l^{-1} NaOH were preheated at 50°C ± 1 K for at least 24 h to reduce dissolved oxygen. Before being poured into the cell, the electrolytes were tempered to 25°C±1 K. When the current density in the oxidation cell fell $i_{BG} = 0.1$ µA cm^{-2} (background current density), the charging cell was filled with oxygen-depleted solution (A or B). According to the literature, the effective hydrogen diffusion coefficient of the steel membrane D_H was determined in permeation measurements on steel membranes of different thicknesses. [19, 20]

Results & Discussion:

In the search for time-constant electrochemical corrosion characteristics that may result in constant hydrogen charging conditions, the following test parameters are varied in this section:

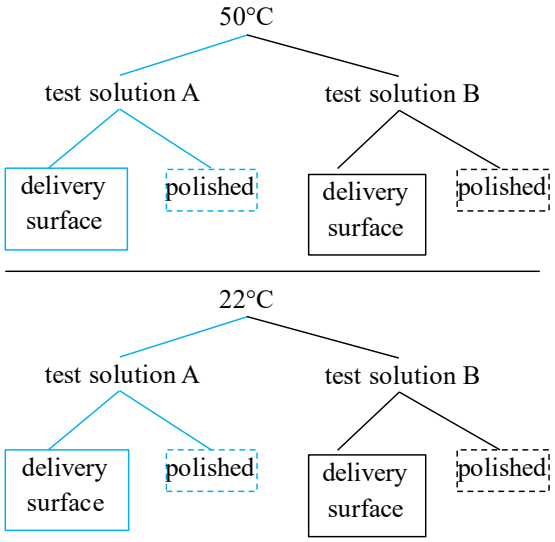

Measurement of free corrosion potential and polarization resistance:

The free corrosion potentials E_{corr} at 50°C over a test-relevant period of 70 h of free corrosion are shown in Figure 6.

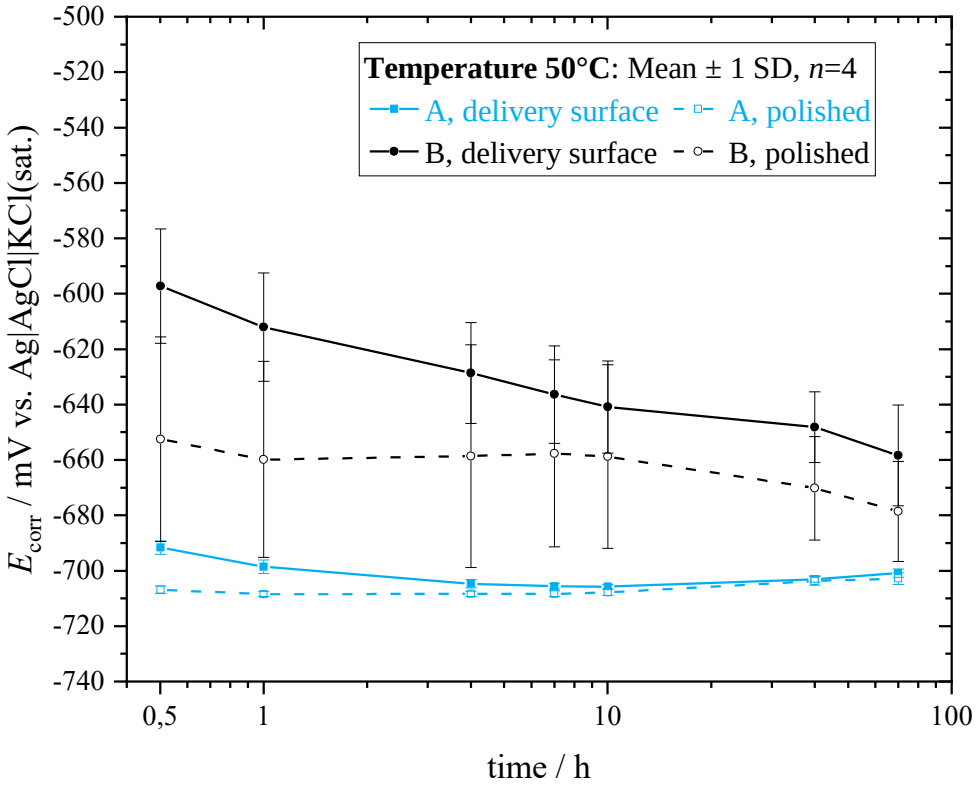

Figure 6: Free corrosion potentials E_{corr} at 50°C over a test-relevant period of 0.5 h to 70 h free corrosion.

At 50°C, after 0.5 h, the E_{corr} of the samples with delivery surface in test solution A is, on average -690 $mV_{Ag/AgCl}$. Over a period of 70 h of free corrosion, it is almost constant. At the time of 70 h it is -700 $mV_{Ag/AgCl}$. The E_{corr} of the samples with a polished surface in test solution A is also constant on average between -710 $mV_{Ag/AgCl}$ and -700 $mV_{Ag/AgCl}$. Figure 6 shows the mean values of E_{corr} with the corresponding standard deviation as scatter of n=4 measurements. The free corrosion potential of the samples with the delivery surface in test solution B drops from -600 $mV_{Ag/AgCl}$ to -660 $mV_{Ag/AgCl}$ over the period investigated. Due to the scattering range, no statement can be made about the course of the E_{corr} for the samples with a polished surface. Statistically, no significant change can be detected. For the polished surface in test solution B the free corrosion potential ranges from -620 $mV_{Ag/AgCl}$ to -690 $mV_{Ag/AgCl}$. Note that lower free corrosion potentials were measured in test solution A than in test solution B for both the delivered and polished surfaces. The pH value of test solution A at 50°C is (5.1 ± 0.3), and that of test solution B is (7.2 ± 0.4), see Table 4.

Table 4: Chemical composition of test solution A and test solution B according to [1]. In addition, the specific conductivities (spec. conductivity) and the pH values of the test solutions at 50°C±1 K are listed.

	Test solution A	Test solution B
Chemical composition	20 m.% NH_4SCN	aqueous solution of K_2SO_4, KSCN, KCl (5.0 g/l SO_4^{2-}; 1.0 g/l SCN^-; 0.5 g/l Cl^-)
spec. conductivity / mS cm^{-1}	(252.2±23.1)	(14.8±0.5)
pH value	(5.1±0.3)	(7.2±0.4)

By comparing potential with pH, it should be assumed that thermodynamically, test solution A should have a higher potential than test solution B. Using a modified Nernst equation, the tendency of the potential level can be estimated as a function of that of the pH value, see Equation 1, where: $\mathrm{pH} = -log[\mathrm{H}^+]$, E_0=standard electrode potential, R=gas constant, z =charge number and F =Faraday constant.

$$E = E_0 - \frac{2{,}3\ R\ T}{zF}\mathrm{pH} \quad (1)$$

Since this is not the case, it indicates that either the anodic or cathodic partial reaction is inhibited. The anodic partial reaction occurs according to Equation 2.

$$\mathrm{Fe} \rightarrow \mathrm{Fe}^{2+} + 2\mathrm{e}^- \quad (2)$$

The cathodic partial reaction for forming adsorbed hydrogen $H_{ad.}$ takes place according to Equation 3.

$$\mathrm{H}^+ + \mathrm{e}^- \rightarrow \mathrm{H}_{ad.} \quad (3)$$

In a further sub-step, adsorbed hydrogen can recombine to molecular hydrogen according to Equations 4 and Equation 5, the so-called hydrogen evolution (HE).

$$\mathrm{H}_{ad.} + \mathrm{H}_{ad.} \rightarrow \mathrm{H}_2 \quad (4)$$

$$\mathrm{H}_{ad.} + \mathrm{H}_3\mathrm{O}^+ + \mathrm{e}^- \rightarrow \mathrm{H}_2 + \mathrm{H}_2\mathrm{O} \quad (5)$$

Equation 4 and Equation 5 are inhibited by the presence of thiocyanate (SCN^-) as a so-called recombination poison. Therefore, the cathodic partial reaction proceeds predominantly according to Equation 3. The lower pH in test solution A results in a higher H^+ concentration. Test solution B has a higher pH and a lower H^+ concentration. The reversed potential levels between A and B can have several causes:

1. The anodic partial reaction, according to Equation 2, may be more uninhibited in test solution A than in test solution B, so the electrons released at the metal surface are not consumed to the same extent according to Equation 3; consequently, the potential decreases.

2. The anodic partial reaction can be inhibited in test solution B by forming locally limited anode areas (in the presence of chlorides). This means that, relative to the total area in solution, fewer electrons can be released to react in the cathodic partial reaction, according to Equation 3.
3. On the test surfaces in test solution B, dissolved oxygen could be reduced in addition to hydrogen evolution (HE). For thermodynamic reasons, oxygen reduction occurs at higher potentials than HE.
4. The formation of a coating layer in test solution B could increase the potential because there are more positive charge carriers at the coating layer/test solution phase boundary than at surfaces without a coating layer. In the case of surface layer formation, potential levels can be reached that cannot be described with thermodynamic equations, such as the Nernst equation. The potential here depends on the kinetics of the interfacial reactions - potential drop across the compact and diffuse Helmholtz layer.

The more extensive scattering range of the E_{corr} of the surfaces in test solution B compared to test solution A indicates both locally limited anodic subareas and the formation of a coating layer.

More detailed information about the corrosion activity of the surfaces in the test solutions is provided by the time course of the polarization resistance R_{P}, see Figure 7.

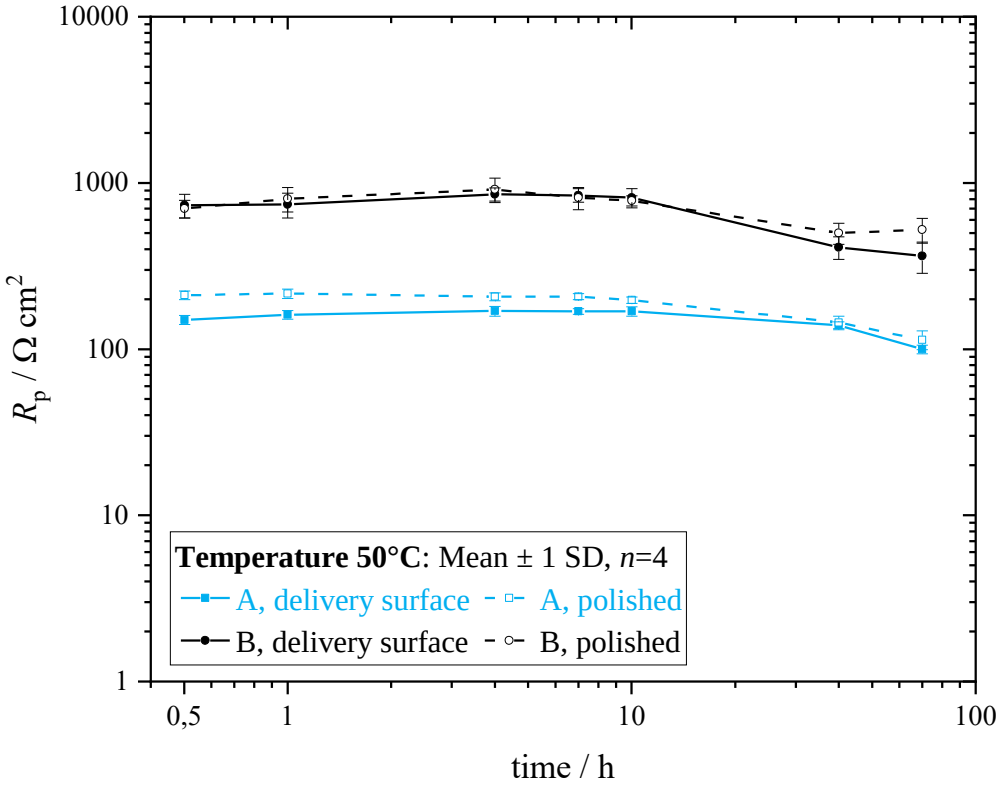

Figure 7: Polarization resistances R_P at 50°C over a test-relevant period of 0.5 h to 70 h of free corrosion (IR-compensated).

At 50°C the R_P values are lower in test solution A than in test solution B. The scatter of R_P is smaller in test solution A than in test solution B. With test solution A, the R_P values of the samples with delivery surface are lower than those of the samples with the polished surface. With test solution B, due to the larger scattering width, no significant difference can be seen between the surface conditions in the period up to 10 h between the surface conditions; in the period from 10 h to 70 h, there is R_P (delivery surface) < R_P (polished). In all variants, the R_P values are almost constant in the period from 0.5 h to 10 h. In the period from 10 h to 70 h, the R_P in both test solutions. In test solution A, from an average of about 200 Ω cm^2 to about 120 Ω cm^2 on samples with polished surface and from about 150 Ω cm^2 to about 100 Ω cm^2 on samples with delivery surface. In test solution B, from an average of about 800 Ω cm^2 to about 500 Ω cm^2 on polished surface condition, down to about 400 Ω cm^2 on delivery surface samples.

The results for the corresponding time course of E_{corr} respectively R_P at a reduced temperature of 22°C are shown in Figure 8 and Figure 9, respectively.

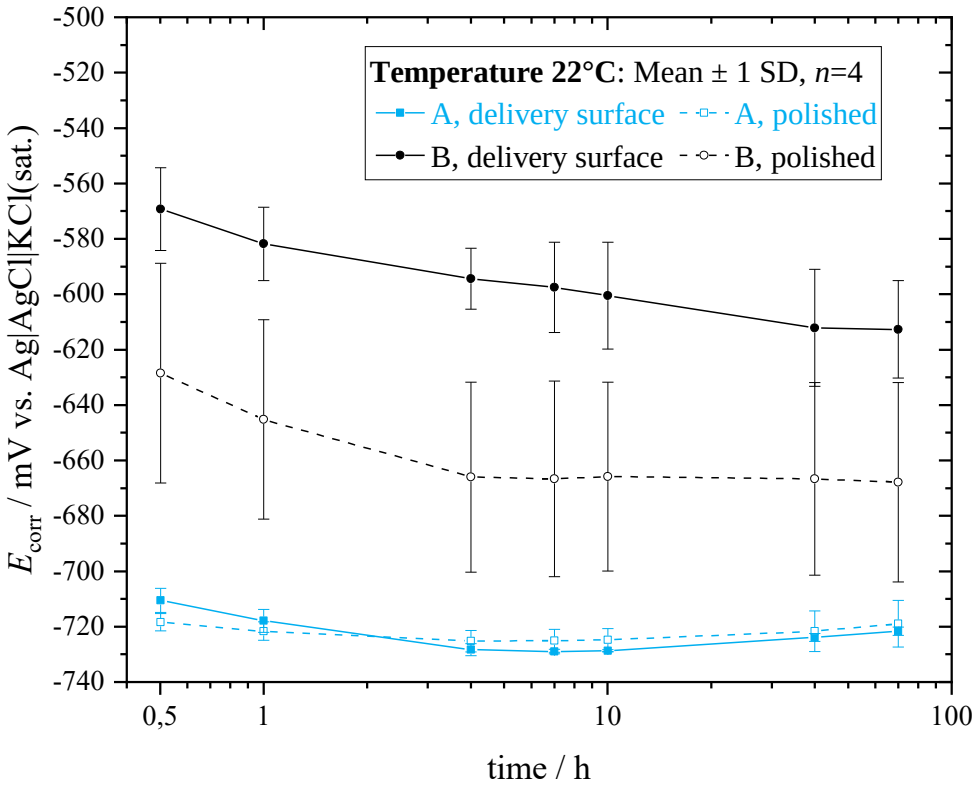

Figure 8: Free corrosion potentials E_{corr} at 22°C over a test-relevant period of 0.5 h to 70 h of free corrosion.

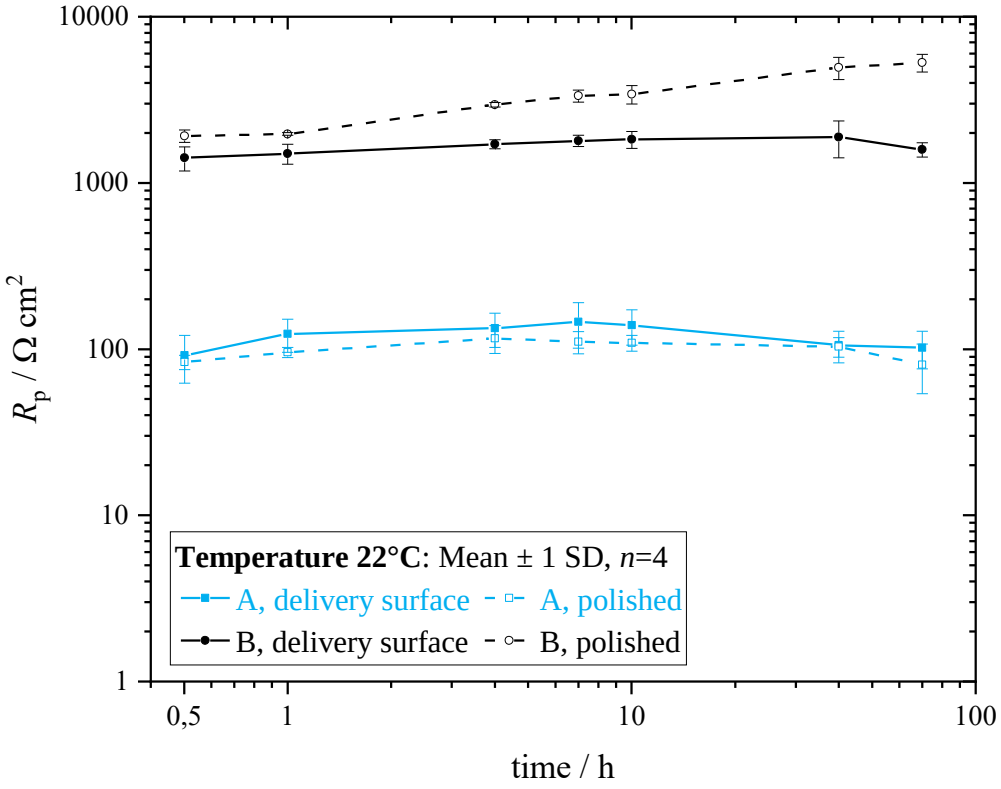

Figure 9: Polarization resistances R_P at 22°C over a test-relevant period of 0.5 h to 70 h of free corrosion (IR-compensated).

At 22°C, the following differences from the experiments at 50°C can be seen:

- At 22°C, E_{corr} and R_P in test solution A is lower than at 50°C
- At 22°C, E_{corr} and R_P of delivery condition samples in test solution B are higher than at 50°C.
- At 22°C, E_{corr} of samples with polished surface in test solution B are not significantly different results at 50°C
- At 22°C, R_P of samples with polished surfaces in test solution B is significantly increased compared to 50°C and increases over time

For the interpretation of the results, the samples in test solution A are significantly more active in terms of corrosion than those in test solution B, as indicated by the significantly lower R_P values. Consequently, test solution B is more inhibited regarding the corrosion processes. The

decisive factor for the corrosion inhibition of test solution B may be the oxygen reduction (OR) as a competing cathodic partial reaction according to Equation 6.

$$\frac{1}{2}O_2 + H_2O + 2e^- \rightarrow 2\ OH^- \quad (6)$$

On the other hand, a coating layer formation can anodically inhibit the corrosion system in that the charge separation, according to Equation 2, is inhibited by the presence of a positively charged coating layer.

Before testing, the temperature was maintained at 50°C for 24 hours to establish constant dissolved oxygen (DO) concentrations. In contrast to the normative test routine, where the DO value decreases with time, the preheating of the test solutions results in an equilibrium state of the DO value at the beginning of the stress corrosion test. The DO values of the test solutions are shown in Table 5.

Table 5: Dissolved oxygen (DO) concentration before starting the electrochemical experiments. A pre-tempering at 50°C for 24 h was performed in each case. After that, the experimental temperature was set. Data for a normal pressure of 100.3 kPa.

Time of DO measurement	Test solution A	Test solution B
after 24 h pre-tempering (50°C) + 30 min at 22°C	3 ppm	3 ppm
after 24 h pre-tempering (50°C) + 30 min at 50°C	3 ppm	3 ppm

Therefore, a low-oxygen test solution containing approximately 3 ppm dissolved oxygen was present for each experiment.

Thermodynamically, the modified Nernst equation (Equation 1) can be used to estimate the tendency to HE and OR based on the potential level as a function of temperature and pH. The linear dependence of the potential on pH according to Equation 1 for the temperatures 22°C and 50°C is shown in Figure 10.

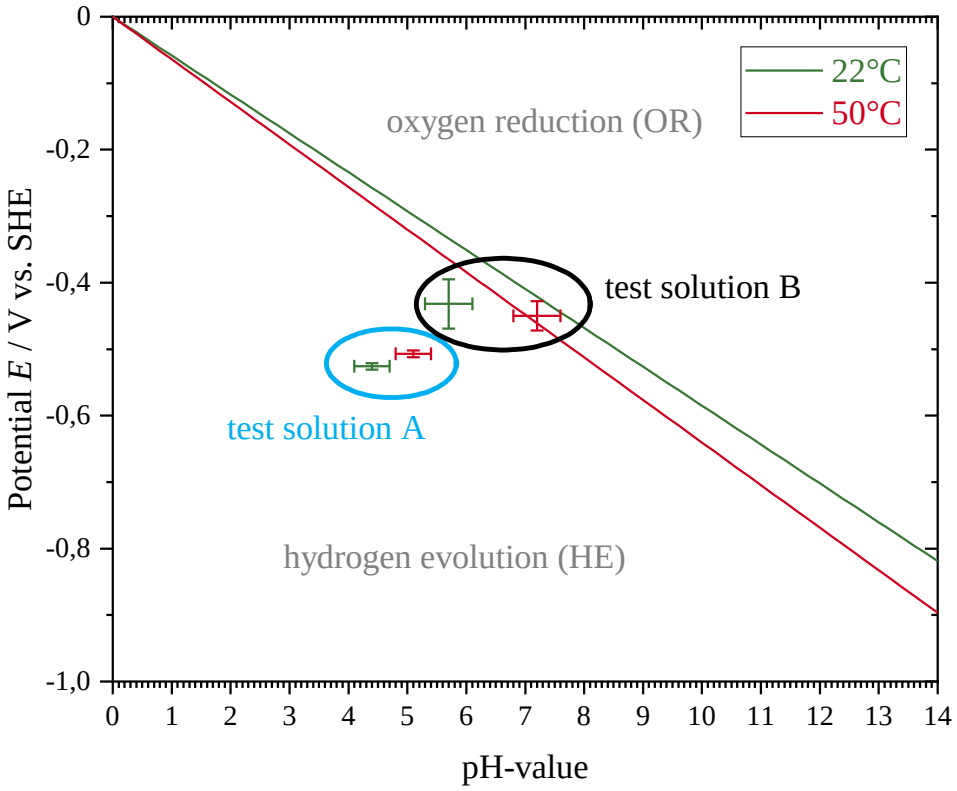

Figure 10: Temperature-dependent potential vs. pH plot for hydrogen evolution (HE) and oxygen reduction (OR).

The drawings of the temperature-dependent potential levels for test solutions A and B show that in test solution A, thermodynamically, hydrogen evolution (HE) tends to be the cathodic partial reaction. In contrast, the surfaces in test solution B have a less clear tendency toward HE. During the measurement, the measured potentials with test solution B at 50°C intersect the straight lines of the Nernst equation for HE. OR is likely to occur at 50°C despite the low oxygen conditions and may change the corrosion characteristics as a function of DO concentration. A change in corrosion characteristics during the test is extremely detrimental to a test method requiring constant hydrogen charging.

Furthermore, the significantly increased polarization resistances with test solution B compared to test solution A and the reversed potential level indicate that test solution B must be a cover layer formation, which interferes with the formation of uniform test conditions. From the sum of the considerations regarding E_{corr} and R_P , test solution B is unsuitable as an electrolyte for

stress corrosion testing. The decision between the two test solutions should be made in favor of test solution A.

The lower free corrosion potentials and polarization resistances of test solution A at 22°C compared to those at 50°C confirm that temperature control can be suspended during the test period to simplify the test method.

However, establishing comparable electrolyte conditions concerning DO concentration by pre-tempering for 24 h followed by cooling to about 22°C±3 K can be beneficial for reproducibility in stress corrosion tests.

Figure 9 shows more constant polarization resistances with less scatter from the polished surface samples in test solution A compared to the delivery surface samples.

An optimized test method should require only polished surfaces in contact with test solution A at 22°C regarding material and test solution properties.

Permeation measurements:

The stronger tendency towards HE in test solution A leads to a higher hydrogen charging intensity, which permeation measurements could determine. In addition, the time aspect of hydrogen permeation could be discussed.

After filling the charging cell, hydrogen adsorption occurs on the steel membrane due to corrosion, according to Equation 3. Adsorbed hydrogen can be taken up (absorbed) into the material in the next step. With a time delay, the total current increases due to oxidation of the permeable hydrogen on the oxidation side. The permeation current density i_{P} is the difference between the total current density i_{total} and the background current density i_{BG}. As an example, Figure 11 shows both the course of the permeation current density i_{P} on the oxidation side as well as the free corrosion potential E_{corr} in the charging cell for a free corrosion hydrogen charge with test solution A at 22°C±1 K. Figure 11 shows that the permeation current - and thus, integrated over time, the hydrogen charge - moves inversely to the time course of the corrosion potential with a delay.

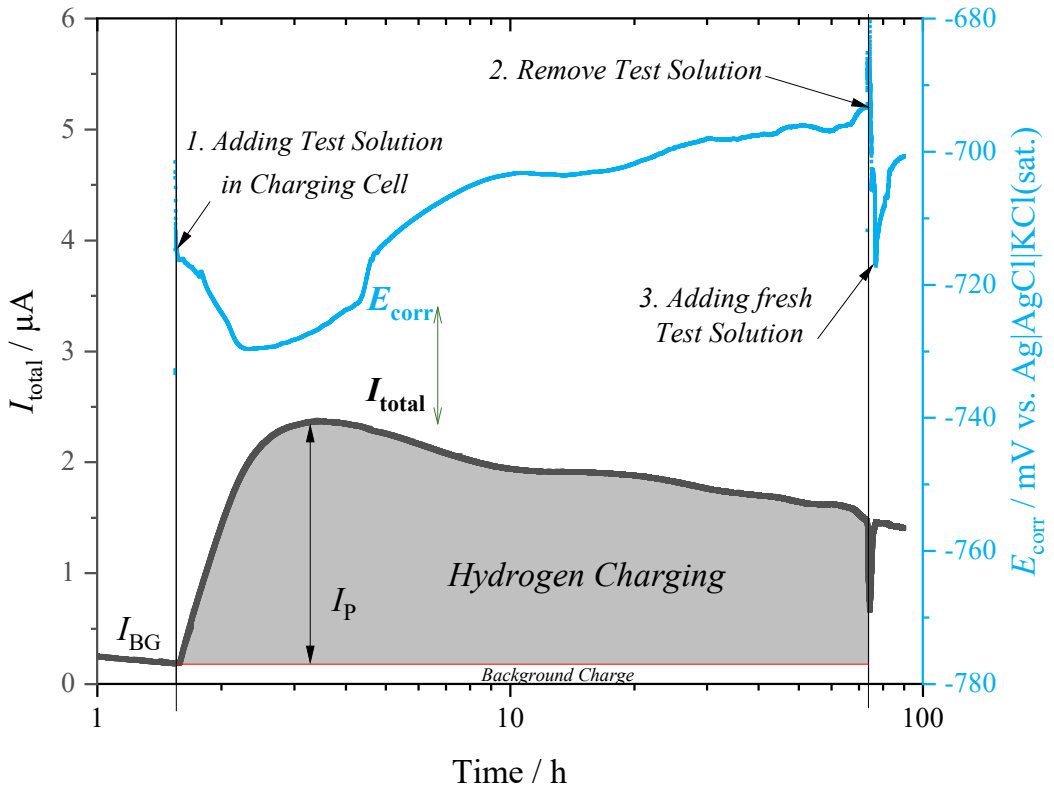

Figure 11: Time course of the total current I_{total} on the oxidation side of an unalloyed steel membrane $d = 0.05$ mm during free corrosion in test solution A at 22°C±1 K (black curve) and the corresponding free corrosion potential E_{corr} over time in the charging cell (blue curve).

The numerical results of the permeation measurements are shown in Table 6 is shown. The permeation measurements were performed at 25°C±1 K for better comparability with the literature hydrogen equilibrium concentration.

Table 6: Results of permeation measurements with a membrane made of unalloyed steel $d = 0.05$ mm with free corrosion in test solutions A and B at 25°C±1 K.

	$t(i_{P,max})$ [h]	$i_{P,ss}$ [µA cm^{-2}]	$a_{H,ss}$
Test solution A	(0.64±0.25)	(0.87±0.15)	(8.90±1.54)
Test solution B	(17.87±3.17)	(0.08±0.03)	(1.08±0.44)

After the addition of the test solution in the charging cell at time $t = 0$, there is a time delay in the passage of the hydrogen through the steel membrane, resulting in an increase in i_P measured on the oxidation side. The time to hydrogen leakage, as well as the time to maximum permeation current, is reached earlier with test solution A than with test solution B, see Table 6. This indicates a delay in hydrogen adsorption in test solution B compared to test solution A. Since

i_P is a direct measure of the hydrogen flux through the steel membrane, Equation 7 can calculate a (subsurface) hydrogen concentration $c_{H,e}$ in the charging cell of the steel membrane.

$$c_{H,e} = \frac{I_{P,ss}\ d}{F\ D_H\ A_{geo}} \tag{7}$$

$I_{P,ss}$ is the steady-state permeation current, F is the Faraday constant, and D_H is the material-specific effective hydrogen diffusion coefficient. The hydrogen diffusion coefficient of the unalloyed steel membrane with material number 1.0978 was determined to be $D_H = (6.0\pm0.5) \cdot 10^{-7}\,cm^2\,s^{-1}$. Using $I_{P,ss}$, the hydrogen activities of the test solutions were calculated using Equation 7 in Equation 8, and the results are listed in Table 6

$$a_H = \frac{c_{H,e}}{c_{H,0}} \tag{8}$$

The equilibrium interstitial hydrogen concentration in the trap-free iron at a partial pressure of $P_{H_2,0} = 1\,bar$ at 25°C is assumed to be $c_{H,0} = 8.425 \cdot 10^{-9}\,mol\,(H)\,cm^{-3}\,(Fe)$. [21] The steady-state hydrogen activity at 25°C±1 K of test solution A is significantly higher than that of test solution B because the following solution-specific process parameters increase the absorbable amount of atomic hydrogen: (i) lower pH, (ii) lower free corrosion potential, and (iii) higher concentration of thiocyanate as a recombination poison. The steady-state hydrogen activity with test solution B at 25°C±1 K is calculated to be 1.08±0.44. In a similar observation of test solution B, steady-state hydrogen activities of 1.13 to 2.12 were calculated for a test temperature of 50°C. [16] The permeation measurements show the difficulty of the test method in the presence of free corrosion. Even when test solution A is used, the maximum possible hydrogen activity is only reached after about 0.6 hours due to the time-dependent formation of the anodic and cathodic sections. This is disadvantageous for a test method in which the time to fracture is the test quantity. Therefore, in work package 3, the possibility of cathodic polarization will be investigated in more detail to develop a new test method in which the maximum possible hydrogen activity could already be reached at the beginning of the stress corrosion test.

2.2.5 Material Characterization

The prestressing wires for stress corrosion tests at BAM are listed in Table 7, which contains information on the strength class, heat treatment condition, geometry, and surface.

Table 7: Used prestressing steels: HENN-BRB according to TGL 12530, CDS-1670 according to DIBt approval Z-12.2-14 and CDS-1770 according to Z-12.2-124. No approval documents have become known for NEPTUN.

Prestressing steel	**Internal Sample-designation**	Heat treatment, surface, geometry	Nominal cross section [mm]^2	Currently approved?
St 145/160 (in kp mm^{-2})	**NEPTUN**	quenched and tempered, ribbed, edged	40.0	no
St 140/160 (in kp mm^{-2})	**HENN-BRB**	oil-quenched and tempered, ribbed, oval	35.0	no
St 1470/1670 (in MPa)	**CDS-1670**	cold drawn, smooth, round	38.5	yes
St 1570/1770 (in MPa)	**CDS-1770**	cold drawn, smooth, round	38.5	yes

The samples with the internal sample designations NEPTUN, HENN-BRB, and CDS-1670 are in a similar strength class, i.e., ≤1670 MPa nominal tensile strength. They have nominal cross sections in the range of 35 to 40 mm^2. The CDS-1770 is in the next higher strength class than the CDS-1670 for the same cross section. To evaluate the test method to be developed, prestressing steels considered highly susceptible (NEPTUN, HENN-BRB) were selected in addition to prestressing wires with current approval (CDS-1670, CDS-1770). In the case of NEPTUN and HENN-BRB, these are prestressing wire sections from tendons of damaged prestressed concrete bridges. In the case of NEPTUN, these are quenched and tempered Neptun N40 wires made by *F&G* from the Hohenzollern Damm bridge in Berlin, and in the case of HENN-BRB, oil-quenched and tempered wires made by *VEB Qualitäts- und Edelstahl-Kombinat, Hennigsdorf* from the Altstädter Bahnhof bridge in Brandenburg an der Havel [6]. The mortar residues were mechanically removed from the prestressing steels, and the absence of cracks in the tested sections was verified using non-destructive magnetic particle testing. The strength values of the crack-free sample sections of the NEPTUN and HENN-BRB met the nominal values from the product designations in tensile tests. The CDS-1670 and CDS-1770 prestressing wires, each with a diameter of 7 mm, were provided as supplied by the associated partner.

The chemical composition was determined by spark emission spectrometry (FES), see Table 8. Where references were available, no differences were found between the measured chemical compositions and the tolerance specifications in the approval documents.

Table 8: Chemical composition of the prestressing steels used in percent by mass [wt%]. The chemical composition of the steel membrane used for permeation measurements has been added.

Sample	C	Si	Mn	P	S	Cr	Ni	Mo	V	Cu	Al	Ti
NEPTUN	0,641	1,322	1,028	0,017	0,016	0,070	0,071	0,010	0,002	0,178	0,008	0,005
HENN-BRB	0,591	0,918	1,076	0,021	0,019	0,133	0,064	0,012	0,002	0,195	0,008	0,003
CDS-1670	0,833	0,285	0,749	0,010	0,012	0,158	0,059	0,013	0,002	0,090	0,002	<0,001
CDS-1770	0,813	0,253	0,895	0,009	0,008	0,271	0,030	0,008	0,032	0,009	0,007	<0,001
Membrane	0,046	0,013	0,204	0,011	0,012	0,012	0,004	0,001	<0,001	0,009	0,053	<0,001

Furthermore, metallographic examinations were carried out to document the sample material used. The respective microstructures were made visible with a Nital *etch.* The metallographic images of the prestressing wires NEPTUN and HENN-BRB (Figure 12 and Figure 13) showed the characteristics of quenched and tempered microstructures with tempered martensite. Edge decarburized layers can be seen in the near-surface region. The metallographic images of CDS-1670 and CDS-1770, see Figure 14 and Figure 15show an elongated grain structure with linearly intercalated MnS inclusions, which is typical for cold-drawn wires.

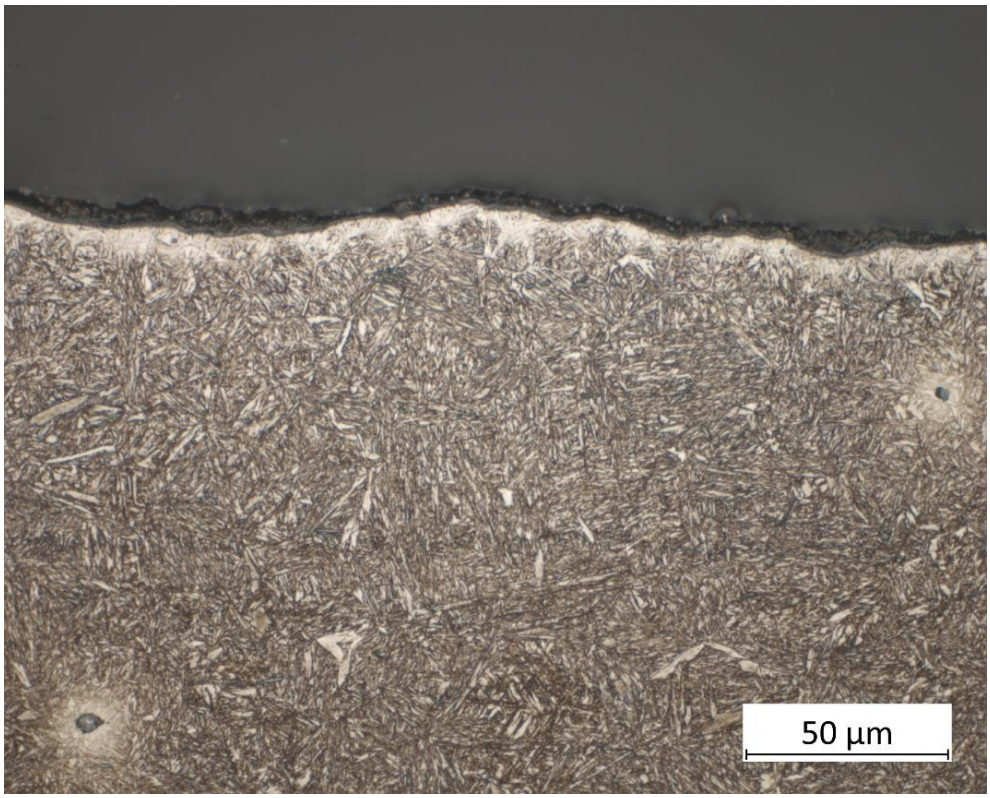

Figure 12: Metallographic image of the NEPTUN edge microstructure (longitudinal section).

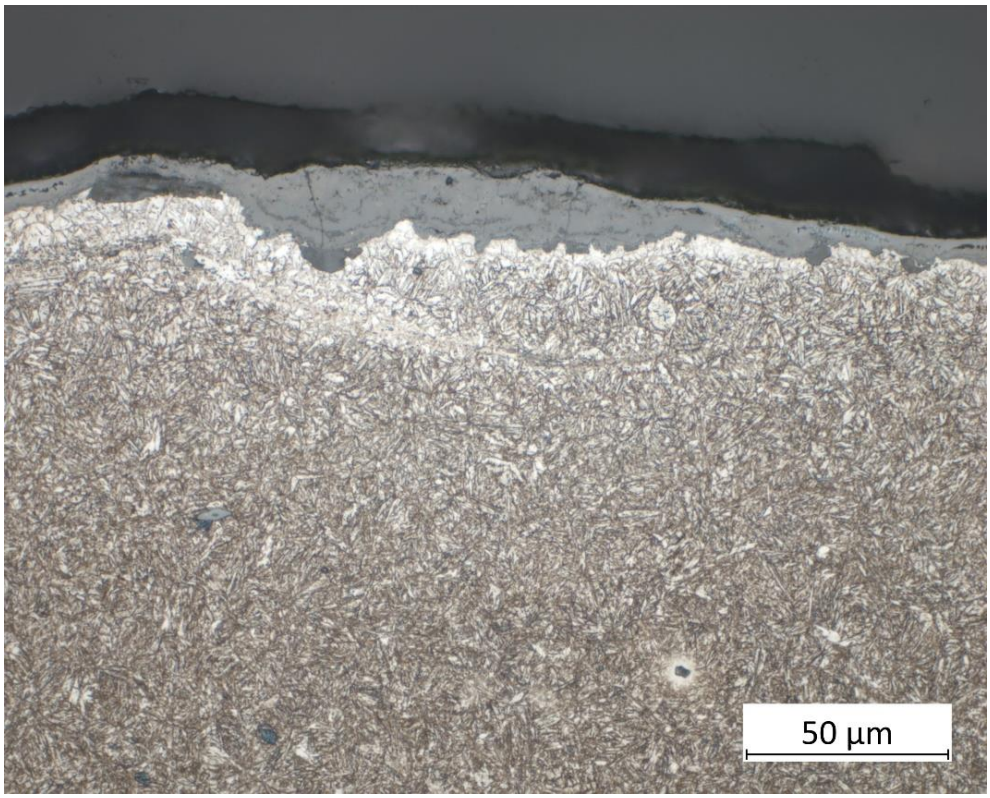

Figure 13: Metallographic image of the HENN-BRB edge microstructure (longitudinal section).

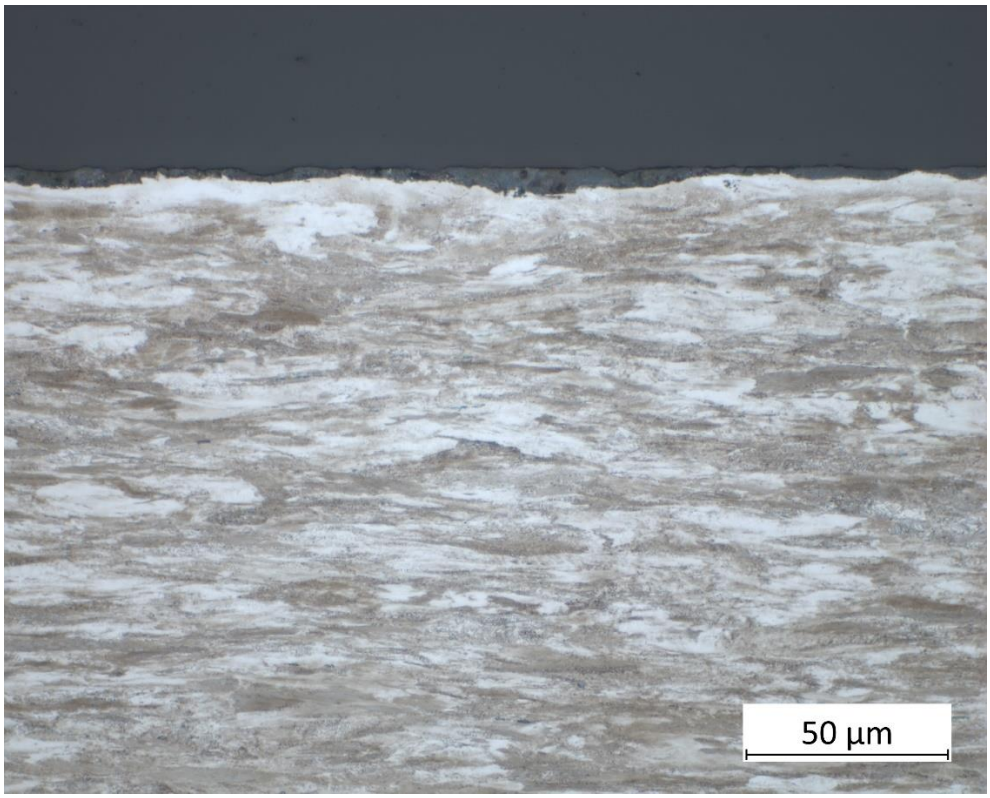

Figure 14: Metallographic image of the CDS-1670 edge microstructure (longitudinal section).

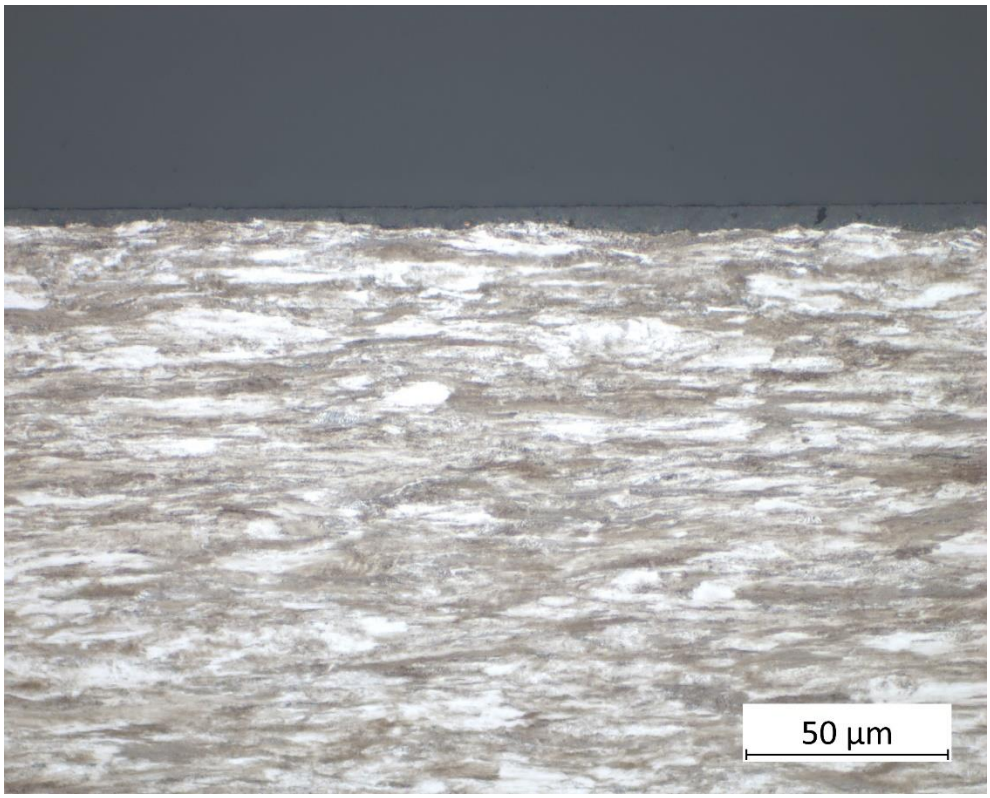

Figure 15: Metallographic image of the CDS-1770 edge microstructure (longitudinal section).

2.3 Work Package 2: Data Evaluation and Sample Production

No.	Goal
2.1.3.1	Historical review, evaluation of old monitoring tests • Anomalies • Relationships with operational or process changes
2.1.3.2	Produce susceptible products (e.g., by heat treatment) as test objects for BAM and Annahütte and characterization of the samples to be provided about: • Mechanical-technological properties • Metallography • Microanalysis

The objective of work package 2 was a historical review of the SAH stress crack tests performed according to DIN EN ISO 15630-3 with test solution A and the evaluation of test data from internal and external monitoring. Furthermore, the characterization of the specimens and their production by heat treatment were tasks of the work package. Finally, the samples produced at SAH were to be made available to BAM for further testing.

2.3.1 Historical Review (Pre-Existing Know-How SAH; not public)

Conclusion: Both the first rough overall evaluation and the more detailed variance and regression analysis show that the test method currently specified by the valid test standard DIN EN ISO 15630-3:2020-02 [1] for testing prestressing steels for their robustness or sensitivity to hydrogen-induced stress corrosion cracking causes a very large and, above all, statistically incomprehensible scatter of results. Thus, the statement of the test uncertainty of the actual test method, already mentioned several times in the overall project description, is confirmed based on SAH's and third-party monitoring results. The motivation to develop a new test method that gives more reproducible and "safe" test values is thus fully supported.

2.3.2 Characterization of the samples as well as the generation of susceptible samples

The task of SAH was to produce samples that were mainly "susceptible" to hydrogen-induced stress corrosion cracking. These samples were then to be tested and characterized at BAM. On the one hand, this characterization was planned on a model scale using miniature samples at BAM. On the other hand, thin SAH real bars in the dimensional range Ø 18.0 mm were also to be pretested at BAM. On the other hand, large real bar specimens (Ø 40.0 mm) were scheduled for testing at SAH due to the newly installed 3 MN stress corrosion cracking test rig at SAH. SAH Table 1 lists the samples manufactured by SAH for BAM. For quality assurance reasons, SAH manufactured 2.5 times the number of specimens of the steel grades rolled in Ø 30.0 mm bars (variants 1, 2, and 3). The proposal to select the steel grades variants 1, 2, and 3 and the heat treatments +QT, +N, +QT(Bainite) came from SAH. The required specimen dimensions, as well as the desired number of specimens, were specified by BAM. The testing of the miniature specimens was original to be carried out exclusively at BAM[1].

SAH-Table 1: Miniature samples manufactured by SAH for BAM.

Miniature samples				
Steel grade	Heat treatment	Number of samples Ø 15,0 mm x 200 mm	Number of samples Ø 30,0 mm x 500 mm	Number of samples per type of steel
Variant 1	+QT	10	3	39
	+N	10	3	
	+QT (Bainite)	10	3	
Variant 2	+QT	10	3	39
	+N	10	3	
	+QT (Bainite)	10	3	
Variant 3	+QT	10	3	39
	+N	10	3	
	+QT (Bainite)	10	3	
Total:		90	27	117

In addition to the miniature samples, real samples of the standard SAH products (SAS950/1050 and SAS 670/800) in Ø 18.0 mm according to SAH-Table 2 in dimensions and number of pieces were requested by BAM in parallel, taken by SAH from the standard production, prepared and

[1] Section 2.5.3 describes the final testing of the ø 30 mm x 500 mm samples at SAH with coupling and post-processing.

sent to BAM subsequently. Again, for quality assurance reasons, SAH prepared 2 times the number of samples.

SAH-Table 2: Real samples produced by SAH for BAM.

Real samples					
Steel grade	Heat -Lot No	Diameter	Sample length	Samples sent to BAM	Material at SAH
SAS 950/1050	VA489331	Ø 18,0 mm	1,80 m	10	ca. 10 m
SAS 670/800	621091	Ø 18,0 mm	1,80 m	10	ca. 10 m
				Total: 20	

All samples were produced by SAH, mechanically processed, thoroughly tested for their mechanical-technological properties, examined for their metallography, and analyzed for their chem. Composition. The heat treatment of the samples for the +QT, +N, and +Q(Bainite) treatment states in variants 1, 2, and 3 were carried out at the Weber und Wallner hardening plant. The necessary tempering treatments +T to adjust the strength for the variant +QT(Bainite) were subsequently carried out at SAH.

The following are excerpts from the test results. SAH-Figure 1, for example, shows the tensile test result for variant 1 for the sample variant 1+QT in ø 15.0 mm x 200 mm in a test diameter of 9.93 mm (standard tensile specimen).

Versuch durchgeführt am 15.01.2021

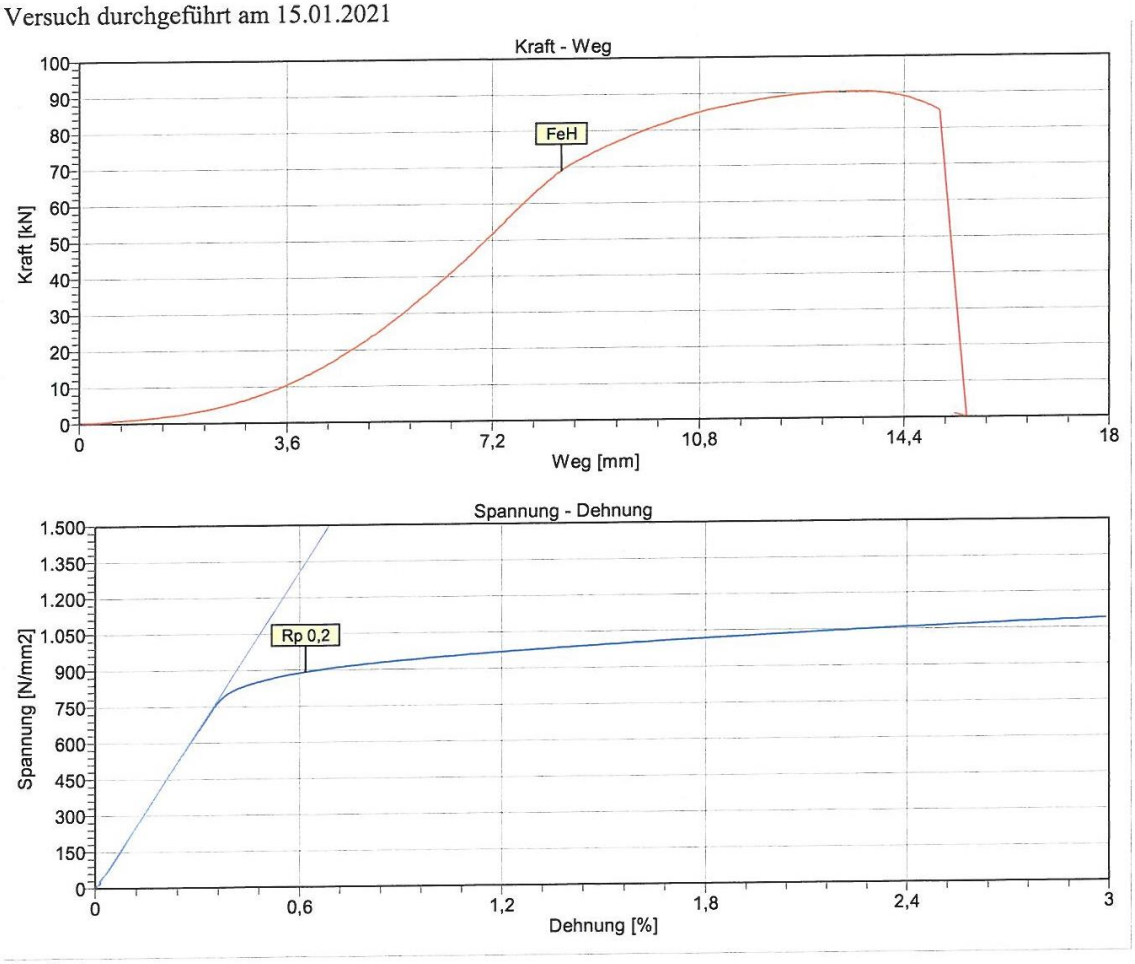

Ergebnisse:

FeH	68,9 kN
ReH	890 N/mm2
Rp 0,2	890 N/mm2
Fm	90,3 kN
Rm	1170 N/mm2

A5	9,96 %
Z	20,2 %
HB o. HRC	
Rm ger.	N/mm²
E	218000 N/mm2

SAH-Figure 1: Mechanical-technological examination (tensile test) of variant 1+QT in ø 15.0 mm x 200 mm in test diameter of 9.93 mm (standard tensile specimen)

SAH-Figure 2 shows the microstructure in the metallographic section with additional hardness value in HRC using the same heat treatment variant 1 +QT in ø 15.0 mm x 200 mm. A tempered martensite, characteristic of this heat treatment condition, is visible.

Edge:

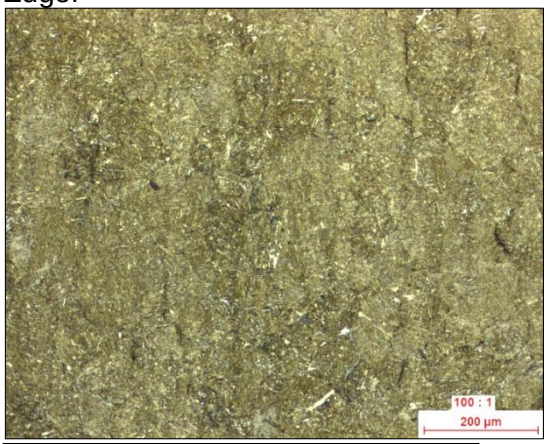

Microstructure: Tempered martensite

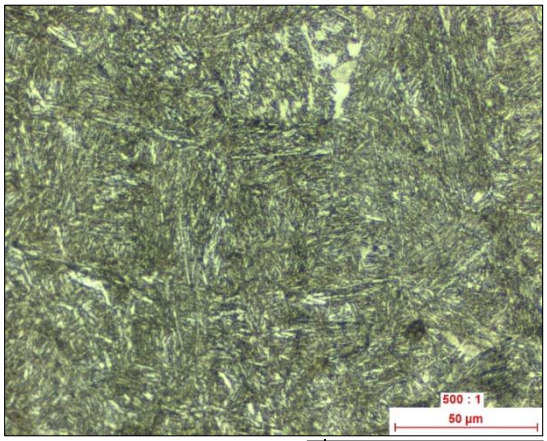

Hardness: 37 HRC

Core:

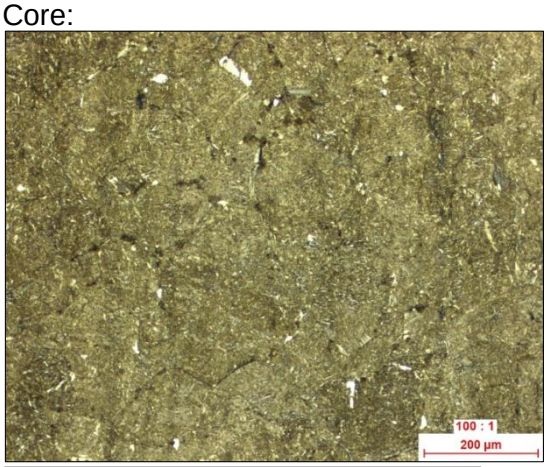

Microstructure: Tempered martensite

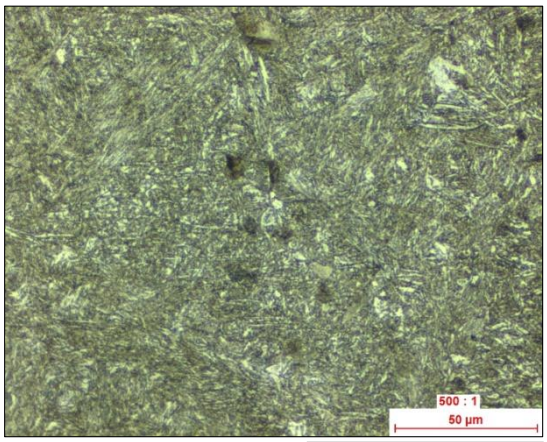

Hardness: 38 HRC

SAH-Figure 2: Metallographic evaluation of the etched section of variant 1+QT in ø 15.0 mm x 200 under the light microscope.

SAH-Figure 3 and SAH-Figure 4 show the same methodology for variant 1, but now in the heat treatment condition + N in ø 15.0 mm x 200 mm. The tensile test (SAH-Figure 3) shows significantly lower strength R_m and yield strength R_e but higher elongation at break A_5. The microstructure shows a normalized annealing structure with pearlite and shallow ferrite content rather than a hardened structure.

Versuch durchgeführt am 15.01.2021

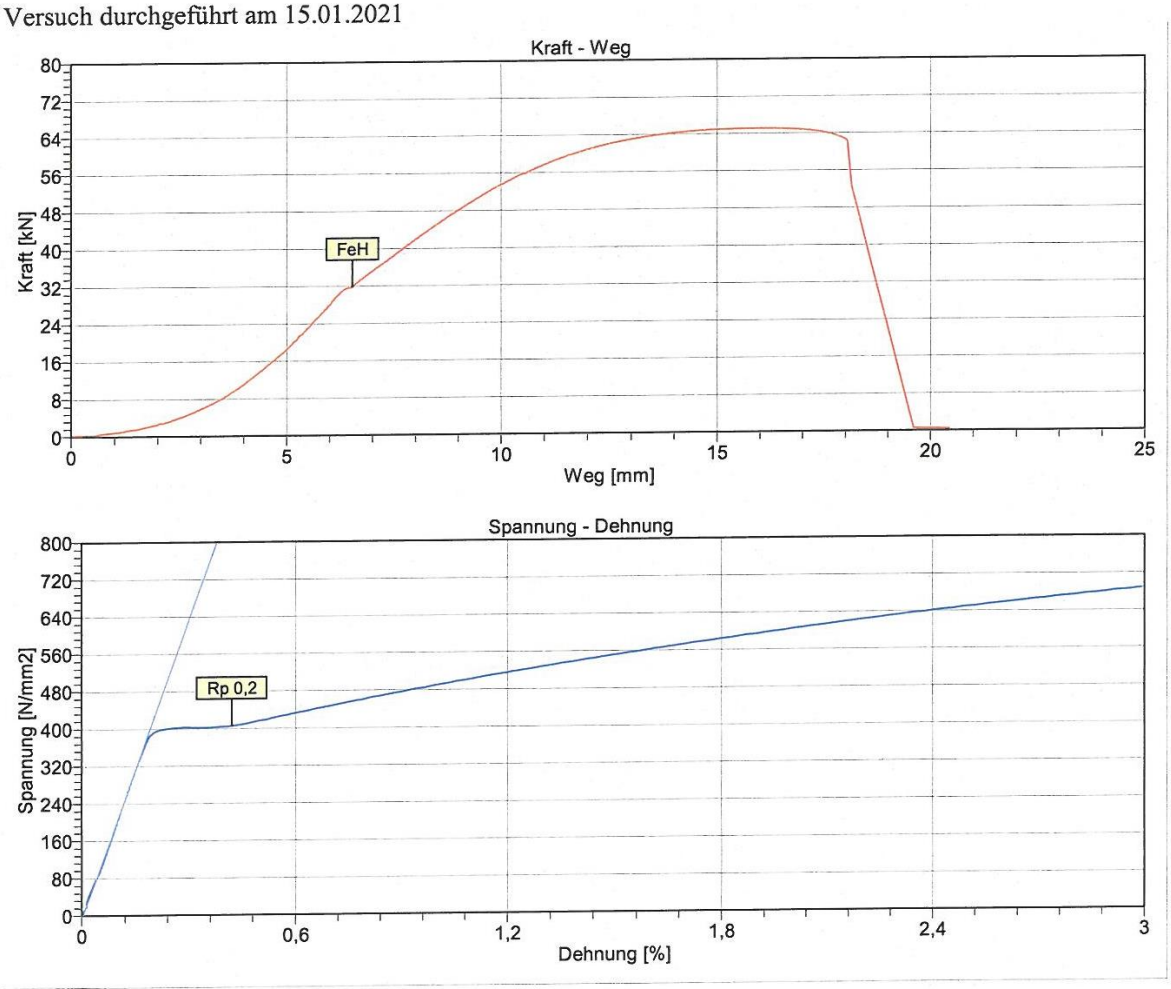

Ergebnisse:

FeH	31,7 kN
ReH	404 N/mm2
Rp 0,2	404 N/mm2
Fm	65,1 kN
Rm	830 N/mm2

A5	15,3 %
Z	20,5 %
HB o. HRC	
Rm ger.	N/mm²
E	215000 N/mm2

SAH-Figure 3: Mechanical-technological examination (tensile test) of variant 1+N in ø 15.0 mm x 200 mm in test diameter of 9.93 mm (standard tensile specimen)

Edge:

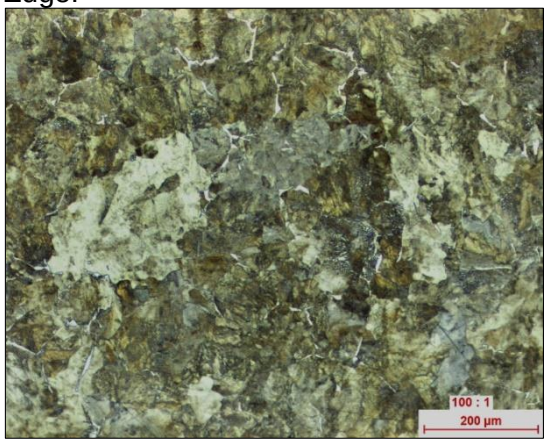

Microstructure: Perlite + Ferrite

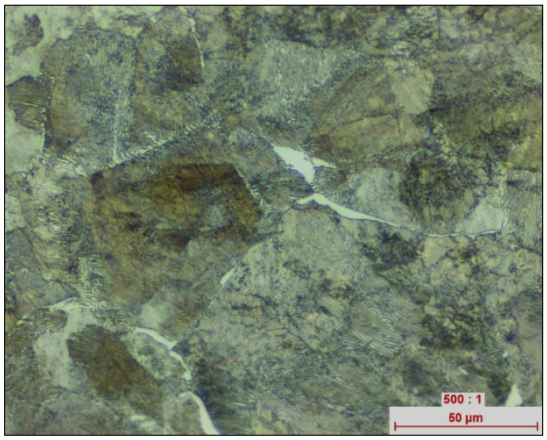

Hardness: 19 HRC

Core:

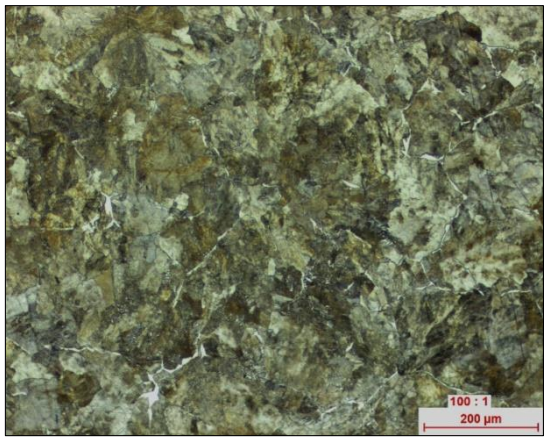

Microstructure: Perlite + Ferrite

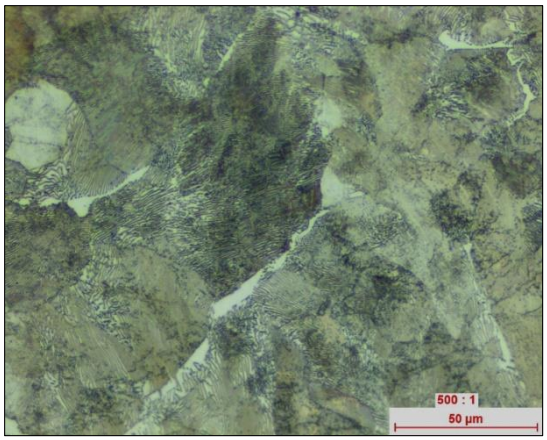

Hardness: 19,5 HRC

SAH-Figure 4: Metallographic evaluation of the etched section of variant 1+N in ø 15.0 mm x 200 mm under the light microscope.

A final example of mechanical and technological testing and documentation of a variant 2+QT(Bainite) sample that is highly susceptible to hydrogen-induced stress corrosion cracking is documented in SAH-Figure 5.

Versuch durchgeführt am 10.06.2021

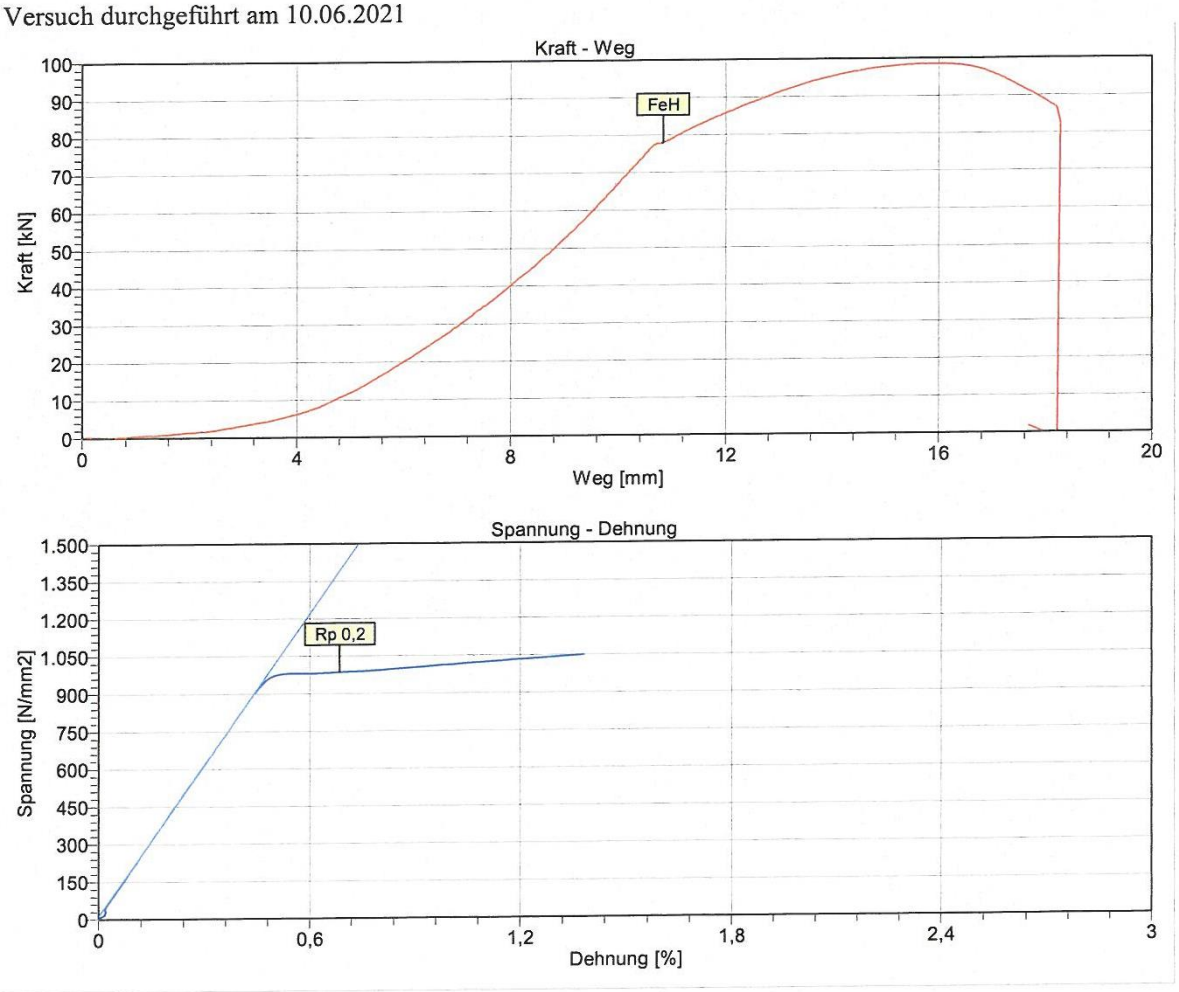

Ergebnisse:

FeH	78,0 kN
ReH	985 N/mm2
Rp 0,2	985 N/mm2
Fm	98,5 kN
Rm	1240 N/mm2

A5	11,6 %
Z	32,0 %
HB o. HRC	
Rm ger.	N/mm²
E	201000 N/mm2

SAH-Figure 5: Mechanical-technological investigation (tensile test) of variant 2+QT(Bainite) in ø 15.0 mm x 200 mm in test diameter of 10.04 mm (standard tensile specimen).

SAH-Figure 6 shows the corresponding metallographic examination. The microstructural constituent Bainiteconforms to the treatment; the microstructural constituents martensite and pearlite are also present in the microstructure due to the alloying and heat treatment processes. The susceptibility of variant 2 was proven by BAM in the miniature specimen test and the SAH tests, as described in section 2.5.3.

Edge:

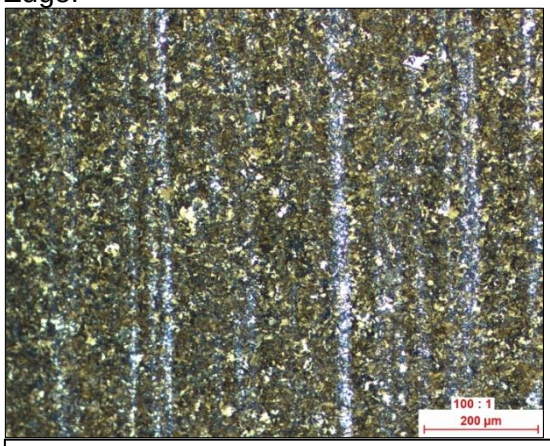

Microstructure: Bainite+ Perlite + Martensite

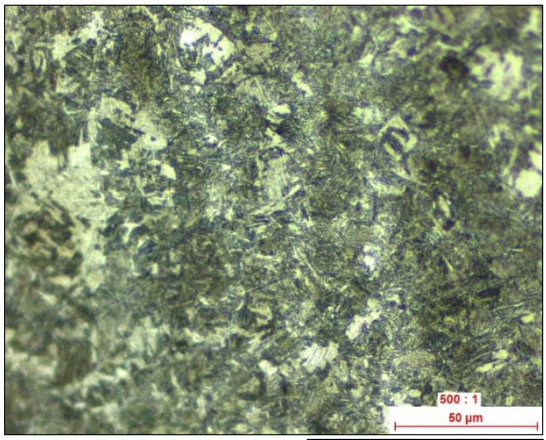

Hardness: 41 HRC

Core:

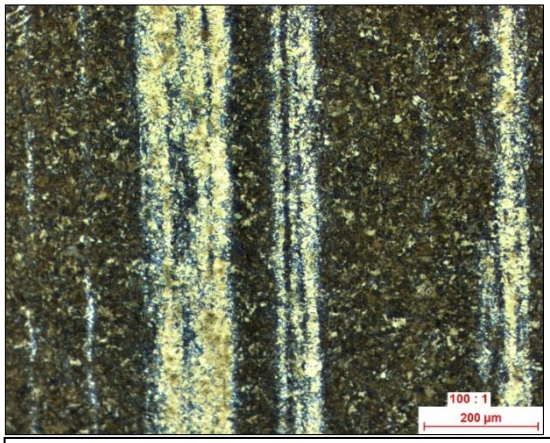

Microstructure: Bainite+ Perlite + Martensite + Martensite segregations

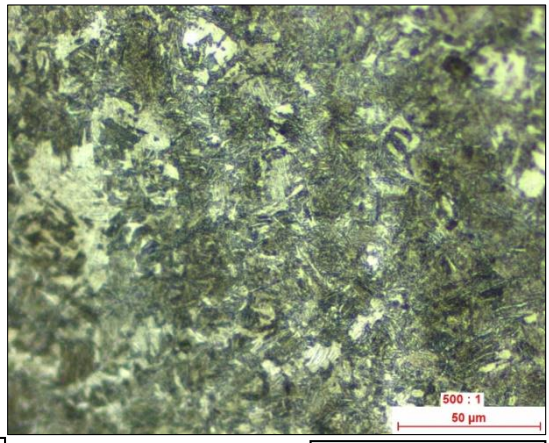

Hardness: 42 HRC

SAH-Figure 6: Metallographic evaluation of the etched section of variant 2+QT(Bainite) in ø 15.0 mm x 200 mm under the light microscope.

2.4 Work Package 3: Development of a New Test Method

No.	Goal
2.1.4.	Development of a new test method based on the findings from WP 1. Test new method.

Experimental:

Permeation measurement: Besides the permeation measurement setup described above, a three-electrode arrangement was set up in the charging cell for cathodic polarization. The steel membrane was used as the working electrode, an additional Ag|AgCl|KCl(sat.) reference electrode, and a titanium mixed oxide grid as the counter electrode.

Stress corrosion tests: For the cathodic polarization stress corrosion tests, the NEPTUN, HENN-BRB, CDS-1670, and CDS-1770 prestressing wires were polished over the central 50 mm of the 510 mm total sample length. Adhesive heat shrink tubing sections were used to limit the central test length L_0 to 10 mm. For the cathodic polarization stress corrosion tests, a measurement cell consisting of a sealed transparent acrylic tube with a titanium mixed oxide grid as the counter electrode was designed. The newly designed test cell is shown in Figure 16. The grid protrudes approximately 10 mm from the test cell for electrical contact.

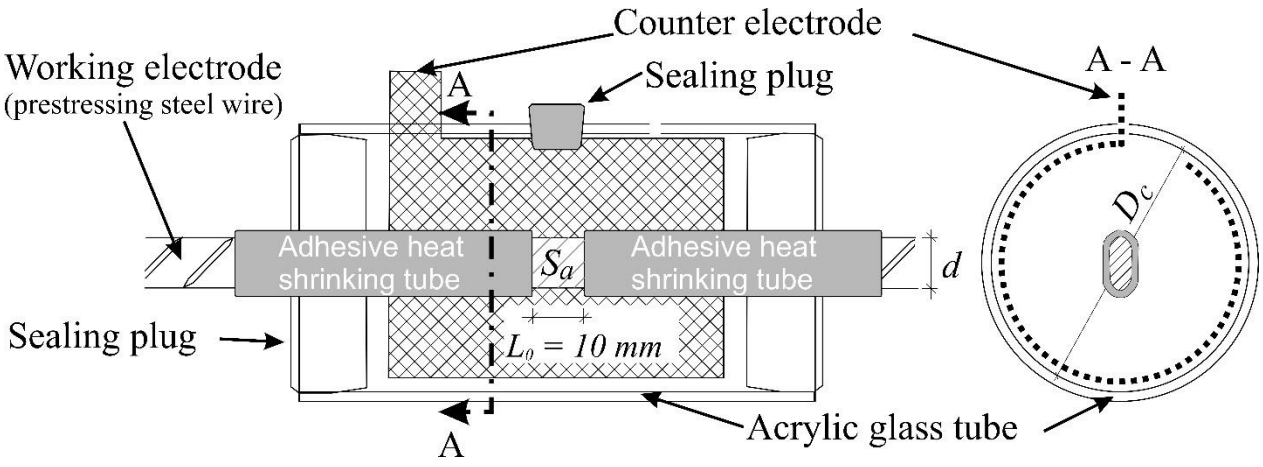

Figure 16: The newly designed test cell is drawn for stress corrosion tests with cathodic polarization.

The surface area of the counter electrode is at least ten times the surface area of the steel in contact with the test solution. The size of the test cell is such that the ratio of electrolyte volume to sample surface area is at least 50 ml cm^{-2}. The specification from [1] of at least 5 ml cm^{-2} is thus met or exceeded. To simplify the test application, the internal diameter D_C and the minimum volume of the test solution for different nominal diameter ranges V_0 have been specified for different nominal diameter ranges; see Table 9.

Table 9: Specifications of the test cell dimensions.

Nominal diameter d of prestressing steel	Inner diameter D_C of the test cell	Minimum electrolyte volume V_0 of the test solution
$d \leq 7.5$ mm	50 mm	≥ 120 ml
7.5 mm < $d \leq 12.5$ mm	50 mm	≥ 300 ml

The prepared sample and the test cell were installed in a tensioning frame, with a hydraulic cylinder to pre-tension the wire. The sample was prestressed at a constant load level of 80% of the nominal tensile strength R_m. To adjust and control the experimental parameters, the output voltage from the force gauge's Wheatstone bridge circuit and the applied current were continuously documented using a Keysight data logger. The output voltage from the gauge's Wheatstone bridge circuit was a function of, and could be converted to the effective force.

Test solution A was tempered at 50°C±1 K for 24 hours before testing and then cooled to a laboratory temperature of 22°C±1 K. During the stress corrosion test, the laboratory temperature was 22°C±1 K. At the start of the test, the test cell was filled with test solution A. The prestressing steel was covered entirely with the test solution at the start of the test. One minute later, the prestressing steel was cathodically polarized in galvanostatic mode using a *Bank's Wenking MP-87* potentiostat/galvanostat.

Experiments were performed at cathodic current densities of 1.000 mA cm^{-2}, 0.500 mA cm^{-2}, 0.375 mA cm^{-2}, 0.250 mA cm^{-2}, and 0.125 mA cm^{-2}. The required DC current was determined by multiplying the current density by the area of the prestressing steel in contact with the test solution. The DC current could be adjusted with an accuracy of ±2 µA. The time measurement started at the time the galvanostatic operation was switched on. The DC current value was reached one second after the start of the experiment. The time to brittle fracture was determined to an accuracy of 0.01 h.

Results & Discussion:

In WP 3, the results of WP 1 were used. The stress corrosion tests continued with the polished surfaces, test solution A, and a test temperature of 22°C. To ensure reasonable test periods in the stress corrosion cracking test, in which it is possible to distinguish between susceptible and robust conditions, the possibility of cathodic polarization is used, in which hydrogen charging is possible and driven independently of free corrosion. The cathodic current densities in galvanostatic operation varied in stress corrosion tests and permeation measurements. The method of WP 3 is outlined in Figure 17.

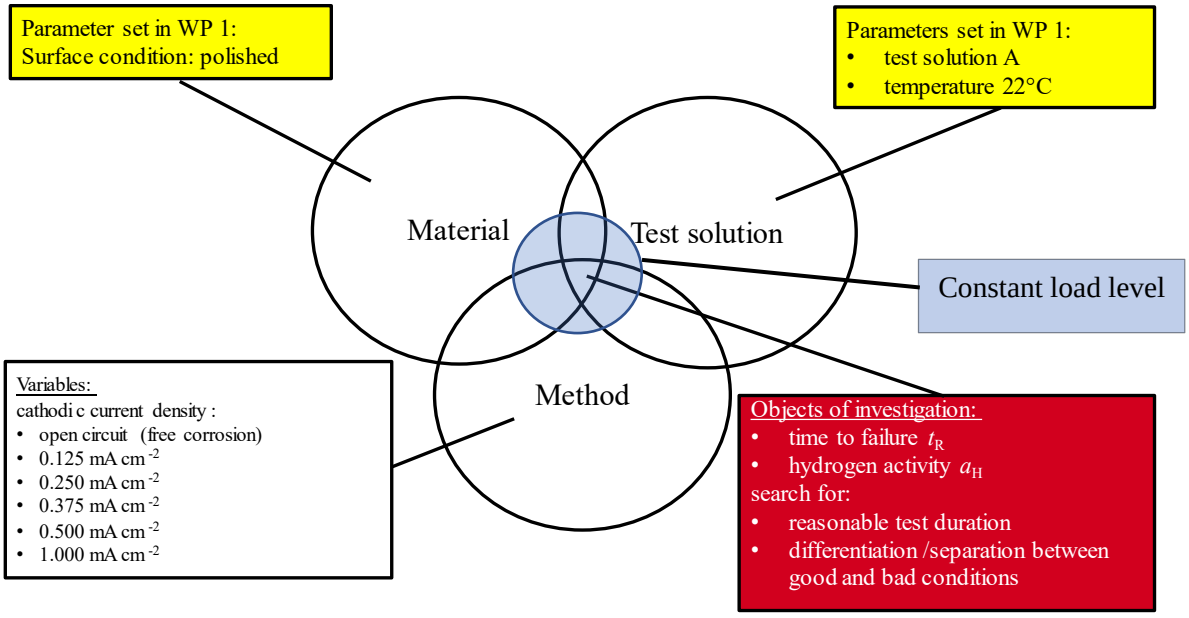

Figure 17: These influences on the test method were investigated in WP 3.

Permeation measurements:

To assess the intensity of hydrogen charging due to cathodic polarization, the permeation current densities, i_P at varying cathodic current densities, were determined in permeation measurements. Figure 18 shows the maximum permeation current density $i_{P,max}$ achieved per experiment as a function of cathodic current density.

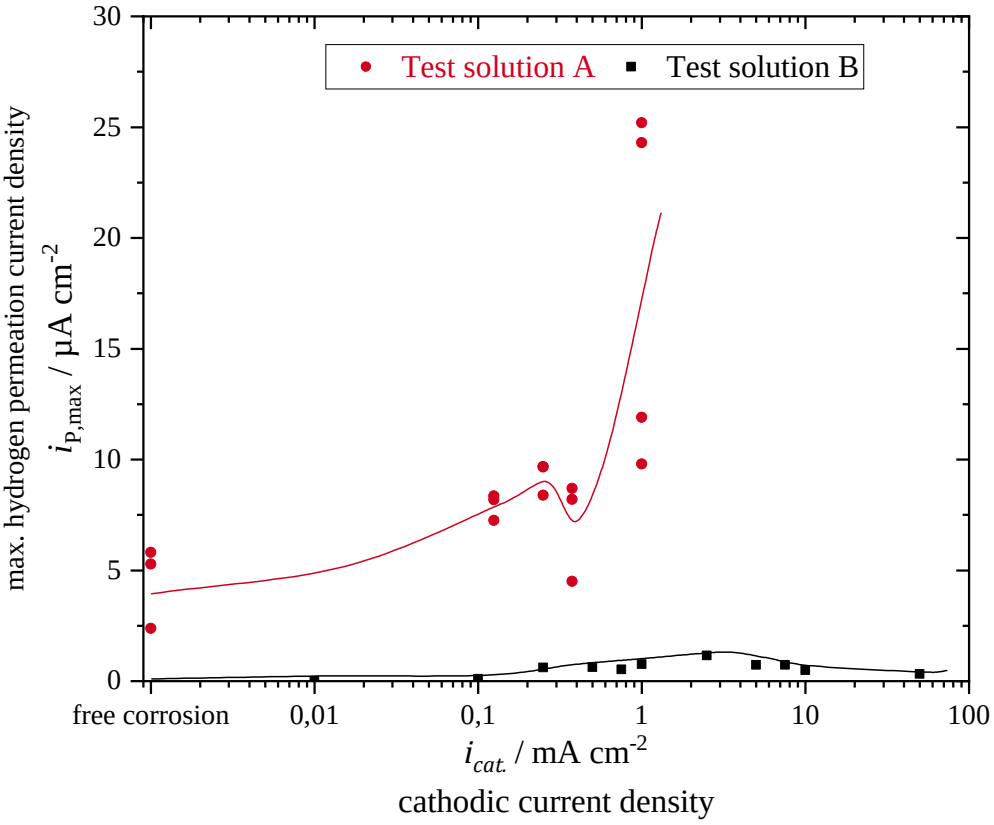

Figure 18: Plot of the maximum hydrogen permeation current density $i_{P,max}$ for individual permeation measurements as a function of the cathodic current density $i_{cat.}$ for the search for suitable cathodic current densities in stress corrosion tests.

With test solutions A and B, it was possible to significantly increase $i_{P,max}$ by cathodic polarization compared to free corrosion. The comparison of the experiments with test solution A and test solution B shows that, at the cathodic current densities set here, the intensity of the hydrogen charge is higher with test solution A than with test solution B. Since further investigations of test solution B were omitted for the reasons discussed in WP 1, a cathodic current density for test solution A is now sought.

Permeation measurements with test solution A were carried out at cathodic current densities $i_{cat.}$ of 1.000 mA cm^{-2}, 0.375 mA cm^{-2}, 0.250 mA cm^{-2}, and 0.125 mA cm^{-2} as well as in free corrosion. The results of these permeation measurements are shown in Table 10.

Table 10: Results of permeation measurements with test solution A at 25°C at various cathodic current densities $i_{cat.}$ and free corrosion in the charging cell.

$i_{cat.}$	Amount of charge Q_i offered in charging cell	Permeable charge quantity Q_H measured in oxidation cell	Q_H/Q_i	Hydrogen activity a_H at 20 h	Calculated mass m of permeable H according to Faraday
mA cm^{-2}	C	C			µg
1.000	81.43	(0.44±0.12)	**(0.5±0.1) %**	(30.7±7.4)	**(4.6±1.3)**
0.375	30.54	(0.29±0.10)	**(0.9±0.3) %**	(24.4±6.1)	**(3.1±1.0)**
0.250	20.36	(0.35±0.06)	**(1.7±0.3) %**	(28.9±5.2)	**(3.7±0.6)**
0.125	10.18	(0.33±0.04)	**(3.2±0.4) %**	(28.6±1.3)	**(3.4±0.4)**
free corrosion	unknown	(0.16±0.07)	**unknown**	(23.4±7.6)	**(1.7±0.7)**

The amount of charge offered, Q_i, was determined over 20 hours according to Equation 9.

$$Q_i = i_{kat.}\, A_{geo}\, t \tag{9}$$

The permeable charge quantity Q_H is the integral of the measured time-dependent hydrogen permeation current I_P over time according to Equation 10.

$$Q_H = \int_{t=0}^{t=20\ h} I_P\ dt \tag{10}$$

The mass of permeable hydrogen that had passed through the membrane in 20 hours was calculated using Faraday's law, see Equation 11.

$$m = \frac{Q_H\, M_H}{z\, F} \tag{11}$$

Where M_H is the molar mass of the hydrogen atom, the charge number is z, which is set equal to one, and F is the Faraday constant. The hydrogen activity at 20 h was calculated according to Equation 7 and Equation 8. The results show that the highest measured charges and hydrogen activities are obtained at 1.000 mA cm^{-2}. There is a tendency for hydrogen activities to increase with increasing cathodic current density. However, hydrogen permeation is more efficient at lower cathodic current densities. Therefore, the charge amounts are similar at 0.125 mA cm^{-2}, 0.250 mA cm^{-2}, and 0.375 mA cm^{-2}. The choice of a cathodic current density below 1.000 mA cm^{-2} for stress corrosion testing seems reasonable since problems with hydrogen charging can occur at higher current densities. On the one hand, too high cathodic current density may favor the recombination reactions according to Equation 4 and Equation 5, which may reduce the charging intensity efficiency by inhibiting hydrogen charging into the material. Second, too high a cathodic current density could reduce the ability to distinguish between susceptible and robust prestressing steels. Since at cathodic current densities of 0.125 mA cm^{-2}, 0.250 mA cm^{-}

^{2}, and 0.375 mA cm^{-2}, the amount of hydrogen passing through the membrane per unit time is a factor of 2 higher than in free corrosion, there is no evidence for a change in the damage mechanism in HiSCC. Considering the charge conversion at 0.125 mA cm^{-2} cathodic polarization current density, the effective hydrogen charge, related to the respective cathodically effective area, is similar.

The critical parameter in hydrogen charging is the cathodic current density, or the ratio of cathode area to anode area, which is clearly defined for external cathodic polarization. It is a 100% area ratio of the cathode since the anode area is 100% located at the counter electrode. Table 10 calculates hydrogen activity for free corrosion for a cathode area ratio of 50% of the total area in contact with the test solution A_{geo}. Since in the case of free corrosion of a heterogeneous mixed electrode without a local element, the area fraction of the cathode, i.e., the area on which the hydrogen charging takes place, is assumed to be equivalent to the anode area, the hydrogen activity is consequently also attributable to 50% of the area. Table 11 shows the calculated hydrogen activities for different surface fractions of the cathode at A_{geo}.

Table 11: Calculated hydrogen activities a_{H} in the "steady-state" for free corrosion in test solution A at 25°C, calculated with different surface areas of the cathode in contact with the test solution.

Area share in %	80%	60%	50%	40%	20%
Effective hydrogen activity	(14.6±4.7)	(19.4±6.3)	(23.3±7.6)	(29.2±9.5)	(58.3±19.0)

Since these area ratios have a decisive influence on the level of the cathodic partial current density and thus on the amount of the hydrogen charge, the hydrogen charge under free corrosion conditions is undefined and can also change during the stress corrosion test. This inevitably also leads to undefined test conditions in the previous stress corrosion cracking tests under free corrosion and thus to the expected scatter of results. For this reason, the statistical scatter of the times to fracture may be reduced in stress corrosion tests with cathodic polarization compared to free corrosion tests.

Stress corrosion tests:

Stress corrosion tests at the 80% load level R_m with test solution A at 22°C were performed on polished surface conditions with different cathodic current densities $i_{cat.}$ on the HENN-BRB and CDS-1670. The results of these stress corrosion tests are shown in Figure 19.

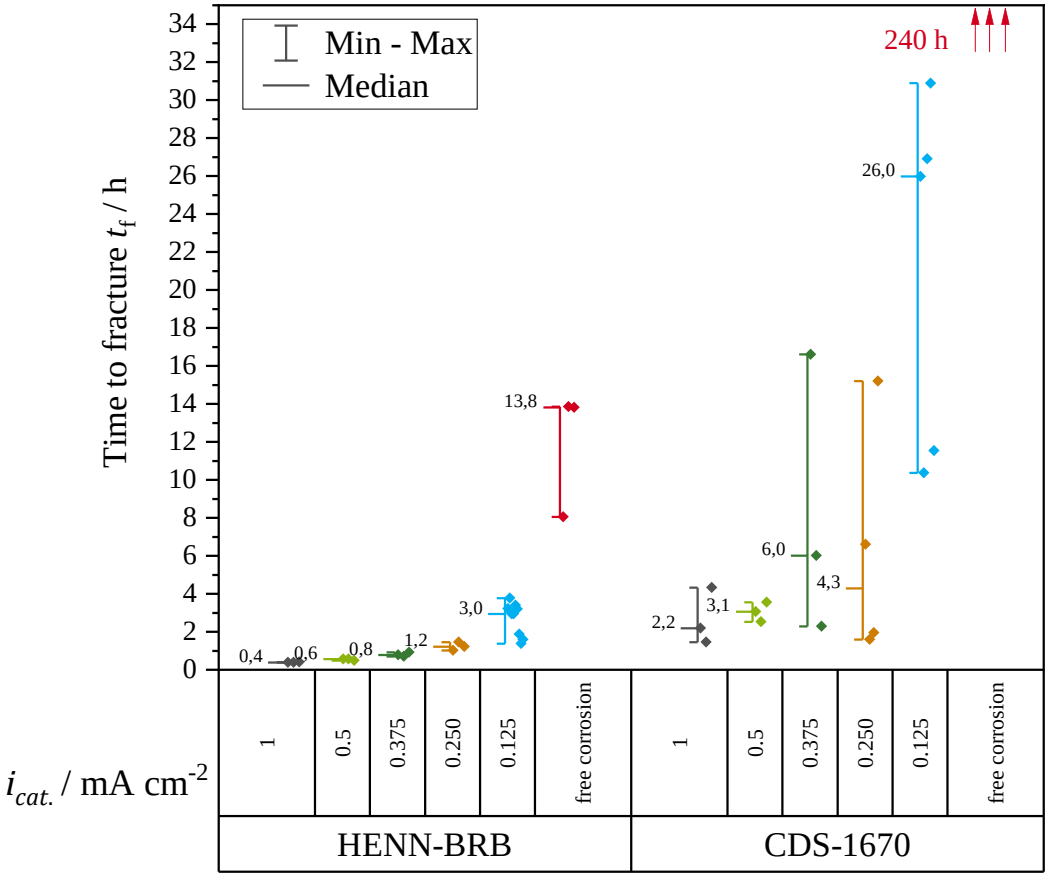

Figure 19: Times to fracture of the HENN-BRB and CDS-1670 at 80% in test solution A at 22°C. R_m in test solution A at 22°C with different cathodic current densities compared to the time to fracture results with free corrosion.

Figure 19 shows that the times to fracture for the highly susceptible HENN-BRB decrease with increasing cathodic current density compared to free corrosion. It is noticeable that the scatter of the results with HENN-BRB decreases with increasing current density. This indicates that highly susceptible prestressing steels can be identified with cathodic polarization. The results with the approved CDS-1670 also show that cathodic polarization shortens the time to fracture compared to free corrosion. Here, the times to fracture at 0.250 mA cm^{-2} are the same as those

at 0.375 mA cm^{-2}. The scatter of the results also tends to decrease with CDS-1670 at higher current densities.

However, the CDS-1670 shows a higher scatter at all cathodic current densities than the HENN-BRB. This indicates a material-dependent result scatter oriented towards the susceptibility to HiSCC.

An advantage of the test method is that the test times on polished samples in test solution A at 22°C can be shortened with cathodic polarization compared to free corrosion. This is most likely since under free unpolarized test conditions, the corrosion processes necessary for hydrogen loading do not start until after a certain incubation period, and thus is time-determinative for the test. With cathodic polarization, the hydrogen loading can now be specifically started and controlled at the beginning of the test.

In addition, the HENN BRB seems to break before the CDS-1670 for each hydrogen charging situation considered. Still, the temporal differentiation between these susceptible and robust conditions is only given at 1.000 mA cm^{-2}, 0.500 mA cm^{-2}, 0.375 mA cm^{-2}, and 0.250 mA cm^{-2}. A clear differentiation between susceptible and robust states is available at a cathodic current density of 0.125 mA cm^{-2}. The clear temporal differentiation between HENN-BRB and CDS-1670 could guarantee the definition of an explicit limit value as a conformity criterion.

Stress corrosion tests were performed at $i_{cat.}$ = 0.125 mA cm^{-2} also using highly susceptible NEPTUN and the approved CDS-1770 to confirm the ability to distinguish between susceptible and robust conditions. The results are shown in Figure 20.

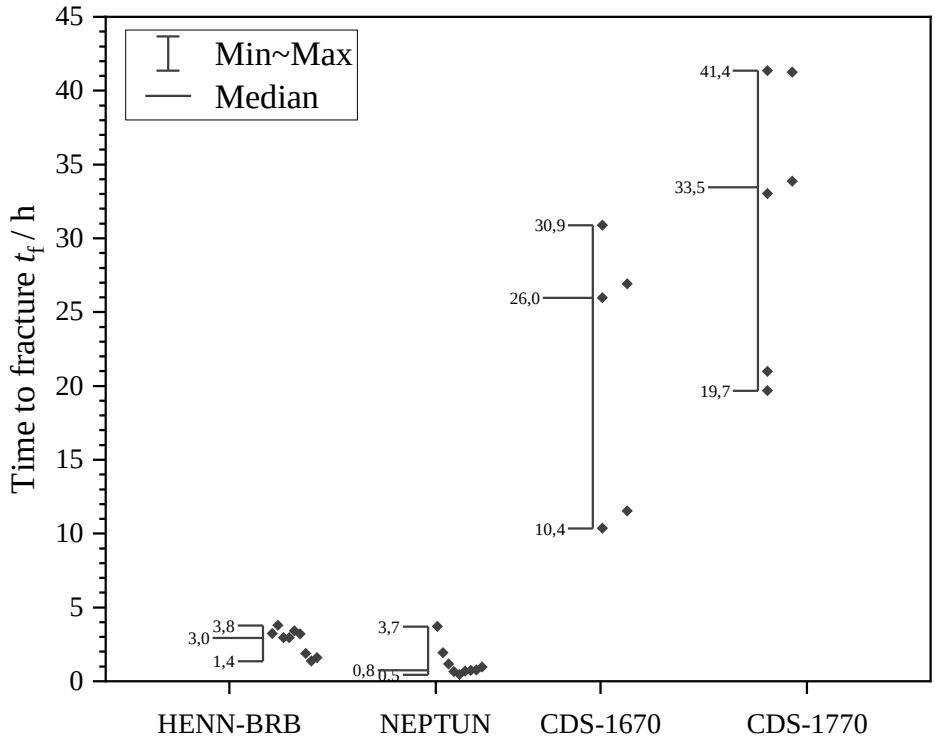

Figure 20: Time to fracture of the prestressing steel wires tested in the project at 80%. R_m in test solution A at 22°C with cathodic polarization at $i_{cat.}$ = 0.125 mA cm^{-2}.

The results in Figure 20 confirm that NEPTUN is considered highly susceptible, and CDS-1670, which is currently approved, also maintains selectivity in the times to fracture. A test method with cathodic polarization at a cathodic current density $i_{cat.}$ = 0.125 mA cm^{-2} is considered suitable for the new test method.

An extension of the results to other prestressing steels with larger diameters will be carried out in WP 4. In WP 5, the newly developed test method will be statistically evaluated for reproducibility in a round robin test. In WP 6, in addition to formulating a draft standard, the results will be summarized in an overview to propose a limit value or a conformity criterion for the new test method based on the statistical evaluation.

Stress corrosion tests with delivery surface vs. polished surface

The previous sections of the report (WP 1) discussed the influence of the surface condition on the stress corrosion cracking test. To verify the electrochemical results obtained in WP 1, i.e., that the surfaces should be polished, samples with delivery surfaces vs. samples with polished surface conditions were directly compared in stress corrosion tests. The stress corrosion tests were performed in each case with test solution A at 80% R_m and 0.125 mA cm^{-2} cathodic

current density at 22°C. The results for comparing CDS-1670 and CDS-1770, each with a delivery surface and polished surface, are shown in Figure 21.

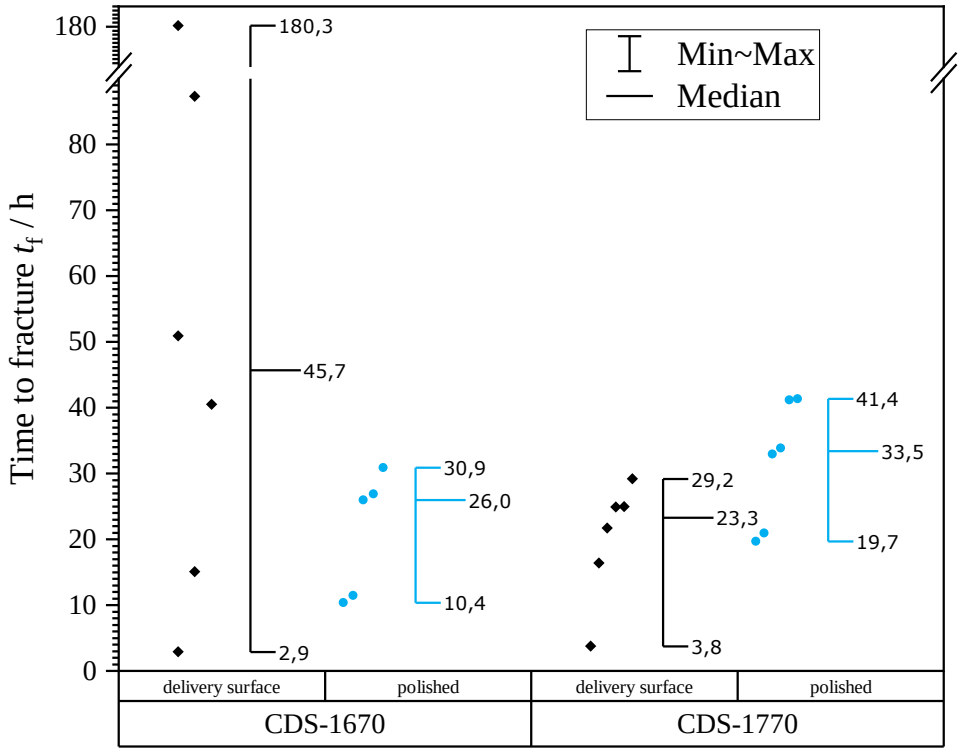

Figure 21: Stress corrosion tests at 80% R_m, test solution A at 22°C on the CDS-1670 and CDS-1770. The scattering of results was compared with the surface conditions in each case: Delivery surface vs. polished surface. Only fractures were considered.

The comparison of the times to fracture with the delivery surface and the polished surface shows that with the polished surface, no early fractures occur far below the median. However, for CDS-1670 (delivery surface), the median is 45.7 h, and the minimum is 2.9 h, and for CDS-1770 (delivery surface), the median is 23.3 h, and the minimum is 3.8 h. In contrast, the difference between the minimum time to fracture and the median is smaller for polished wires: for CDS-1670 (polished), the median is 26.0 h, and the minimum is 10.4 h (or CDS-1770 (polished), the Median is 33.5 h, minimum 19.7 h). Thus, the scatter on polished wires is significantly reduced, resulting in fewer "early" fractures well below the median. From a testing point of view, the polishing of the surface offers advantages since, on the one hand, the

minimum time to fracture can be used as a conformity criterion, as also regulated in prEN 10138, parts 1-4 [3], and on the other hand the differentiation to highly susceptible prestressing steels is maintained.
After reviewing all the studies on the electrochemical surface influence on stress corrosion cracking testing, it was concluded that testing on delivery surfaces is not helpful but that the test surfaces should be homogenized using a non-abrasive polish as sample preparation.

The problem with delivery surfaces is localized damage caused by the manufacturing or transportation process before testing. In the case of prestressing steel, artifacts (scratches or cracks) in the drawing layer cannot be excluded.

From an electrochemical point of view, it was shown in WP1 that polished surfaces without drawing layers have a lower polarization resistance with less scattering than delivered surfaces. Thus, surfaces without a drawing layer can be cathodically polarized more easily and in a more defined manner.

In cathodic polarization tests, hydrogen charging is controlled by applying direct current and a defined cathodic current density and begins immediately upon application of the direct current. Using the delivery surface with its artifacts (scratches or cracks) in the drawing layer effectively disturbs the polarization. Since the current seeks the path of least resistance, and in the case of delivery surfaces, lower polarization resistances act in the area of the scratches than in the rest of the surrounding drawing layer; consequently, only the scratches' area is cathodically polarized. Thus, the current density changes depending on the number, distribution, and size of the artifacts on the drawing layer. Since the hydrogen charge intensity depends on the current density, the charge intensities vary greatly from sample to sample, accounting for the more extended fracture scattering with the delivery surface.

It was decided with the project consortium to evaluate the newly developed test method with polished surfaces, test solution A at 22°C, and a cathodic polarization with $i_{cat.}$ = 0.125 mA cm^{-2} to be evaluated in WP 4 and WP 5, see Figure 22.

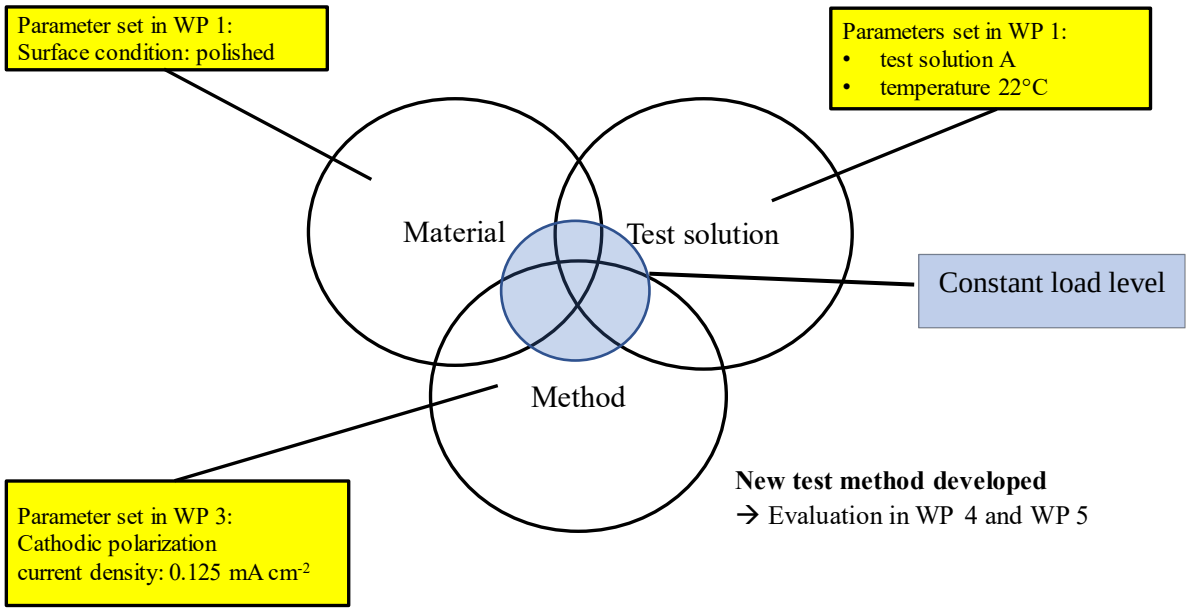

Figure 22: Parameter overview of the newly developed test method.

2.5 Work Package 4: Implementation of the New Process

No.	Goal
2.5.1.	Constructive preparation
2.5.2	Implementation of the new test procedure
2.5.3	Test series according to the newly developed test method
2.5.4	Design of Experiments (DOE) on 11 mm samples

The task of work package 4 was commissioning a new test stand for large bar diameters. For this purpose, the design preparation and construction of a large 3 MN stress corrosion cracking test stand was already carried out before the start of the project. Subsequently, the work package task was to install the new test method on the stress corrosion cracking test stands available at SAH and to carry out the test series. Within the scope of the implementation, the specifications of BAM – resulting from the prestressed wire and miniature specimen test series carried out by BAM – were to be implemented in the best possible way for the industrial SAH stress corrosion cracking test stands.

A partial study with the sample material produced by SAH was carried out at BAM. The results of this study are described below:

2.5.1 Constructive Preparation

Based on the preliminary consultations before the project's actual start, the desire was formulated to realize testing possibilities for hydrogen-induced stress corrosion cracking for large prestressing steel bar diameters. In response to this request, SAH constructed a 3 MN stress corrosion cracking test rig, as shown in SAH-Figure 7 and SAH-Figure 8, especially for the present project.

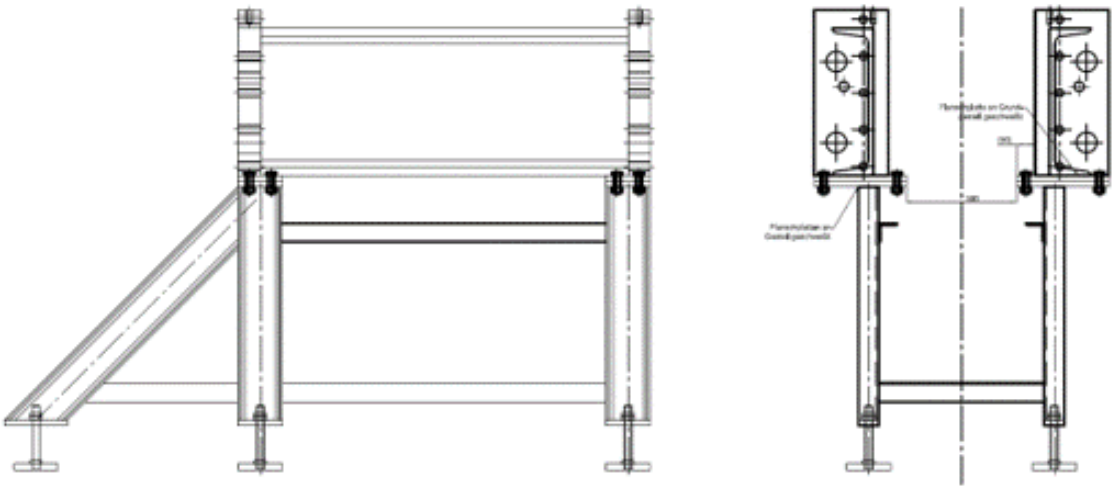

SAH-Figure 7: Design drawing of the 3 MN stress corrosion test rig constructed by SAH for the project.

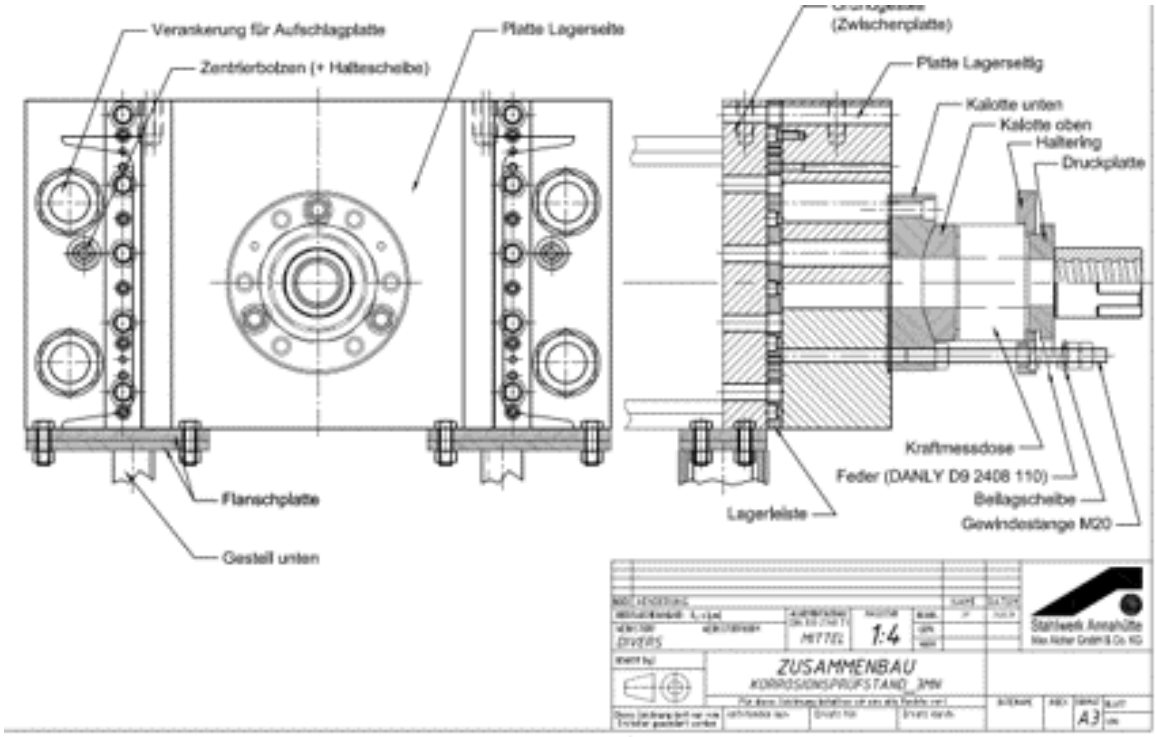

SAH-Figure 8: Construction drawing of the test rig plate designed by SAH for the project, including spherical cap and 3 MN ring load cell.

The new 3 MN stress corrosion cracking test stand, which was built before the start of the project using SAH's funds, has the following capacity in the actual design according to SAH-Figure 9 and SAH-Figure 10

- 3 MN Test force to be generated and metrologically monitored
- Bars with a length of 2,800 mm to be tested.

The measured values are recorded using the measuring cabinet shown in SAH-Figure 10 at the rear left.

SAH-Figure 9: After completion, the newly built 3 MN stress corrosion cracking test rig at SAH.

SAH-Figure 10: New stress corrosion cracking test rigs in the SAH test laboratory.

2.5.2 Implementation of the New Test Procedure

The new 3 MN stress corrosion cracking test's commissioning phase was characterized by integrating the classical force-time measurement. In addition, the conventional test vessel (cf. SAH-Figure 11) was replaced by a test vessel newly developed and manufactured by BAM and integrated metrologically. The specification was to polarize the prestressing steel cathodically, i.e., electrically negatively (-), and the corresponding grid counter electrode positively (+).

SAH-Figure 11: Conventional test vessel according to DIN EN ISO 15630-3:2020-02, incl. curing tube.

The test cell concept developed by BAM is shown in Figure 16. Following this concept, SAH-Figure 12 shows the concept implementation as a test cell manufactured by BAM for testing ø 40 mm SAS 950/1050 prestressing steel. The prestressing steel is polarized as a cathode, electrically negative (-). In contrast, the grid counter electrode in the test vessel, which is sealed using rubber sleeves and a clamping band, is polarized anodically electrically positive (+). The test solution filling opening and the current supply to the counter-electrode grid using an alligator clip can also be seen in SAH-Figure 13.

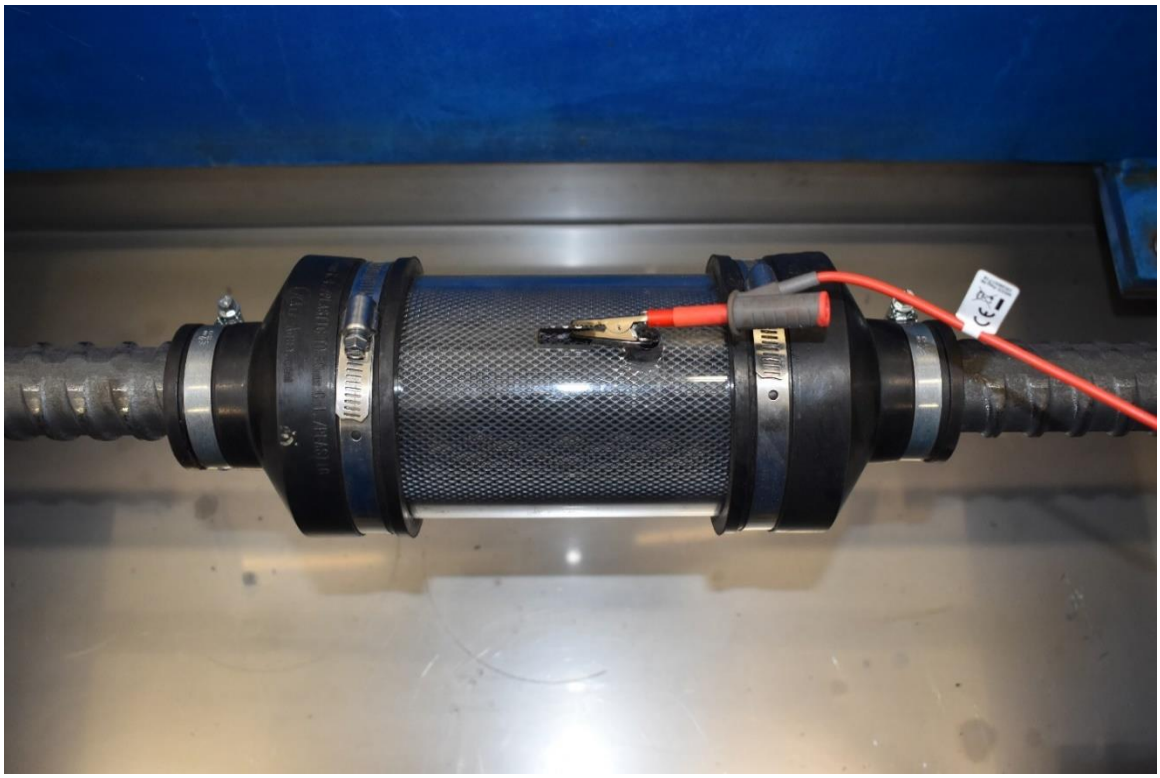

SAH-Figure 12: Newly developed test cell for a ø 40 mm SAS 950/1050 prestressing steel in the new 3 MN stress corrosion cracking test stand.

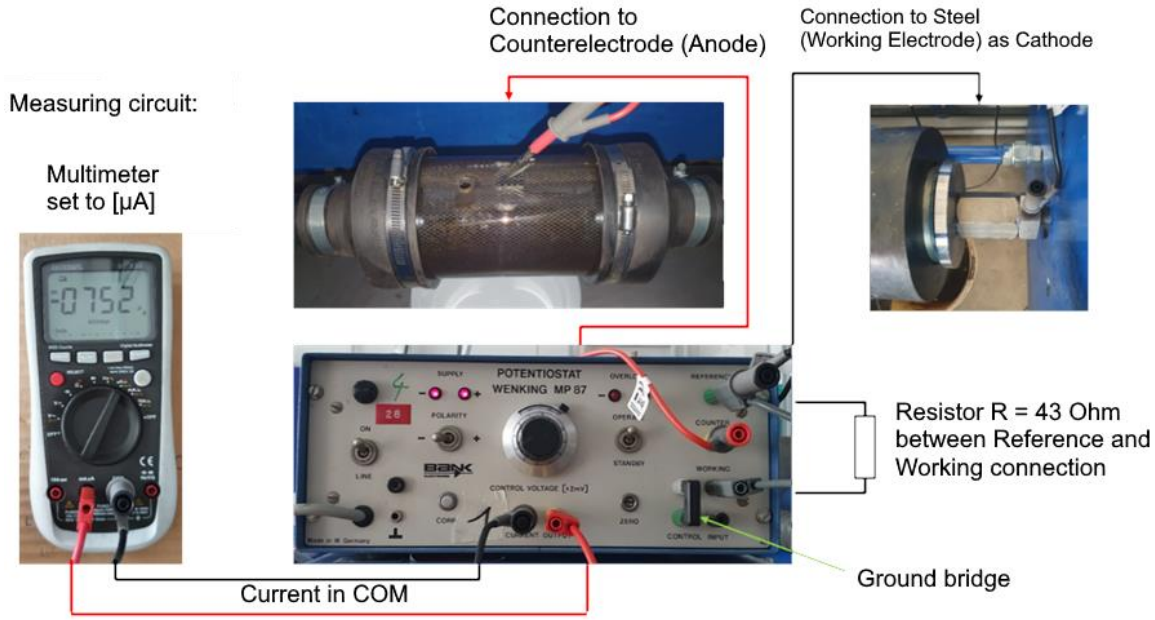

SAH-Figure 13: Electrical test setup for the newly developed test method on the 3MN stress corrosion cracking test stand.

2.5.3 Test series with the new test method

On the ø 18 mm SAS 950/1050 prestressing steel, 15 active stress corrosion cracking tests (0.6 MN test stand in the front left of the picture, the 1 MN test stand in the center of the picture) were carried out using the new test method during the project. The accumulated test time was 10,480.8 h, which corresponds to approx. 437 days. The SAH-Table 3 shows the following quantities.

- Test No.
- Heat Lot No.
- Clamping force factor related to tensile strength R_m
- (Test) current in $\mu A/mm^2$ applied to the affected surface area
- (Test) running time in h
- Statement fracture yes/no
- Yield strength F_{eH}
- Yield strength R_{eH}
- Maximum (bearable) tensile force F_m
- Tensile strength R_m
- Elongation at break A_{10}
- Elongation under maximum load A_{gt} as well as the
- Reduction of the area at fracture Z

On an unloaded reference bar (highlighted in yellow), the mechanical-technological values (see above list) of the underlying test melt were recorded in advance. For the unbroken bars, with one exception, a downstream tensile test was carried out after the bars had been removed from the stress corrosion cracking test stand, and the listed mechanical-technological steel properties were again recorded. It should be noted that only 1 test from the ø 18 mm SAS 950/1050 prestressing steel specimen series broke after 1345.8 hours (approx. 56 days). For the unbroken test bars, a slight drop in the mechanical-technological properties (elongation at break A_{10}, elongation at maximum load A_{gt}, and reduction of the area at fracture Z) can be observed in some cases.

SAH-Table 3: Tests on ø 18 mm SAS 950/1050 prestressing steel with the new test method

Test No.	Heat Lot No.	Force Factor x Rm	Current density µA/mm²	Run Time h	Fracture? yes/no	F_{eH} kN	R_{eH} N/mm²	F_m kN	R_m N/mm²	A_{10} %	A_{gt} %	Z %
	624455					242	979	275	1112	9,6	7	29,6
0	VA489331	0,8	1,25	1148,3	no	234	960	267	1095	4,1	6,3	14,5
1	624455	0,8	1,25	239,9	no	238	959	273	1100	7,1	4,8	25,5
2	624455	0,8	1,25	239,5	no	238	959	273	1100	9,4	7,3	30,3
3	624455	0,8	1,25	240,0	no	237	962	267	1084	8,3	6,7	27,7
4	624455	0,8	1,25	240,0	no	237	954	270	1087	8,8	7,7	25,0
5	624455	0,8	1,25	240,0	no	243	986	276	1120	9,2	6,2	27,3
6	624455	0,8	1,25	240,0	no	242	985	278	1131	8,7	5,9	26,7
7	624455	0,8	1,25	237,0	no	238	970	266	1085	9,1	6,3	26,7
8	624455	0,8	1,25	236,5	no	237	963	268	1089	9,2	7,1	26,2
9	624455	0,8	10	718,0	no	241	940	267	1042	8,8	6,4	28,7
10	624455	0,8	10	718,0	no	239	938	272	1067	9,2	6,9	27,4
11	642455	0,9	1,25	650,5	no	240	980	268	1094	6,3	6,2	27,4
12	624455	0,9	1,25	650,5	no	240	975	272	1105	8,1	5,4	17,3
13	624455	0,8	1,25	1345,8	Fracture in test cell							
14	624455	0,8	1,25	3336,8	no							

Similarly, six stress corrosion cracking tests with a total test time of 1914.3 h, corresponding to about 80 days, were carried out on the ø 40 mm SAS 950/1050 prestressing steel on the newly built 3MN stress corrosion cracking test stand. Also, in this series of tests, no fractures occurred on the product within the respective selected test time. The decrease in the mechanical and technological values of the unloaded test is shown in SAH-Table 4.

SAH-Table 4: Tests on ø 40 mm SAS 950/1050 prestressing steel with the new test method

Test No	Heat Lot No.	Force Factor x Rm	Current density µA/mm²	Run Time h	Fracture ? yes/no	F_{eH} kN	R_{eH} N/mm²	F_m kN	R_m N/mm²	A_{10} %	A_{gt} %	Z %
	323625					1240	994	1375	1102	7,8	7	15,9
1	323625	0,8	1,25	239,8	no	1239	995	1375	1104	5,0	4,7	10,9
2	323625	0,8	1,25	239,5	no	1232	986	1377	1102	5,8	6,1	11,6
3	323625	0,8	1,25	240,0	no	1240	991	1371	1096	5,9	5,3	11,7
4	323625	0,8	1,25	240,0	no	1238	992	1382	1107	6,5	6,1	13,7
5	323625	0,8	1,25	237,0	no	1238	988	1380	1101	6,7	6,1	9,0
6	323625	0,8	10	718,0	no	1234	985	1382	1104	6,1	5,6	11,3

Based on the results of the test on real prestressing steel specimens[2] listed in SAH-Table 3 and in SAH-Table 4, the samples of variant 2 QT(Bainite) tested as susceptible in the miniature test (see Section 2.5.4) were still tested on the 3 MN stress corrosion cracking test stands. Due to the specimen dimensions (short length), the samples had to be sleeved in the 3 MN stress corrosion cracking test stands (required specimen length = 2,800 mm). For this purpose, metric

[2] Only in the case of the prestressing steel SAS 950/1050, ø 18 mm, sample 13 failed after 1345.8 h, i.e., one sample out of 14 samples from one and the same melt.

threads were cut at the ends of the specimens (ø 30 mm) and adapted via coupling sleeves and extension rods for clamping in the test stand. Test bars 3 and 4 in the test area were turned down to ø 24 mm for stress corrosion cracking testing and tested; see SAH-Table 5. As expected, both samples failed after short test times in the intended measuring range S_a, according to Figure 16, thus confirming the susceptibility of this sample variant compared to the miniature samples of the same variant tested at BAM. (cf. Section 2.5.4)

SAH-Table 5: Tests on samples of variant 2 QT(Bainite) susceptible to heat treatment

Test No.	Heat Lot No.	Force Factor x Rm	Current density µA/mm²	Run Time h	Fracture ? yes / no	F_{eH} kN	R_{eH} N/mm²	F_m kN	R_m N/mm²	A_{10} %	A_{gt} %	Z %
	VA389835					603	860	874	1247	10,6		26,6
	VA389835								1270			
3 - Ø24,0 mm	VA389835	0,8	1,25	0,5	Fracture in test cell							
4 - Ø24,0 mm	VA389835	0,8	1,25	0,8	Fracture in test cell							

The susceptibility of variant 2 QT(Bainite) could thus also be confirmed for larger diameters (ø 24 mm) based on two tests.

2.5.4 Design of Experiments (DOE) on 11 mm Samples

For stress corrosion tests with larger diameters, the Annahütte produced samples for corresponding tests at BAM. Round tensile samples with a diameter of 11 mm were prepared at BAM from the supplied prestressing bar material with a diameter of 15 mm, not to exceed the maximum test stand forces of 100 kN at BAM. The round tensile samples are shown in the longitudinal section in Figure 23.

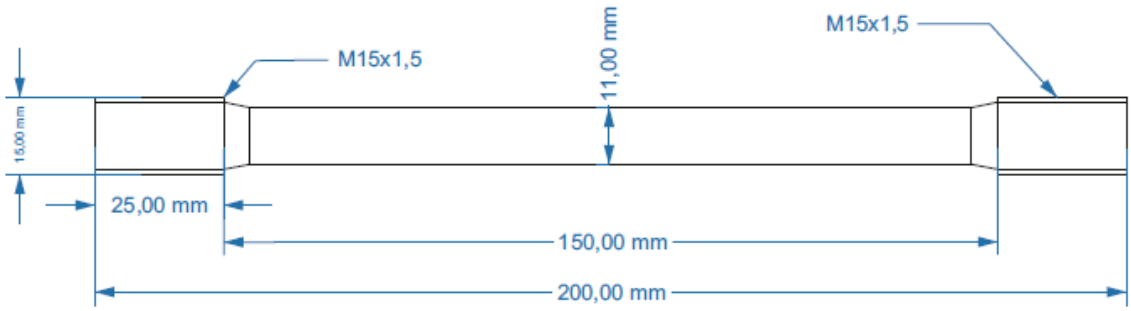

Figure 23: Dimensions of the round tensile samples with thread.

The variants with different starting materials in terms of chemical alloy composition, anonymously named Variant 1, Variant 2, and Variant 3 to protect the trade secrets of the Annahütte (SAH), were used. Each of the three variants was produced in three heat treatment states: normalized (+N), quenched and tempered (+QT), and quenched and tempered through the Bainitestage (+QTB). In a series of 42 tests, the influence of the cathodic current density in stress corrosion testing on the time to fracture of the 9 specimen variants was investigated. The three cathodic current densities studied were 0.125 mA cm^{-2}, 0.250 mA cm^{-2}, and 0.375 mA cm^{-2}. The experimental design and analysis were performed using *DesignExpert Version 13* statistical design software *from Stat-Ease, Inc., Minneapolis, USA,* to determine the interaction between the variables influencing the time to fracture and to derive statistical models from them. The results of the design of experiments (DOE) are shown in Table 12.

Table 12: Time to fracture results of the design of experiments (DOE) at 80%. R_m with test solution A at 22°C. (red arrow ↑ = sample was removed).

Run	Cathodic current density $i_{cat.}$	Alloy variant	Heat treatment condition	Time to fracture
#	mA cm^{-2}			h
1	0.375	Variant 2	+N	0.47
2	0.250	Variant 3	+QTB	0.58
3	0.375	Variant 1	+QT	2.66
4	0.375	Variant 3	+N	1.27
5	0.375	Variant 2	+QT	0.52
6	0.250	Variant 1	+QT	2.02
7	0.125	Variant 1	+N	23.82
8	0.375	Variant 3	+N	0.42
9	0.125	Variant 2	+QTB	0.35
10	0.375	Variant 2	+N	1.07
11	0.250	Variant 1	+QTB	3.45
12	0.250	Variant 2	+QT	1.07
13	0.125	Variant 1	+QT	0.95
14	0.375	Variant 2	+QTB	0.19
15	0.375	Variant 2	+QT	1.17
16	0.125	Variant 1	+QTB	1.27
17	0.250	Variant 2	+N	3.83
18	0.125	Variant 2	+QT	2.42
19	0.250	Variant 3	+N	2.32
20	0.125	Variant 1	+QTB	1.08
21	0.125	Variant 2	+QTB	0.45
22	0.250	Variant 2	+QTB	0.25
23	0.125	Variant 3	+N	19.15
24	0.375	Variant 2	+QTB	0.17
25	0.125	Variant 1	+QT	1.10
26	0.375	Variant 1	+N	12.28
27	0.375	Variant 1	+QTB	1.23
28	0.375	Variant 1	+QTB	0.42
29	0.375	Variant 3	+QT	↑ 90.00
30	0.375	Variant 3	+QT	↑ 90.00
31	0.125	Variant 2	+N	1.43
32	0.125	Variant 3	+QT	31.78
33	0.125	Variant 1	+N	↑ 90.00
34	0.125	Variant 2	+QT	1.58
35	0.375	Variant 3	+QTB	0.14
36	0.125	Variant 1	+N	↑ 90.00
37	0.250	Variant 1	+N	13.97
38	0.125	Variant 3	+N	20.90
39	0.125	Variant 3	+QTB	1.58
40	0.125	Variant 3	+QT	↑ 90.00
41	0.250	Variant 3	+QT	↑ 90.00
42	0.375	Variant 3	+QTB	0.22

A reduced two-factorial (2FI) model with transformation by a decadic logarithm function was selected for model building. The hypothesis tests ANOVA and Lack-of-Fit were performed for the selected model type. The calculated characteristics of these hypothesis tests are listed in Table 13.

Table 13: Characteristics of the hypothesis tests ANOVA and Lack-of-Fit for the selected reduced two-factorial model (2FI) with a decadic logarithm function transformation.

	Sum of squares	df	Mean value of squares	F-value	P-value
Model	**28.44**	**11**	**2.59**	**32.28**	**< 0.0001 significant**
A-Cathodic current density	1.48	1	1.48	18.44	0.0002
B-alloy variant	5.08	2	2.54	31.73	< 0.0001
C heat treatment condition	8.80	2	4.40	54.92	< 0.0001
AC	1.23	2	0.6161	7.69	0.0020
BC	8.35	4	2.09	26.06	< 0.0001
Residuals	**2.40**	**30**	**0.0801**		
Lack-of-Fit	1.68	15	0.1119	2.32	0.0569 not significant
pure errors	0.7233	15	0.0482		
Overall correlations	30.84	41			

The F value of the selected model is 32.28, indicating a significant model. There is only a 0.01% chance that an F value of this magnitude occurs due to noise. P-values less than 0.05 indicate significant model terms. Values greater than 0.10 indicate non-significant model terms. For this reason, the interaction AB reduced the model, which had a P value greater than 0.10. A, B, and C are significant model terms and the interactions between AC and BC. The lack-of-fit F value of 2.32 implies a 5.69% chance that a lack-of-fit F value of this magnitude occurs due to noise. The Lack-of-Fit is insignificant, so no model terms have been omitted that could have a relevant effect on the time to fracture.

To assess the quality of the model, the coefficient of determination R^2 is given in the statistics for the model's fit in Table 14.

Table 14: Statistics on the fit of the model.

Mean value $\bar{x}$	0,462 h	R^2	0,922
Standard dev. SD σ	0,283 h	adjusted R^2	0,894
Variation coef. S	69,66		

The value of R^2 ranges from 0 to 1, with larger values representing more accurate model fits and 0.922 representing a high goodness of fit. In addition to the R^2, there is the adjusted R^2, which may decrease as non-significant factors are added. The adjusted R^2 of just under 0.9 also provides a satisfactory value for the goodness of fit.

Model diagnostics test the following model assumptions: (i) the residuals are normally distributed, (ii) the residuals are homoscedastic, and (iii) the individual measurements are independent. The normal-quantile plot tests the normal distribution assumption (see Figure 24).

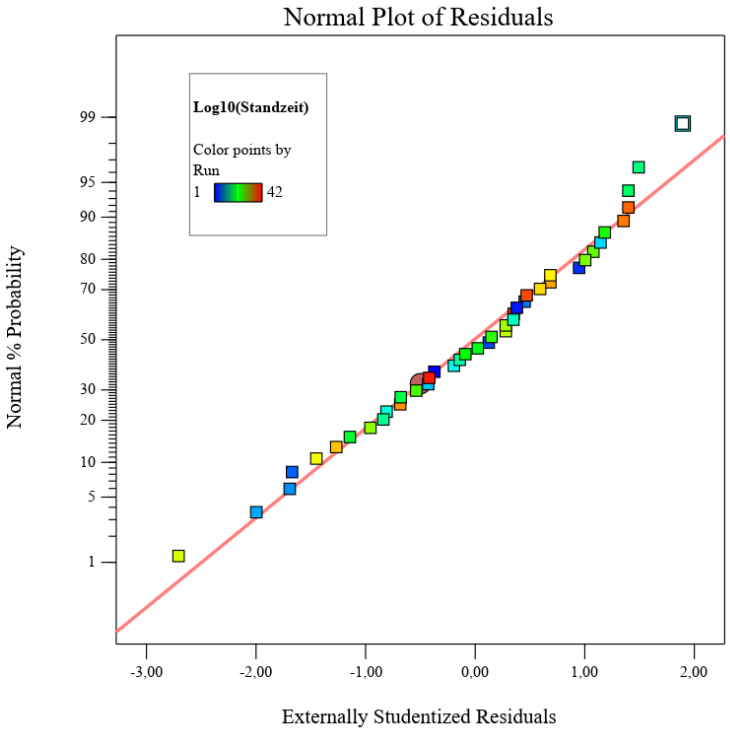

Figure 24: Normal-quantile plot of the model of interest.

In the normal-quantile plot, most residuals are close to the plotted straight line and describe a symmetrical shape. The assumption of normal distribution of the residuals is correct. To check the assumption of homoscedasticity, i.e., that the same dispersion of random errors is expected for all possible settings of the influencing factors, the residual plot (Figure 25) is considered.

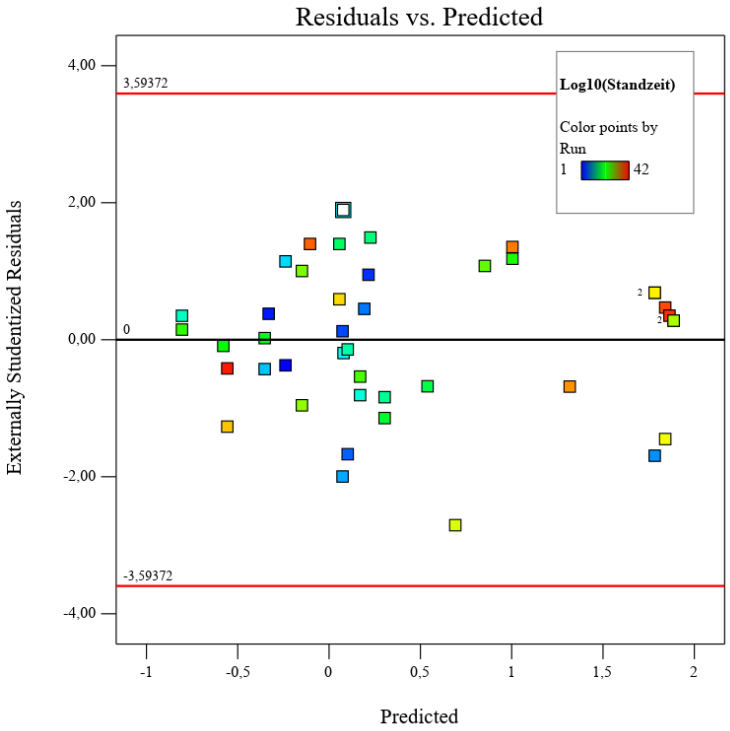

Figure 25: Residual plot of the model of interest. Measured residuals vs. predicted residuals.

The residuals' dispersion over the predicted residuals' range is mostly constant. The assumption of homoscedasticity appears to be met, although there is a structure at negative values of the predicted residuals. This may indicate that higher-order (quadratic) model terms may influence the fracture time, which was not modeled in this case. In this case, a reduced, two-factorial model was chosen.

To check the time independence of the residuals, the time series of the residuals were considered, see Figure 26.

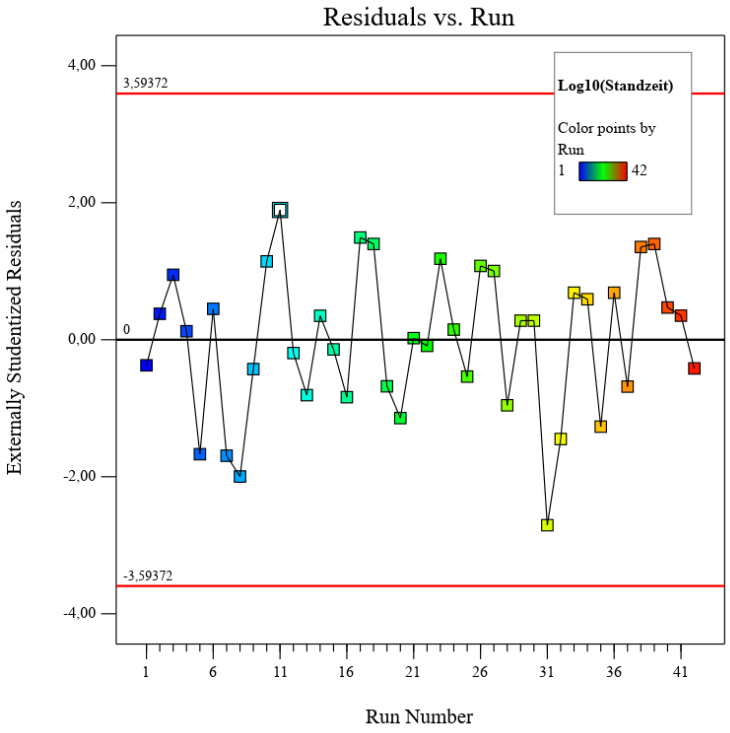

Figure 26: Time series of measured residuals.

No clear structures can be identified in the time series of the residuals. The assumption that the individual values are independent of each other in time is plausible.

With the model now diagnosed, the time to fracture results are plotted as a function of current density and various heat treatment conditions:

- For alloy variant 1, see Figure 27
- For alloy variant 2, see Figure 28
- For alloy variant 3, see Figure 29

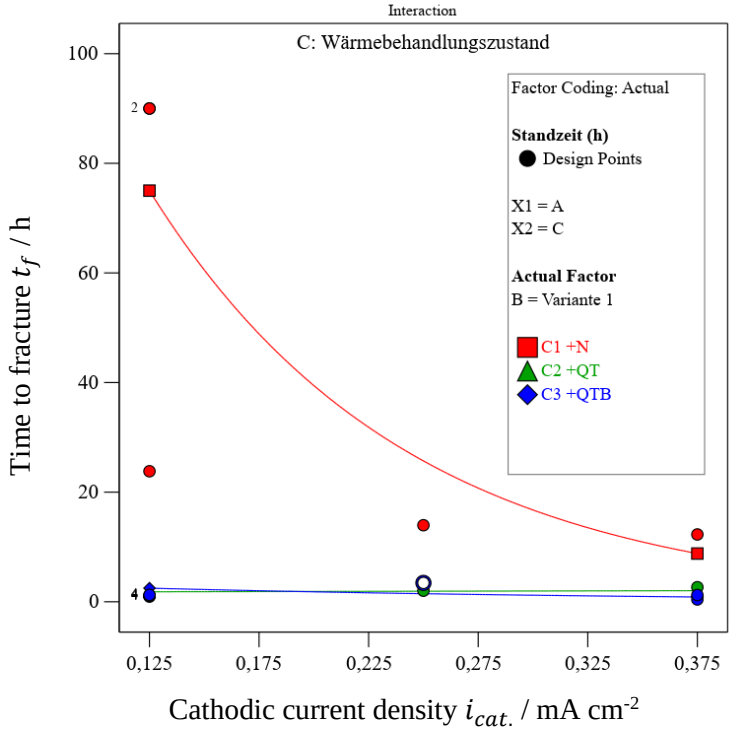

Figure 27: Time to fracture model as a function of the cathodic current density $i_{cat.}$ in mA cm^{-2} and the heat treatment condition for alloy variant 1.

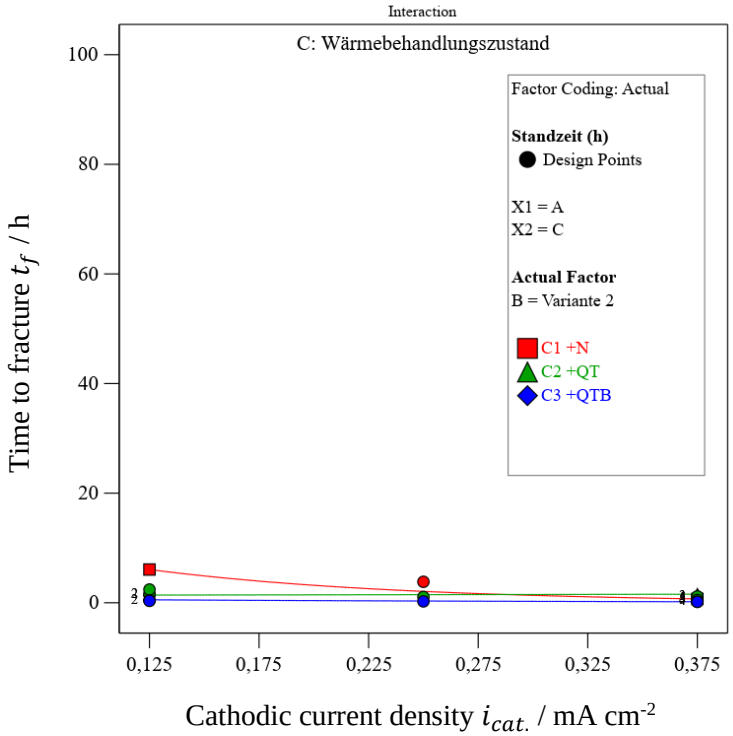

Figure 28: Time to fracture model as a function of the cathodic current density $i_{cat.}$ in mA cm^{-2} and the heat treatment condition for alloy variant 2.

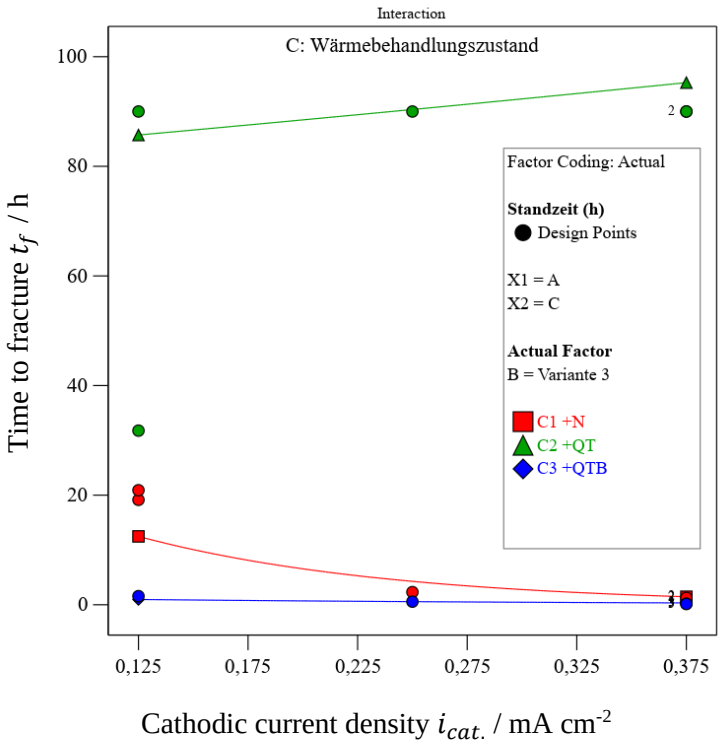

Figure 29: Time to fracture model as a function of the cathodic current density $i_{cat.}$ in mA cm^{-2} and the heat treatment condition for alloy variant 3.

For alloy variant 1 (Figure 27), it was shown that the time to fracture (in the range of approximately 0.4 h to 3.5 h) of the +QT and +QTB heat treatment conditions is independent of the cathodic current density. The time to fracture of the +N heat treatment condition increases with decreasing current density.

For alloy variant 2 (Figure 28), the time to fracture of each heat treatment condition is short regardless of the cathodic current density.

For alloy variant 3 (Figure 29), the time to fracture of the +QTB heat treatment condition is low regardless of the cathodic current density. For +N, the time to fracture increases with a cathodic current density of 0.125 mA cm^{-2}; for +QT, the time to fracture is relatively high regardless of the cathodic current density.

The time-to-fracture model shows that higher current densities do not significantly reduce fracture time, except for the heat treatment condition +N of the respective alloy variants 1 and 3. The observations from the permeation measurements in WP 3 can explain the results from the stress corrosion tests. In the permeation measurements with steel membranes of the same type, the three cathodic current densities of 0.125 mA cm^{-2},

0.250 mA cm^{-2}, and 0.375 mA cm^{-2} provided similar amounts of permeable hydrogen. The comparison with DOE is appropriate at a current density of 0.125 mA cm-2, where NEPTUN, HENN-BRB, CDS-1670, and CDS-1770 gave the best differentiation between susceptible and robust conditions.

The tested round tensile samples have more than twice the cross section (at 11 mm diameter approx. 95 mm^2) as the wire material tested in WP 3 (from approx. 35 mm^2 to approx. 40 mm^2). Still, the times to fracture of the putative susceptible and bad materials are similar. Therefore, the new test method (test solution A, at 80% R_m, 22°C) is suitable at a cathodic current density of 0.125 mA cm^{-2} on bar material without a scale layer up to a cross-section of approx. 100 mm^2 and can significantly differentiate between susceptible and robust conditions. The sample material with a larger cross section could be classified as high- or low-susceptible, like CDS-1670 and CDS-1770, analogous to HENN-BRB and NEPTUN.

The small number of test results at the 0.125 mA cm^{-2} model point and the statistical model suggest that for variant 1, the normalized +N heat treatment condition should be considered low-susceptible. In contrast, the experimental results suggest that the +QT (quenched and tempered through the martensite stage) and +QTB (quenched and tempered through the Bainitestage) heat treatment conditions are highly susceptible. The small number of individual measurements at 0.125 mA cm^{-2} and the statistical model suggests that alloy variant 2 can be classified as highly susceptible in each of the heat treatment conditions studied. For alloy variant 3 at 0.125 mA cm^{-2} cathodic current density, the +N heat treatment condition is classified as less susceptible. The +QT heat treatment condition provided the longest times to fracture and can be classified as low-susceptible. Regardless of the alloy variant, the heat treatment condition +QTB (quenched and tempered via the Bainitestep) is classified as highly susceptible and unsuitable for use in prestressed concrete construction.

The influence of the different alloy variants and heat treatment conditions on the time to fracture results was not investigated in detail. As an experiment, the influence of the hydrogen transport of the different steel variants and heat treatment conditions was investigated in permeation measurements. For this purpose, permeation measurements were performed on steel membranes of different thicknesses of the steel mentioned above variants, and the effective hydrogen diffusion coefficients D_H, a measure of the integral hydrogen transport rate in a

material, were approximated. The values for D_H are in the same order of magnitude for the steel grades studied, ranging from $2 \cdot 10^{-6}$ cm^2 s^{-1} and $9 \cdot 10^{-6}$ cm^2 s^{-1}. Therefore, a direct correlation between D_H and time to fracture could not be found. There was also no correlation between strength and fracture time in this test series. The long time to fracture of Variant 3 + QT appears to be due to the chemical composition of Variant 3 alloy. Variant 3 + QT loses significant susceptibility due to a higher chromium and/or vanadium content.

The new test method thus offers the fundamental possibility of being used in the product development of prestressing steels. The test method can differentiate samples up to 100 mm^2 cross-section in different alloy variants and heat treatment states at 0.125 mA cm^{-2} cathodic current density based on time to fracture.

2.6 Work Package 5: Round Robin Test

No.	Goal
2.1.6	Install new process on existing test stands
	Evaluation of the tests with the new method

Install new method:

In WP 5, the newly developed test method was tested for its reproducibility on sections of the same batch's prestressing steel wire product. The test objects were cold-drawn prestressing wires of a batch of St 1470/1670, diameter 7 mm (round, smooth) from *Nedri* with current building authority approval in Germany. These were made available to BAM as supplied. The new test method worked at 80% R_m with polished surfaces, tested under cathodic polarization with $i_{cat.}$ = 0.125 mA cm^{-2} in test solution A at 22°C. For better comparability of the forces between the round robin test participants, a constant load level of 80% of the nominal tensile strength was R_m (1670 MPa) was required. It was not necessary to determine the actual tensile strength of the samples beforehand since the purpose of this round robin test was to verify the applicability and reproducibility of the new test method and not to obtain a new approval for this prestressing wire product.

The new test method and technical set-up resulting from cathodic polarization were implemented at the participating testing institutes and companies with factory production control. BAM implemented the new test method at the round robin test participants through business trips. Among them were the following institutes and companies:

- cbm TU München, München, D
- Institut für Baustoffforschung RWTH Aachen (ibac), Aachen, D
- Bundesanstalt für Materialforschung und -prüfung (BAM), Berlin, D
- IBMB MPA TU Braunschweig, Braunschweig, D
- NEDRI Spanstaal B.V., Venlo, NL
- MPA Nordrhein-Westfalen, Dortmund, D
- Stahlwerk Annahütte (SAH), Ainring-Hammerau, D

The test institutes have been replaced by capital letters in alphabetical order for anonymity. The order of the list of participants does not correspond to the alphabetical order. During the

implementation of the test procedure, the new test cell was adapted for vertical and horizontal test stands; examples of test setups are shown in Figure 30.

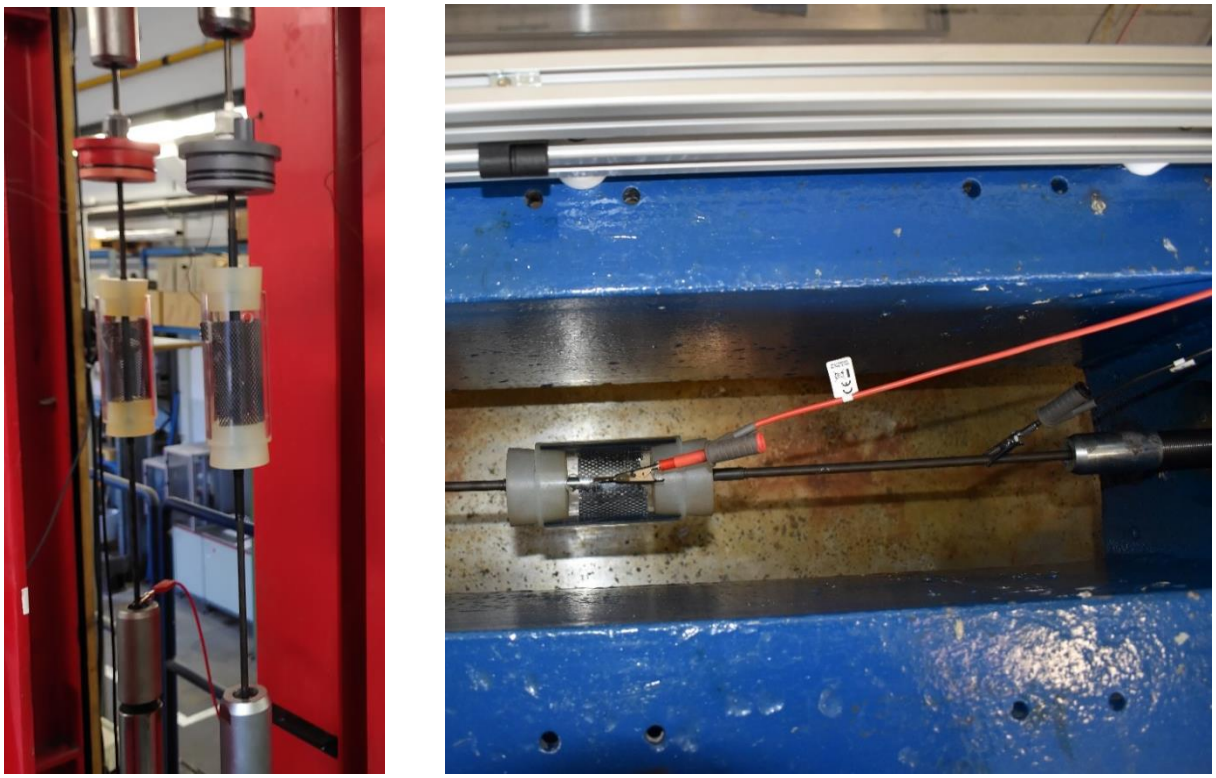

Figure 30: Test setup for standing (left) and horizontal test stands (right).

Detailed test instructions for sample preparation, test setup, and test execution were prepared by BAM and given to the participants. The electrical contact was made by clamps on the clamping steel and counter electrode via insulated measuring leads to the inputs of the *Wenking MP-87* potentiostats/galvanostats from *Bank* provided for the tests, which were switched in galvanostatic mode. During the on-site visits, BAM advised the test institutes and companies on performing the first test. Common sources of error in incorrectly performed tests were:

- Improper contact of the test solution with ferrous materials during preparation and pre-tempering of the test solution.
- Inaccurate determination of the test surface, which is in contact with the test solution during the test. This will result in an incorrect current setting.
- Incorrect handling of the potentiostat/galvanostat
- Leakage of the test solution during the test due to improper sealing of the test cell

Appropriate text and notes were added to the draft standard to avoid these serious implementation errors.

The pH value and the specific conductivity of the test solution A from the respective test institutes/companies were determined at the same temperature of 22°C in the BAM laboratories using portable measuring instruments from Knick. The measured values are intended to indicate whether the participants in the round robin test have correctly prepared the normative test solution A. Figure 31 shows the pH values and Figure 32 shows the specific conductivity of the test solution samples from the individual test institutes.

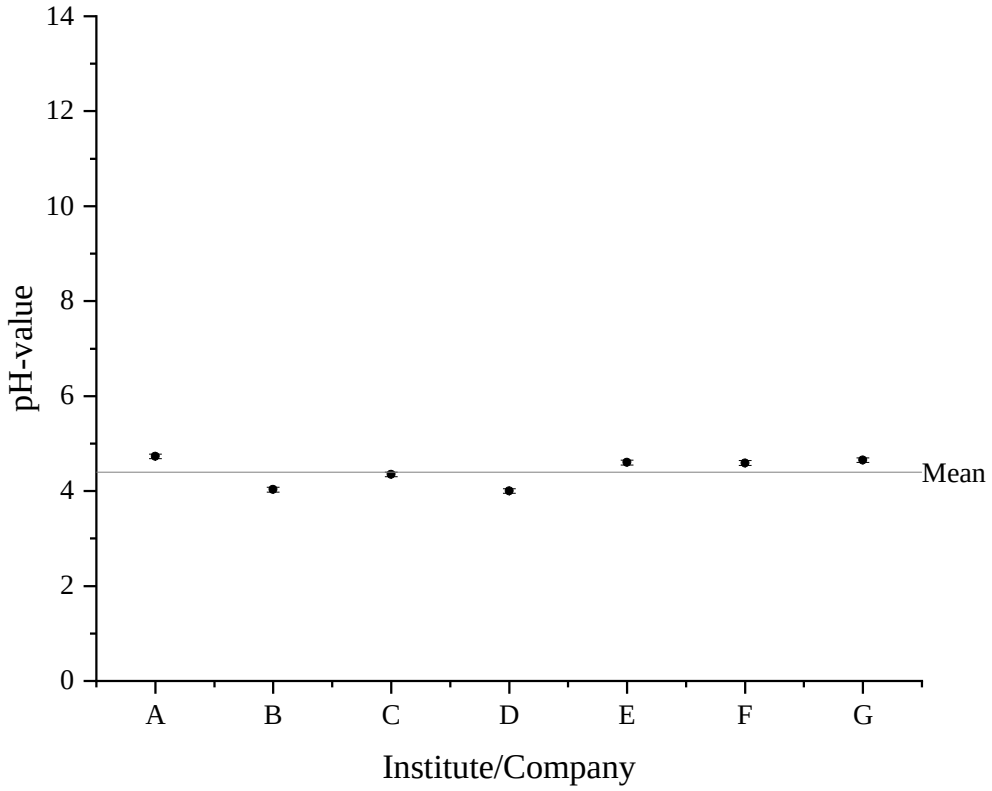

Figure 31: pH values of the samples of test solution A prepared in the respective test laboratories. The BAM laboratories determined the pH values at a temperature of 22°C.

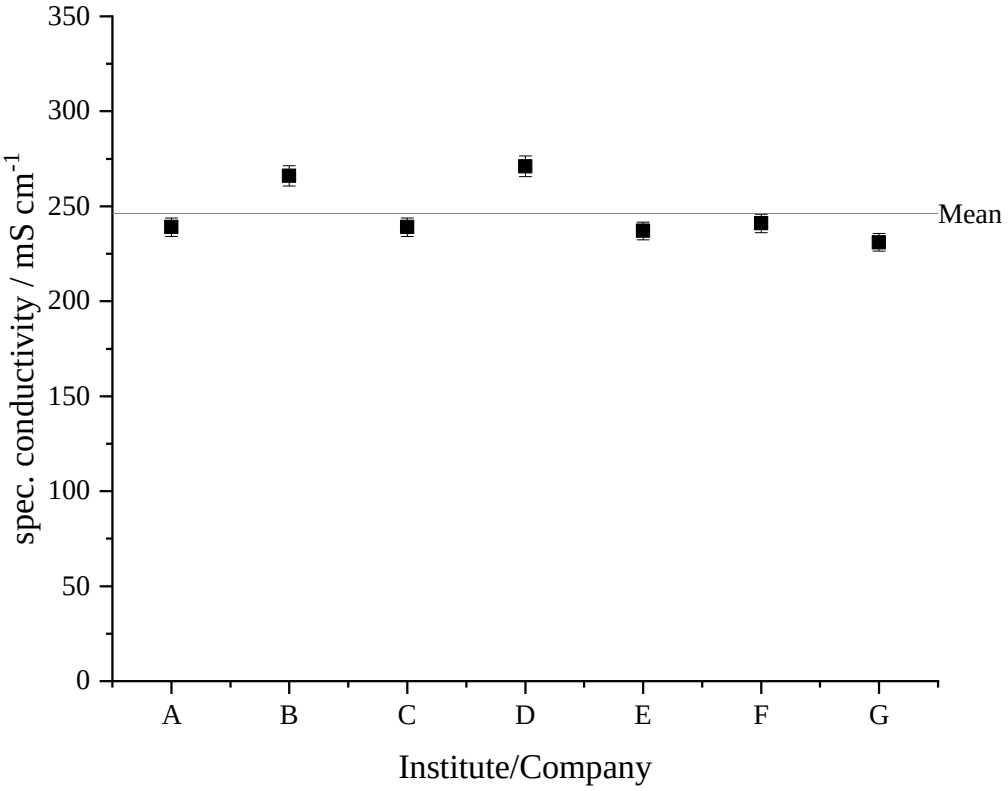

Figure 32: Specific conductivities of the samples of test solution A prepared in the respective test laboratories. The BAM laboratories determined the specific conductivities at a temperature of 22°C.

Differences in pH are measurable but show a slight deviation from the mean. There are also differences between the institutes in the specific conductivity. At the same temperature, the specific conductivity increases as the pH in test solution A decreases. The specific conductivities are generally in an elevated range, typical of aqueous electrolytes with a high concentration of dissolved salts. It can be assumed that test solution A was prepared correctly for each participant in the round robin test according to [1]. An influence of the pH value and the specific conductivity on the time to fracture in the round robin test is not to be expected. The mean laboratory temperature of the individual test laboratories of the first test is shown in Figure 33.

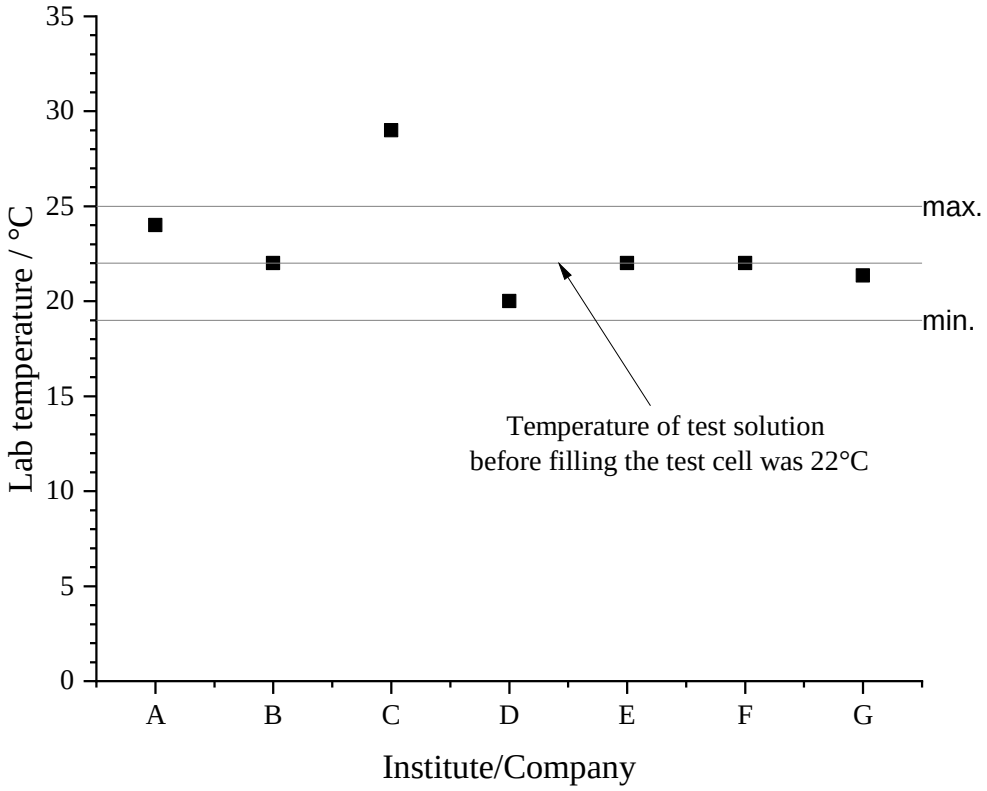

Figure 33: Laboratory temperature in the respective test laboratories of the test institutes and companies, measured at the start of the first tests.

In the test instructions for the round robin test, a temperature range of 22°C±3 K was required. Samples A, B, D, E, F and G could comply with the limits in their test rooms; in sample C, the measured laboratory temperature was above the required range. The test solution temperature was 22°C initially, but laboratory temperatures can change throughout the test. For test solution A, temperature changes can affect the specific conductivity and pH. However, from the thermodynamic consideration in WP 1, a temperature increase up to about 50°C is unlikely to change the tendency for other interfacial reactions to occur with test solution A. Beyond that, however, temperature changes can alter the potential level and the kinetics of the reactions at the steel/test solution phase boundary; for example, the IR drop corrected polarization resistance increases, cf. WP 1. Therefore, the time-to-fracture results should be examined for an influence of the pH value, the specific conductivity, and the laboratory temperature.

Evaluation of the round robin test:

The time to fracture results of the round robin test are presented as raw data in Table 15.

Table 15: Time to fracture in hours (h) of the round robin test batch CDS-1670 with newly developed test methods at the individual anonymized test institutes and companies. (Red arrow ↑ = run)

Institute/Company	A	B	C	D	E	F	G
	28.7	1.6	58.4	2.8	1.3	22.7	44.6
	28.9	28.8	↑ 72.0	25.6	50.1	36.3	47.9
	29.8	35.4	↑ 72.0	28.5	56.8	47.2	53.8
	30.7	38.5	↑ 72.0	30.4	72.7	94.4	58.7
		49.7	↑ 72.0	32.7	83.5	113.7	60.5
		52.2	↑ 72.0	33.6	90.8	↑ 217.6	76.2
		53.6		44.1	91.9		
		55.2		50.6			

Figure 34 shows a box plot of each sample. The whiskers are the range between minimum and maximum, and the boxes show the range of the interquantile distance (distance from 25% to 75% quantile) around the median (50% quantile).

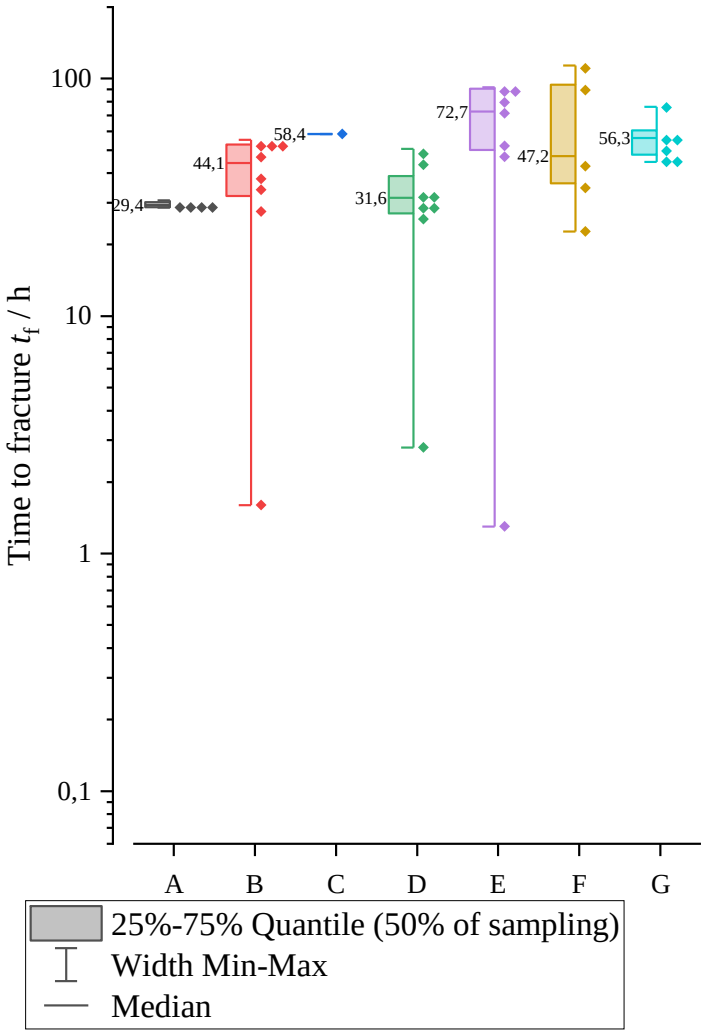

Figure 34: Boxplot for the descriptive statistics of the round robin test results with only wire breaks.

As expected, the medians of a batch of CDS-1670 in each sample should be above 10 h with high confidence; the results of WP 3 suggest this. In each sample, i.e., test institutes A-G, the median is above 20 h, the interquantile range from 25% to 75% quantile can be given for samples A, B, D, E, F, and G, and is also above 20 h time to fracture.

Reproducibility and applicability of the new test method seem to be given.

However, early fractures are well below the medians and the 25%-75% quantile range for samples B, D, and E.

More detailed statistical analysis is required to evaluate these results. Descriptive statistical characteristics for each sample are shown in Table 16.

Table 16: Descriptive statistics of the round robin test results. Only wire breaks were considered.

Institute/Company	A	B	C	D	E	F	G
n	4	8	1	8	7	5	6
Median	29.4	44.1	58.4	31.6	72.7	47.2	56.3
Mean value $\bar{x}$	29.5	39.4	-	31.0	63.9	62.9	57.0
SD σ	0.9	18.0	-	14.1	32.0	39.2	11.2
Variation coef. S	0.031	0.458	-	0.455	0.500	0.623	0.197
Minimum	28.7	1.6	-	2.8	1.3	22.7	44.6
Maximum	30.7	55.2	-	50.6	91.9	113.7	76.2

When comparing samples, the coefficient of variation S, the quotient of the standard deviation and the mean value, is a good measure of the relative scatter. Since the standard deviation is smaller than the mean for each sample, S<1. Sample A has the smallest dispersion of results, and Sample F has the largest. No further descriptive statistics can be used for test institute C since only one time to fracture result was obtained in addition to 5 runs, so only the median can be determined.

To compare the samples with each other, it must first be clarified whether all collected data should be included in the analysis or whether some can be neglected as outliers. To do this, a Grubbs test was performed on each sample using the statistics function of the *Origin 2021* software to identify outliers. The results of the outlier test are shown in Table 17.

Table 17: Outlier test statistic (Grubbs test) of times to fracture per sample (fractures only, no removed wires) at 95% confidence level.

Institute/Company	A	B	C	D	E	F	G
Value with largest G	30.7	1.6	-	2.8	1.3	113.7	76.2
G Statistical	1.280	2.093	-	1.999	1.958	1.297	1.714
critical G-value	1.481	2.127	-	2.127	2.020	1.715	1.887
estimated P	0.57	0.07	-	0.12	0.09	0.82	0.22
P limit	0.05	0.05	-	0.05	0.05	0.05	0.05
Outliers?	no	no	-	no	no	no	no

No outlier was identified in any of the samples at the 95% confidence level. Therefore, all measured times to fracture with fracture must be included in the evaluation of the round robin test. As a further check of the individual samples, whether the sample data were drawn from a normally distributed overall population was statistically tested. For this purpose, a Kolmogorov-Smirnov test for normal distribution was performed, and the results are presented in Table 18.

Table 18: The normal distribution test results according to Kolmogorov and Smirnov.

Institute/Company	A	B	C	D	E	F	G
n	4	8	1	8	7	5	6
Kolmogorov/Smirnov p-value	0.252	0.216		0.225	0.190	0.255	0.209
p limit value	1	0.829		0.774	1	0.898	1
Population normally distributed?	yes	yes		yes	yes	yes	yes

With 95% confidence, the sample data are from a normally distributed population. This is expected in a round robin test where only one batch of prestressing steel was tested and is another indication of the reproducibility and applicability of the new test method. This is also a criterion for considering the individual samples together. Several t-tests were performed to compare the means of two samples at a 95% confidence level to validate this on the one hand in the case of equal variance and on the other hand in the case where equal variance was not assumed. The t-test was performed on the sample pairs with the largest differences between their means. The interpretation of the t-tests is presented in Table 19.

Table 19: T-test statistic for comparison of two samples. Case 1: equal variance assumed; Case 2: equal variance not assumed. Null hypothesis mean1-mean2 = 0.

Institute/Company	Mean1	Mean2	significantly different? in case 1	significantly different? in case 2
A/B	29.5 h	39.4 h	no	no
B/D	39.4 h	31.0 h	no	no
D/E	31.0 h	63.9 h	no	no
E/F	63.9 h	62.9 h	no	no
F/G	62.9 h	57.0 h	no	no

Since the samples are comparable according to the t-test and the assumption of a normal distribution, a joint consideration of the times to fracture is also valid.

To estimate the probability distribution of the normally distributed population, the one-sided Student t distribution is used to determine the distribution's 5% and 1% quantiles. In addition to the median, the 5% or 1% quantile of the round robin test results could be used for a compliance criterion. Equations 12 and 13 were used to determine the quantiles of the student t distribution.

$$t_{0.05/0.01} = \bar{x} - \left(k_{0.95/0.99}\frac{\sigma}{\sqrt{n}}\right) \tag{12}$$

$$t_{0.95/0.99} = \bar{x} + \left(k_{0.95/0.99}\frac{\sigma}{\sqrt{n}}\right) \tag{13}$$

The t-constants $k_{0.95/0.99}$ are tabulated for each confidence level and number of degrees of freedom. The t-distribution allows, especially for small sample sizes, to calculate the distribution of the difference between the sample mean and the true population mean. Thus, for the small sample sizes in this interlaboratory comparison, the student's t-distribution provides a reliable estimate of the distribution and quantiles.

For samples A, B, D, E, F, and G, the corresponding $t_{0.05}$ and $t_{0.01}$ quantiles of the student t distribution were determined, representing an estimate of the distribution of the unknown, normally distributed total population for early break times. For larger values, the $t_{0.95}$ and $t_{0.99}$ quantiles were determined.

The $t_{0.05}$ means that in 5 out of 100 cases, or 95% confidence, the times to fracture are less than the corresponding values. At the next higher level of conformity, $t_{0.01}$ means that in 1 out of 100 cases, i.e., with 99% confidence, the times to fracture are below the corresponding values.

The specification of the lower quantiles $t_{0.01}$ and $t_{0.05}$ can be decisive for determining a limit value.

As shown in WP 3, CDS-1670 is a prestressing steel wire product with low susceptibility to HiSCC. Prestressing steel products that achieve similar times to fracture as CDS-1670 can also be considered low-susceptible. Consequently, the $t_{0.95}$ or $t_{0.99}$ quantile of the CDS-1670 can be used as a guide to limit the maximum test duration. Tests longer than the $t_{0.95}$ or $t_{0.99}$ quantile can be marked as passed and removed. All quantiles discussed for each sample are listed in Table 20.

Table 20: Estimates, quantiles by Student t distribution for the one-sided confidence interval at the 95% and 99% confidence levels, respectively.

Institute/Company	A	B	C	D	E	F	G
n	4	8	1	8	7	5	6
Mean value $\bar{x}$	29.5 h	39.4 h	-	31.0 h	63.9 h	62.9 h	57.0 h
SD σ	0.9 h	18.0 h	-	14.1 h	32.0 h	39.2 h	11.2 h
Degree of freedom df = n-1	3	7	0	7	6	4	5
$k_{0.95}$	2.353	1.895	-	1.895	1.943	2.132	2.015
$t_{0.05}$	**28.4 h**	**27.0 h**	**-**	**21.6 h**	**40.4 h**	**25.5 h**	**47.7 h**
$t_{0.95}$	**30.6 h**	**51.5 h**	**-**	**40.5 h**	**87.3 h**	**100.2 h**	**66.2 h**
$k_{0.99}$	4.541	2.998	-	2.998	3.143	3.747	3.365
$t_{0.01}$	**27.4 h**	**19.8 h**	**-**	**16.1 h**	**25.9 h**	**-2.8 h**	**41.5 h**
$t_{0.99}$	**31.6 h**	**58.7 h**	**-**	**46.0 h**	**101.8 h**	**128.5 h**	**72.4 h**

In each evaluable sample $t_{0.05}$ is not less than 20 h, i.e., in 5 out of 100 cases, the times to fracture are below the $t_{0.05}$ quantile or vice versa the times to fracture are over 20 h with 95% certainty. This statistically puts the early breaks in samples B, D, and E into perspective. The largest value from the round robin test is again estimated to be about 100 hours to break. Increasing the statistical certainty by choosing wider intervals, for A, B, D, E, and G, a range from 15 h (for $t_{0.01}$) to approximately 100 h (for $t_{0.99}$) is estimated. In sample F, however, negative $t_{0.01}$ quantiles are calculated. Negative values for $t_{0.01}$ are impossible to test and indicate that the sample size in F, with its comparatively high relative dispersion (coefficient of variation S=0.623), was too small to indicate a 99% confidence level.

Since there is comparability and normal distribution among the samples, it could be statistically concluded that the data come from the same overall population. Table 21 calculated the

quantiles for the one-sided confidence interval at the 95% and 99% confidence levels of all time-to-fracture results for the Student t-distribution estimate.

Table 21: The quantiles by Student-t distribution for the one-sided confidence interval at 95% and 99% confidence level estimated for the total round robin test results (only prestressing steel fractures considered).

	Total
n	39
Mean value $\bar{x}$	47.2 h
SD σ	25.3 h
Coefficient of variation S	0.536
Degree of freedom df = n-1	38
$k_{0.95}$ for df=30	1.697
$t_{0.05}$ (Total)	**40.3 h**
$t_{0.95}$ (Total)	**54.1 h**
$k_{0.99}$ for df=30	2.457
$t_{0.01}$ (Total)	**37.3 h**
$t_{0.99}$ (Total)	**57.2 h**

The overall observation estimates the $t_{0.01}$ (total) to be 37.3 h. The coefficient of variation here is S=0.536. However, the $t_{0.01}$ (total) is not suitable as a limit value since a conformity criterion must be robust for larger relative scatters, which can occur in individual institutes or companies, and such an exact estimate of the distribution for small sample sizes of about 6 trials can only be represented in exceptional cases.

From a test engineering point of view, the goal is to achieve a practical cutoff that is robust to the different scatter of results from individual testing institutes. As a further possibility, a superior $t_{0.05}$ quantile of each sample, a superior 5% quantile of these values could be determined so that in 5 out of 100 cases, the $t_{0.05}$ cannot be below a value. Thus, the different scatter of each sample could be neglected. Using the $t_{0.05}$ or $t_{0.95}$ quantiles from Table 20, the upper $t^*_{0.05}$ quantile is calculated according to Equation 14 or the upper $t^*_{0.95}$ quantile is calculated according to Equation 15:

$$t^*_{0.05} = \overline{t_{0.05}} - \left(k_{0.95/0.99} * \sigma_{0.05} \frac{1}{\sqrt{n}}\right) \quad (14)$$

$$t^*_{0.95} = \overline{t_{0.95}} + \left(k_{0.95/0.99} * \sigma_{0.95} \frac{1}{\sqrt{n}}\right) \quad (15)$$

Both the variables for the calculation and the results for the superior quantiles $t^*_{0.05/0.95}$ are shown in Table 22.

Table 22: The calculation of the superior quantiles by Student t distribution for the one-sided confidence interval at 95% and 99% confidence level estimated from the $t_{0.05}$ and $t_{0.95}$ Quantiles of the individual samples.

	for the $t_{0.05}$ individual values	for the $t_{0.95}$ individual values
Mean values $\overline{t_{0.05/0.95}}$	$\overline{t_{0.05}}$ = 31.8 h	$\overline{t_{0.95}}$ = 62.7 h
Standard deviation σ	$\sigma_{0.05}$ = 10.1 h	$\sigma_{0.95}$ = 27.1 h
for $k_{0.95}$ for df=5	2.015	2.015
$t^*_{0.05}$ (P=95%)	**22.7 h**	-
$t^*_{0.95}$ (P=95%)	-	**87.2 h**
for $k_{0.99}$ for df=5	3.365	3.365
$t^*_{0.05}$ (P=99%)	**16.6 h**	-
$t^*_{0.95}$ (P=99%)	-	**103.5 h**

To interpret the round robin results for the superior quantile $t^*_{0.05}$ (P=95%) = 22.7 hours:

- In 5 out of 100 cases, test institutes estimate their sample with a $t_{0.05}$ quantile below 22.7 h. Thus, the estimate of $t_{0.05}$ is above 22.7 h with 95% confidence.
- $t^*_{0.05}$ (P=99%) means that in 1 out of 100 cases, test institutes estimate their sample with a $t_{0.05}$ quantile below 16.6 h. This means there is a 99% certainty that the estimate of the $t_{0.05}$ quantile is above 16.6 h.
- $t^*_{0.95}$ (P=95%) means: In 5 out of 100 cases, test institutes estimate their sample with a $t_{0.95}$ quantile above 87.2 h. This means that with 95% certainty, the estimate of the quantile is $t_{0.95}$ is below 87.2 h.
- $t^*_{0.95}$ (P=99%) means: In 1 out of 100 cases, test institutes estimate their sample with a $t_{0.95}$ quantile above 103.5 h. This means that with 99% certainty, the estimate of the quantile based on the $t_{0.95}$ quantile based on the round robin test results is below 103.5 hours.

The calculated higher-order quantiles may guide WP6 to recommend limit values (compliance criteria) and set a maximum test duration.

From comparing the round robin test results with the measured differences in pH, specific conductivity, and measured laboratory temperatures, no conclusions could be drawn regarding an influence on the test. Thus, the new test method appears robust to such "minor" changes in test parameters.

No conclusions could be drawn from the review of the force gauge calibration documents, which, among other things, classified the force gauges used into specific quality classes of 0.5, 1, 2, and 3, and from the comparison of this information with the respective coefficients of variation, S.

2.7 Work Package 6: Evaluation and Drafting of a New Test Standard

No.	Goal
2.1.7	Summary of results
	Elaboration of a new test standard

Summary of results:

The results obtained on prestressing steel wires are summarized in this WP 6. The round robin test results from WP 5 on CDS-1670 were compared with those on CDS-1770, HENN-BRB, and NEPTUN. The time to fracture results for these wires are shown in Table 23.

Table 23: Times to fracture in hours (h) of CDS-1770, HENN-BRB, and NEPTUN with newly developed test methods.

Prestressing steel wire	CDS-1770	HENN-BRB	NEPTUN
Time to fracture in h	19.69	1.38	0.47
	20.99	1.61	0.66
	33.04	1.88	0.68
	33.88	2.96	0.73
	41.25	3.21	0.76
	41.36	3.23	0.98
		3.40	1.18
		3.79	1.95
			3.72

Analogous to the round robin test evaluation in WP 5, these wires were also evaluated using the same statistical methods. The results of the statistical evaluation are shown in Table 24.

Table 24: Statistics on the time to fracture results of the CDS-1770, HENN-BRB, and NEPTUN.

Statistics data	CDS-1770	HENN-BRB	NEPTUN
n	6	8	9
Median	33.46	3.09	0.76
Mean value $\bar{x}$	31.70	2.68	1.24
SD σ	9.49	0.92	1.03
Variation coef S	0.299	0.34	0.83
Minimum	19.69	1.38	0.47
Maximum	41.36	3.79	3.72
Outlier test (Grubbs test) at 95% confidence level			
Value with largest G	19.69	1.38	3.72
G Statistical	1.266	1.420	2.415
Critical G-value	1.887	2.127	2.215
Outliers?	no	no	yes
Normal distribution test according to Kolmogorov and Smirnov at 95% confidence level (without outliers)			
Kolmogorov/Smirnov p-value	0.223	0.244	0.264
p limit value	0.969	0.663	0.555
Population normally distributed?	yes	yes	yes
Quantile values according to one-sided Student t distribution (without outliers)			
df=n-1	5	7	7
$k_{0.95}$	2.015	1.895	1.895
$\boldsymbol{t_{0.05}}$	**23.9**	2.1	0.6
$\boldsymbol{t_{0.95}}$	39.5	**3.3**	**1.2**

A Grubbs test at 95% confidence level shows no significant outliers in the samples of CDS-1770 and HENN-BRB. For NEPTUN, the time to fracture result of 3.72 hours was identified as an outlier. The Kolmogorov-Smirnov test for normal distribution at the 95% confidence level, with the outliers eliminated, confirms that the times to fracture of CDS-1770, HENN-BRB, and NEPTUN come from a normally distributed population so that a normal distribution can be assumed, as with the results of the round robin test with CDS-1670.

The quantiles $t_{0.05}$ and $t_{0.95}$ were determined using a one-sided Student t distribution. For comparison with the results of the Round Robin, the quantiles determined are in the confidence interval from $t_{0.05}$ to $t_{0.95}$, so it is estimated with 95% confidence that the values of CDS-1770, HENN-BRB, and NEPTUN are between $t_{0.05}$and $t_{0.95}$. As a cold-drawn wire with expected low susceptibility to HiSCC, the estimated $t_{0.05}$ quantile of CDS-1770 is 23.9 h. Thus, despite the higher nominal strength, CDS-1770 is comparably low-susceptible to HiSCC as CDS-1670 in the lower strength class.

The $t_{0.95}$ quantiles as upper estimates of the HENN-BRB and NEPTUN prestressing wires, which are considered highly susceptible, are 3.3 h and 1.2 h, respectively. Both steel grades are now statistically confirmed to be highly susceptible to HiSCC, and they must fail the test by setting an appropriate conformity criterion. New prestressing wires that achieve similar times to fracture as HENN-BRB and NEPTUN in initial or re-approval tests must be considered unsuitable for use in prestressed concrete construction. The test results of the investigated prestressing wires with estimated normal distribution curves as well as important quantiles, determined according to the Student t-distribution, are graphically summarized in Figure 35.

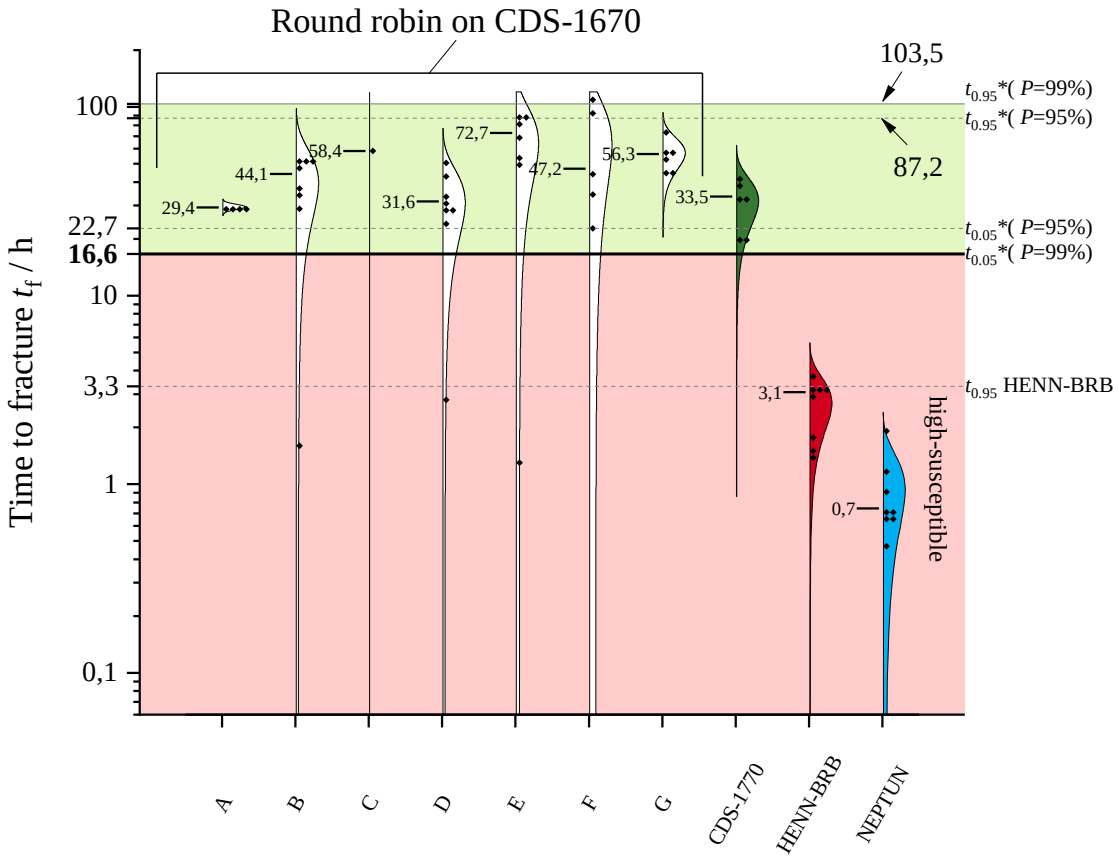

Figure 35: Comparison of results on prestressing steel wires in the WIPANO project with important quantiles.

According to the recommendation of the project consortium, a limit value of 16.6 h should be applied as a conformity criterion. The limit value of $t^*_{0.05}$ (P=99%) = 16.6 h provides a good

differentiation between cold-drawn prestressing wires with current building authority approval and quenched and tempered prestressing wires, which are considered to be highly susceptible to HiSCC.

The comparison between $t^*_{0.05}$ (P=99%) = 16.6 h with a confidence level of 99% as a lower estimate and $t_{0.95}$ = 3.3 h from HENN-BRB with a confidence level of 95% as the upper estimate is valid because the 16.6 h value of $t^*_{0.05}$ (P=99%) was calculated from the individual $t_{0.05}$ sample estimates, these sample estimates have a confidence level of 95%. Consequently, testing with the 16.6 h limit is robust to mis-estimates of the $t_{0.05}$ quantile at the 95% confidence level for low-susceptibility prestressing steels but additionally provides a required time to fracture level at which high-susceptibility prestressing steels will statistically fail.

Therefore, a procedure for assessing the conformity of prestressing wires can be recommended. See the diagram in Figure 36.

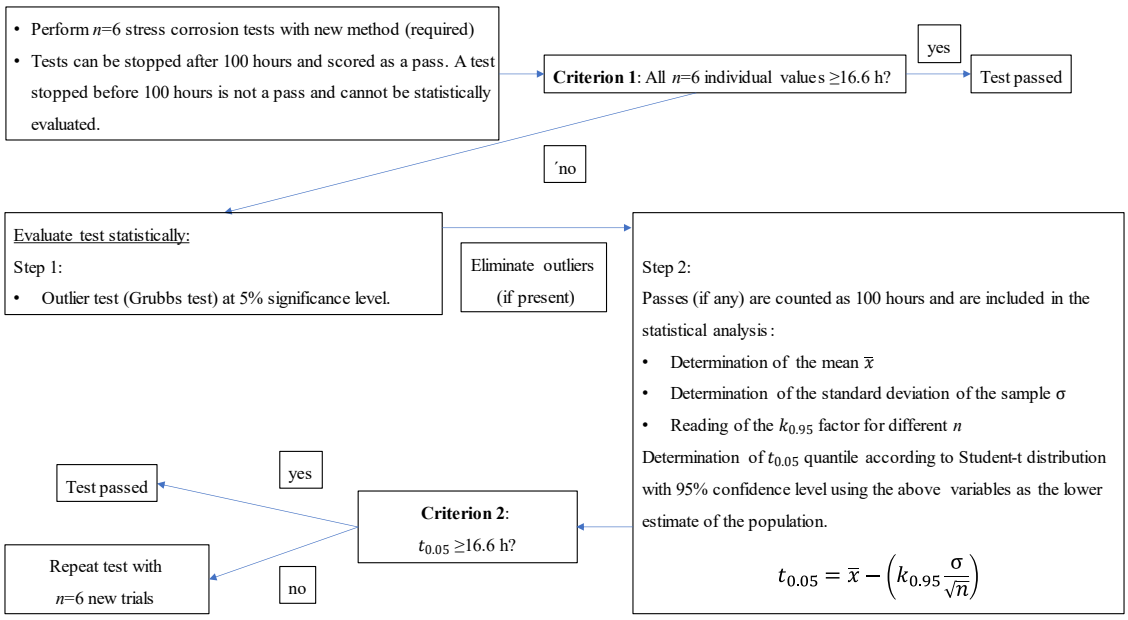

Figure 36: Scheme for the recommended evaluation procedure for conformity tests of prestressing steel wires with the new test method.

Six stress corrosion tests are required. Statistically valid individual tests can be stopped after 100 h and scored as a pass. The test is passed if all six individual time-to-fracture values are

≥16.6 h (criterion 1). If at least one time to fracture is less than 16.6 hours, a statistical evaluation with an outlier test (Grubbs test) at the 95% confidence level is mandatory. If outliers are identified, they must be used to estimate the $t_{0.05}$ quantile (according to Equation 12).
In this case, the passes (if any) are counted as single values of 100 h in the statistical evaluation as if they were fractures. A test termination before 100 h is not a pass and must not be statistically evaluated. Determining the mean $\bar{x}$, the standard deviation σ, and the sample size n of the data without outliers is mandatory. The corresponding $k_{0.95}$ factors of the Student-t-distribution with sample size n can be taken from Table 25.

Table 25: $k_{0.95}$ Factors for 95% confidence in statements according to Student t distribution as a function of sample size n.

n	$df = n-1$	$k_{0.95}$
3	2	2.920
4	3	2.353
5	4	2.132
6	5	2.015

If the 5% quantile estimate according to the Student-t-distribution is $t_{0.05} \geq 16.6$ h (criterion 2), the test is passed; if. $t_{0.05} < 16.6$ h, the sample is considered failed and would have to be repeated with six new trials.
Considering the passers with 100 h values in the statistical evaluation is controversial because the samples are supposedly "worse" evaluated, and the standard deviation is reduced. However, this is accepted for evaluating the sample to be able to make a statistic with six experiments at all. In addition, the test method only evaluates the $t_{0.05}$ quantile as the lower estimate (criterion 2) in the statistical evaluation, which is why an upper estimate is practically negligible. Nevertheless, the maximum test duration of 100 h allows a clear differentiation between susceptible and robust conditions.

Elaboration of a new testing standard:

In the project's final phase, a draft standard was developed in cooperation between Max Aicher GmbH & Co. KG (MAF) and the Bundesanstalt für Materialforschung und -prüfung (BAM)—the draft standard, which was submitted to the responsible ISO committee and for approval.

The objective of incorporating the results of the research project into standardization has been achieved. The new test method can be available as an informative annex of ISO 15630-3 in the future and can be referred to by product standards. In addition, the new test specification can be applied worldwide by being included in ISO 15630-3 as Annex B. The new test specification is expected to be widely used, and further results will enable further development, e.g., regarding the application of strands and bars.

In the project, the new testing method was evaluated on prestressing steel wires and also tested on prestressing steel bars. The testing problem for prestressing steel strands is that due to the product geometry with twisted individual wires, the actual contact area with the test solution is unknown. The specific cathodic current density required for the test cannot be guaranteed due to the undefined surface reference. A technical solution for testing prestressing steel strands was not developed during the project, but ideas for a possible implementation have been developed. Possible solutions should, therefore, be investigated in a further research project.